AN EXPERIMENTAL INVESTIGATION OF THE EFFECTS OF VACUUM ENVIRONMENT ON THE FATIGUE LIFE, FATIGUE-CRACK-GROWTH BEHAVIOR, AND FRACTURE TOUGHNESS OF 7075-T6 ALUMINUM ALLOY

by

CHARLES MICHAEL HUDSON

A thesis submitted to the Graduate Faculty of
North Carolina State University at Raleigh
in partial fulfillment of the
requirements for the Degree of
Doctor of Philosophy

DEPARTMENT OF MATERIALS ENGINEERING

RALEIGH

1 9 7 2

APPROVED BY:

A. A. Tobey — Roy B. Beason, Jr.

Wm. L. Bryan — Charles R. Manning
Chairman of Advisory Committee

ABSTRACT

HUDSON, CHARLES MICHAEL. An Experimental Investigation of the Effects of Vacuum Environment on the Fatigue Life, Fatigue-Crack-Growth Behavior, and Fracture Toughness of 7075-T6 Aluminum Alloy (Under the direction of Dr. C. R. Manning.)

Axial-load fatigue-life, fatigue-crack propagation, and fracture toughness tests were conducted on 0.090-inch thick specimens made of 7075-T6 aluminum alloy. The fatigue life and fatigue-crack propagation experiments were conducted at a stress ratio (ratio of the minimum gross stress to the maximum gross stress) of 0.02.

Maximum stresses ranged from 33 to 60 ksi in the fatigue life experiments, and from 10 to 40 ksi in the fatigue-crack propagation experiments. Fatigue life experiments were conducted at gas pressures of 760, 5×10^{-1}, 5×10^{-2}, 5×10^{-4}, and 5×10^{-8} torr. Fatigue-crack-growth and fracture toughness experiments were conducted at gas pressures of 760 and 5×10^{-8} torr.

Residual stress measurements were made on selected fatigue life specimens to determine the effect of such stresses on fatigue life.

The fracture surfaces of typical specimens were examined after failure using both transmission and scanning electron microscopes to study fracture modes in vacuum and air.

Analysis of the results from the fatigue life experiments indicated that fatigue life progressively increased as the gas pressure decreased. At a pressure of 5×10^{-8} torr fatigue lives were fifteen to thirty times

longer than at 760 torr, and the fatigue limit was approximately 11 ksi higher. It appeared that the reduction of the available water vapor around the test specimen is responsible for this increase in fatigue life.

Analysis of the results from the fatigue-crack-growth experiments indicates that at low values of stress-intensity range, the fatigue crack growth rates were approximately twice as high in air as in vacuum. However at higher values of stress intensity range, the fatigue crack growth rates were nominally the same in vacuum and air. An empirical equation developed by Forman et al was fitted to the crack propagation data using least squares techniques. This equation gave an excellent fit to the data generated in both vacuum and air.

Analysis of the fracture toughness data showed there was essentially no difference in the fracture toughness of 7075-T6 in vacuum and in air.

The X-ray stress analysis portion of the investigation indicated there was no consistent variation of fatigue life with residual stress level.

Fractographic examination of the specimens tested in both vacuum and air indicated that fatigue striations occurred in both vacuum and air, although the striations were considerably more numerous on the surfaces of air tested specimens than on the vacuum tested ones.

BIOGRAPHY

The author was born on [redacted] He received his elementary education at St. Paul's Catholic School, and his high school education at Benedictine High School both in Richmond, Virginia. He graduated from high school in June of 1953. The author attended St. Procopius College, Lisle, Illinois for two years and then transferred to Virginia Polytechnic Institute in Blacksburg, Virginia. He graduated from VPI in June 1958 with a Bachelor of Science degree in Civil Engineering. He subsequently received a Master of Science in Engineering Mechanics from VPI in June, 1965. From June 1958 until the present time he has been employed as an Aerospace Technologist at the Langley Research Center of the National Aeronautics and Space Administration, Hampton, Virginia. At Langley, he has conducted research in the field of fatigue of metals and has authored fifteen technical reports published by NASA. The author has also completed a Procurement Management Seminar (1964), and a Clear Writing Course (1968) sponsored by NASA. In addition he has completed short courses in Aerospace Structural Analysis (1965) at the University of Michigan, Ann Arbor, Michigan, and Nondestructive Test Techniques (1966) at the Illinois Institute of Technology, Chicago, Illinois.

The author is married to the former Miss Jean Carol [redacted] of Roanoke, Virginia. They have two children and now reside in Williamsburg, Virginia.

ACKNOWLEDGMENTS

The author wishes to express his sincere thanks for the assistance given by the Advisory Committee: Dr. C. R. Manning, Dr. A. A. Fahmy, Dr. R. B. Benson, Jr., and Dr. W. L. Bingham. Special thanks is due Dr. Manning, Chairman of the Advisory Committee, for his assistance and guidance throughout the author's studies at N. C. State.

The author would also like to thank his colleagues at NASA - Langley for their encouragement and assistance during this investigation, especially Mr. W. Illg, and Dr. H. A. Leybold. Thanks is also due Mrs. Alberta Saunders and Mrs. Elsie D. Illg for their help in the electron microscope and X-ray stress analysis studies; Mrs. Sue K. Seward for her assistance in gathering material for the literature survey; Mr. C. A. Rogers for his help in running the fatigue experiments; Mrs. Nancy H. White for her help in developing the computer programs used in the data analysis; and Mrs. Marcella Dobbins for her assistance in typing the manuscript.

The author would also sincerely like to thank his wife, Jeanie, and his children, Michael and Celeste, for their encouragement and for the sacrifices they willingly accepted in order that this investigation could be completed.

TABLE OF CONTENTS

TABLE OF CONTENTS (continued)

LIST OF TABLES

LIST OF TABLES (continued)

LIST OF FIGURES

LIST OF FIGURES (continued)

LIST OF FIGURES (continued)

INTRODUCTION

The effects of vacuum environment on the fatigue behavior of pure metals have been studied by several investigators. Generally these investigators found that fatigue lives were longer in vacuum than in air. However, space vehicles are generally constructed of high-strength metal alloys rather than pure metals, and the fatigue behavior of these high strength alloys is not generally known. In order to provide some of this knowledge a series of axial-load fatigue-life, fatigue-crack-propagation, and fracture toughness experiments have been performed on sheet specimens made of 7075-T6 aluminum alloy. (This alloy was selected because of its frequent usage for aerospace applications.) These tests were performed at gas pressures ranging from 760 to 5×10^{-8} torr to determine how fatigue behavior varied with decreasing gas pressure; and at stress levels ranging from 60 to 10 ksi to determine the effects of different stress levels on fatigue resistance.

In addition, selected specimens were X-rayed prior to testing to determine the residual stress state on the specimen surface and thus study the effects of these residual stresses on overall fatigue behavior.

The fracture surfaces of selected specimens were also examined using transmission and scanning electron microscopes techniques to determine whether there were different fracture modes in vacuum and in air.

The fatigue-crack-growth and fracture toughness data were analyzed using stress-intensity analysis procedures. Figge and Newman (1967) showed that by using these procedures, the data from simple sheet specimens could be used to predict fatigue-crack-growth behavior in simulated structural configurations.

An empirical equation developed by Forman, Kearney, and Engle (1967) was fitted to the data generated in this investigation by using least-squares techniques.

LITERATURE REVIEW

As explained in the Introduction section of this dissertation, a vacuum environment generally increases the fatigue resistance of pure metals.

Only the fatigue resistance of the precious metals gold and silver was unaffected by the vacuum environment. The mechanism or mechanisms responsible for this increase in fatigue resistance have not been identified as yet, but some very perceptive research aimed at identifying this mechanism(s) has been conducted. The primary objective of this literature review is to collate the findings of the various researchers, and determine the most likely mechanism(s) to explain the observed increase in fatigue resistance in vacuum. In addition, this review will consider the overall fatigue behavior which was observed in the various vacuum-fatigue experiments. Included in this overall fatigue-behavior review are: (1) the variation of fatigue life with decreasing gas pressure, (2) the microscopic and macroscopic surface morphology of the fatigue-fractured specimens, (3) the phase of fatigue affected by the environment, i.e., the fatigue-crack-initiation or fatigue-crack-propagation phases, (4) the effects of prolonged exposure to vacuum prior to testing, (5) the effects of different gas environments on fatigue behavior, and (6) the gasses given off by the specimen during fatigue cycling.

A detailed discussion of the six preceding review topics will be given in the last section of the Literature Review.

Variation of Fatigue Life With Decreasing Gas Pressure

The variation of fatigue life with gas pressure, in the range 760 to 10^{-8} torr, has not been clearly established to date. In some instances, a continuous variation between fatigue life and gas pressure was found, whereas in other instances, a stepped variation occurred.

An example of continuous variation is shown in figure 1. In this figure, the fatigue life of pure copper, pure aluminum, and an aluminum alloy has been replotted from a paper by Wadsworth (1959) as a function of gas pressure. Similar continuous variations of fatigue life with decreasing gas pressure were observed by Snowden (1961) in tests on pure aluminum, by Kramer and Podlaseck (1961) testing pure aluminum crystals, and by Christensen (1963) in tests on 2014-T6 aluminum alloy.

A number of possible mechanisms were proposed to explain how the interaction of the environment and the material could produce the observed increase in fatigue life with decreasing gas pressure. Wadsworth and Hutchings (1958) suggested that the oxygen molecules in the atmosphere combine with the freshly exposed atoms at the tip of the fatigue crack, which weakens the material and thus accelerates fatigue-crack propagation. At a lower gas pressure, there are fewer oxygen molecules available to combine with and weaken the material; consequently, the rate of fatigue-crack growth is longer.

Wadsworth and Hutchings (1958) also suggested that coldwelding could be responsible for the observed increase in fatigue life in vacuum. Materials studies by Ham (1962) have shown that two uncontaminated

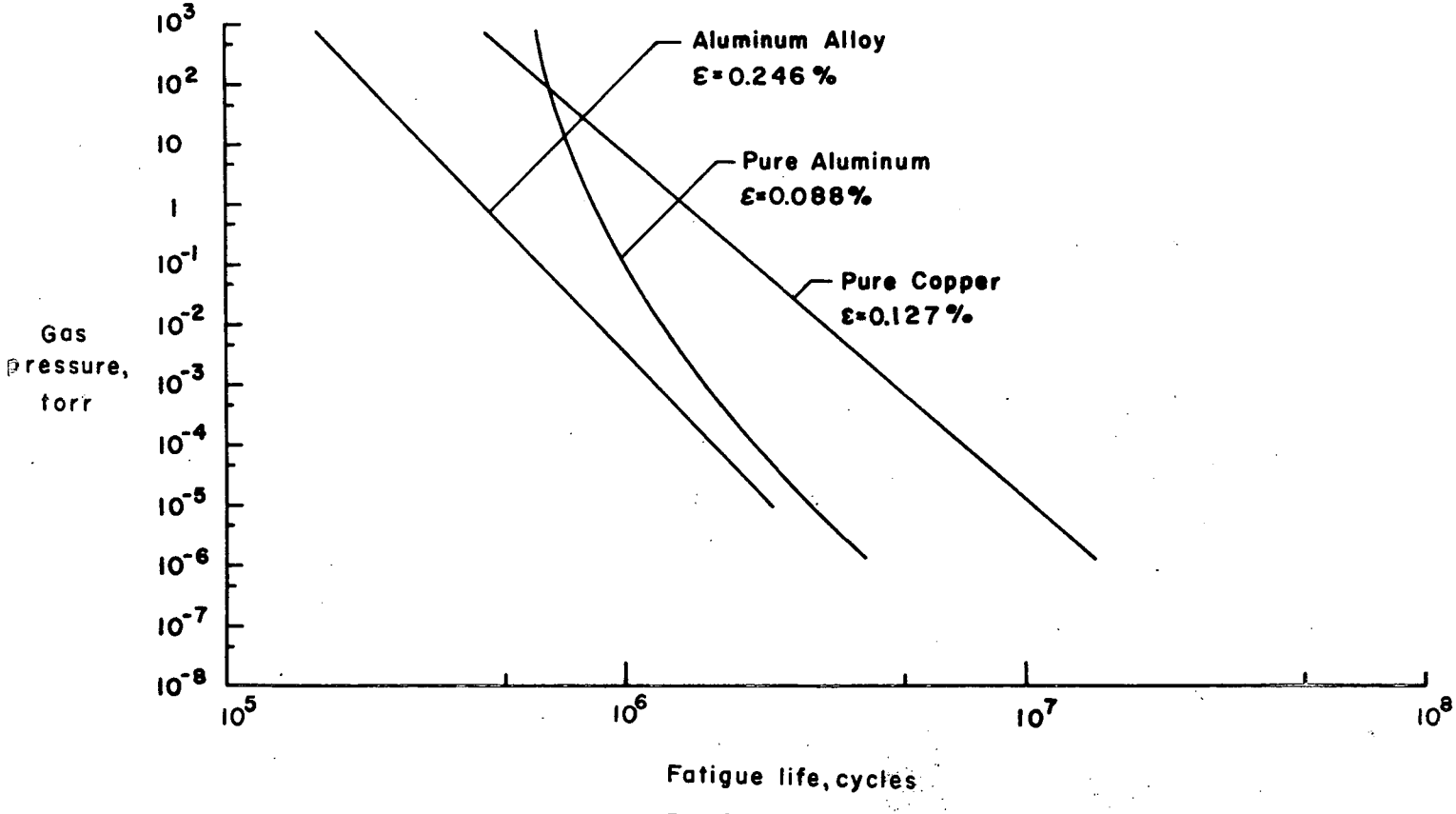

Figure 1.- Continuous variation between fatigue life and gas pressure (from Wadsworth (1959)). R = - 1.

metal surfaces, e.g., the fracture surfaces of a specimen fractured in high vacuum, when placed in contact and subjected to a moderate compressive stress will actually coldweld together. Wadsworth and Hutchings proposed that at low gas pressures, the new fatigue-crack surface that developed under the tension loading is only partially contaminated because of the limited number of contaminating molecules available. During the compression portion of the cycle, the uncontaminated portions of the surface are brought back together under pressure and coldwelding occurs. The net effect is a delay in fatigue crack-propagation and an extended life at the lower gas pressures. Ishii and Weertman (1969) also indicated they believed coldwelding of freshly cracked surfaces was a contributing factor to the increased fatigue life in vacuum.

Broom and Nicholson (1961) suggested that hydrogen was responsible for the difference in fatigue behavior in vacuum and air. They proposed that hydrogen ions are produced at clean metal surfaces when the water vapor in the air combines with the clean metal to form an oxide. Broom and Nicholson proposed three possible mechanisms by which these ions could affect overall fatigue behavior. In the first mechanism, the hydrogen ions diffuse into the metal and accumulate at voids which exist in the metal. The constant diffusion of these ions builds up internal pressure in the voids which facilitates crack initiation. In the second mechanism, the diffusion of hydrogen ions alters the surface energy of cracks and, thus, modifies the rate at which the cracks propagate. In the third suggested mechanism, the rate of diffusion of the

hydrogen ions governs the generation of voids by controlling the clustering of vacancies formed by moving dislocations.

Bradshaw and Wheeler (1965) similarly proposed that some form of hydrogen embrittlement was responsible for the increased fatigue-crack-propagation rates in air.

Grosskreutz and Bowles (1965) proposed that, in vacuum, freshly exposed slip steps are not immediately oxidized when they form (as they are in air). Consequently, reversible motion of the dislocation loops near the surface of the metal can occur when the fatigue loading reverses direction. Under such conditions, Grosskreutz and Bowles state, the rate of strain hardening would be decreased as would be the rate of slip-step formation and dislocation dipole formation. Conversely, in air, the atmosphere would oxidize the freshly exposed surfaces introducing obstacles to dislocation movement. These obstacles would cause higher rates of work-hardening, slip-step formation, and dislocation dipole formation. Grosskreutz and Bowles contended that these higher rates constituted a higher rate of fatigue-damage accumulation in air and consequently, a shorter fatigue life. Grosskreutz and Bowles presented supporting experimental data on aluminum single crystals which were obtained using replica and transmission electron microscopy. These data showed that for a given number of fatigue cycles, the specimens tested in air exhibited more numerous and more intense slip bands than specimens tested in vacuum. Also, specimens tested in air contained many dislocation dipole clusters on the primary glide planes while

specimens tested in vacuum contained dislocation dipole clusters with much less frequency.

Pelloux (1969) proposed a similar mechanism for explaining the difference in fatigue-crack propagation in vacuum and in air. In air, Pelloux suggests an oxide forms on the slip steps generated by growth of the fatigue crack and blocks reversed slip when the load direction changes from tension to compression. In vacuum, of course, no such oxide film forms and consequently, reverse slip can occur. Pelloux explains that this model accounts for the existence of fatigue striae on specimens tested in air, and the absence of such striae on vacuum-tested specimens.

Wilkov and Applewhite (1967) similarly proposed that in air an oxide film forms on the freshly exposed slip-step surfaces and inhibits dislocation movement. Wilkov and Applewhite suggest that such inhibition leads to more rapid fatigue-damage accumulation. In vacuum, they propose that no such oxide film forms, therefore dislocations can escape to the surface of the metal more easily and fatigue damage does not occur as rapidly as in air.

A typical example of the stepped variation of fatigue life with decreasing gas pressure is shown in figure 2 which is replotted from Hordon and Wright (1968). This figure shows that the fatigue life of 1100-H14 aluminum was nearly constant from 760 torr (atmospheric pressure) to approximately 10^{-1} torr, increased steadily from 10^{-1} to 10^{-4} torr, and was again nearly constant for lower pressures. Snowden (1961)

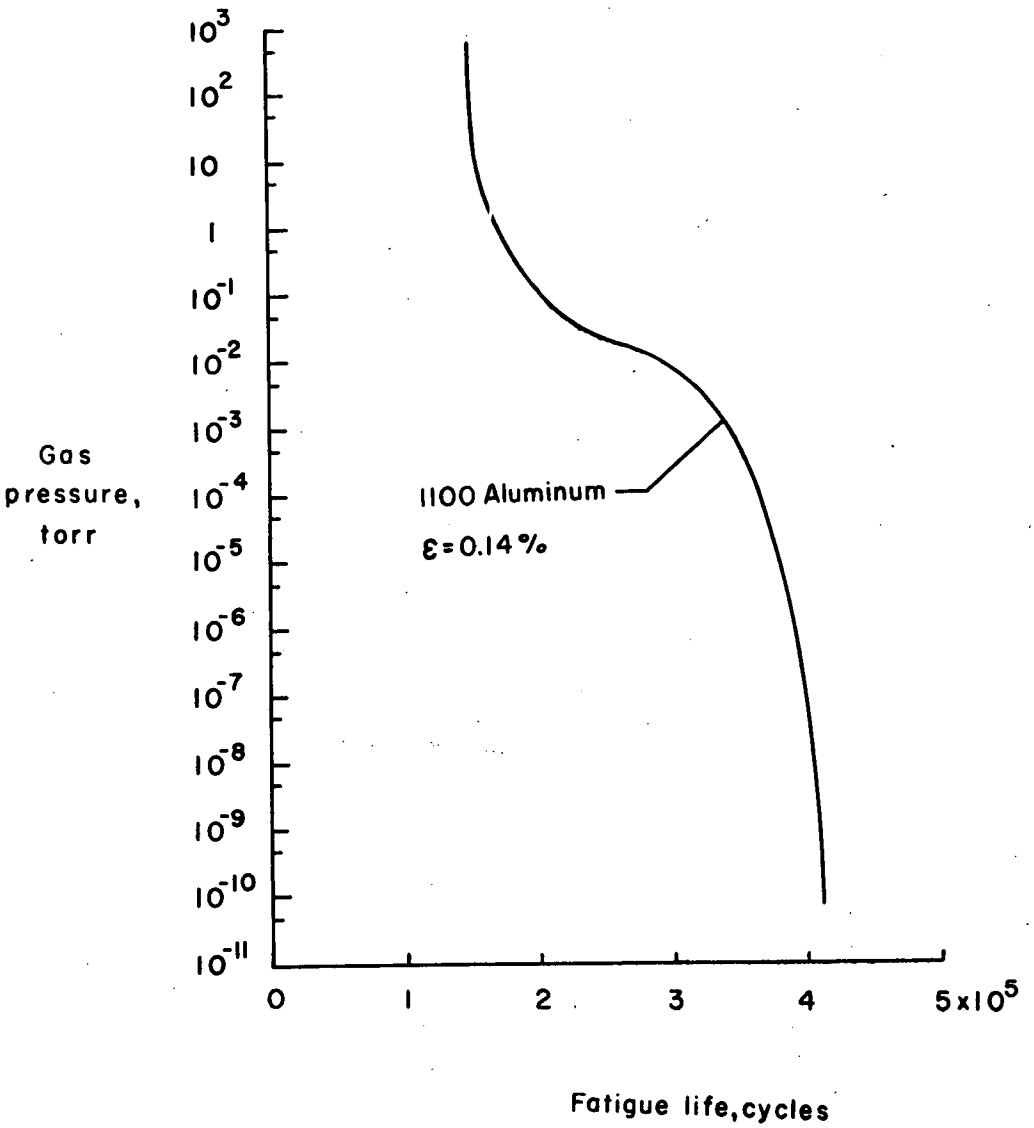

Figure 2.- Stepped variation between fatigue life and gas pressure (from Hordon and Wright (1968)). R = - 1.

in tests on pure lead, Sumsion (1968), and Nelson and Williams (1967) in tests on pure magnesium, Ham (1963) and Shen (1967) in tests on 1100-H14 aluminum, and Shen, Podlaseck and Kramer (1966) in tests on pure aluminum found similar stepped variations of fatigue life with decreasing gas pressure. In all of these investigations in which the stepped variation in fatigue life was found, the pressure range over which the fatigue life increased rapidly with decreasing gas pressure was approximately 10^{-1} to 10^{-4} torr. There were minor variations for different materials, however.

Three somewhat similar mechanisms were proposed to explain this stepped variation of fatigue life with gas pressure. Ham (1963) proposed that in the initial stage of fatigue-damage accumulation in 1100-H14 aluminum (prior to crack initiation) localized plastic deformation occurs in some surface crystals as a result of fatigue loading. It was assumed that some of this deformation occurs in the form of reversible slip, which initially exposes clean-surface material to the gas molecules of the surrounding environment. The buildup of aluminum oxide on this clean surface is time-dependent but tends towards an equilibrium thickness at a given pressure; at a higher pressure, the thickness is greater. At higher pressures, a sufficient oxide thickness forms the structure characteristic of Al_2O_3. Ham proposed that only this structure can be bound tightly enough to the base metal to be carried into the metal when reverse slip occurs. Rebonding of the surfaces is thus inhibited and a crack nucleated. If there is an insufficient thickness

of oxide to form Al_2O_3, the attached oxygen can be displaced upon reversal of slip, and the rebonding of the surfaces can be accomplished. It was proposed, therefore, that above approximately 10^{-1} torr there is always a sufficient thickness of oxide to form Al_2O_3 and, consequently, fatigue life is governed by the nucleation of oxide-caused cracks. Below 10^{-4} torr, there is an insufficient thickness of attached oxygen to form Al_2O_3, and fatigue life is assumed to be influenced by some other damage phenomenon. Between 10^{-1} and 10^{-4} torr, there is a transition range, and life varies rapidly within this range.

A mechanism similar to Ham's (1963) was suggested by Sumsion (1968) to explain the stepped variation in fatigue life with decreasing gas pressure. Sumsion hypothesized that in vacuum no reaction occurs between the new metal surface created by a fatigue crack and the environment, since there is little reactive gas present in the vacuum. The absence of a resultant surface film (since no reaction occurs) will permit the unimpeded egress of dislocations from the metal surface, easier deformation of the metal at the crack tip, and therefore, greater blunting of the crack tip. Consequently, there should be a lower rate of fatigue-crack propagation and an increase in fatigue life in vacuum. Sumsion cited the following experimental results on magnesium to support his mechanism: (1) the fracture surfaces of the specimens tested in vacuum showed more ductile fracture areas than did the air-tested specimens, and (2) fatigue life was not pressure-dependent below or above a certain critical range, i.e., above a certain pressure, a surface film forms, and below a certain pressure, no surface film forms.

Shen, Podlaseck, and Kramer (1966) have found that a so-called "debris" layer containing a high concentration of dislocations forms in the base metal near the surface of a specimen during plastic deformation. The formation rate of this "debris" layer is a function of the ease with which dislocations can escape through the specimen surface. The oxide film at the surface of the base metal retards the progress of dislocations to the surface and consequently, increases the formation rate of this layer. Shen, Podlaseck, and Kramer proposed that a "debris" layer also accumulates in the surface regions of a fatigue crack. Under fatigue loading, the accumulation process is continually repeated in the newly created surface of a propagating fatigue crack. When a metal surface is exposed to the air, the surface regions are immediately covered by an oxide film. Therefore, the dislocation-escape rate is low and the accumulation rate and concentration of dislocations in the surface region will be high. Consequently, the formation of voids and cavity dislocations due to dislocation interactions will be high. The formation of these voids and cavity dislocations are proposed to facilitate the growth of the fatigue crack. In vacuum the oxide film forms slowly on the newly created crack surface. The absence of this oxide film permits easy dislocation escape from the metal surface. Consequently, the accumulation rate of voids and cavity dislocations occurs at a lower rate, and the fatigue crack will propagate more slowly than in air. This lower crack-growth rate will lead to longer fatigue lives in vacuum.

Effect of Vacuum on Specimen Deformation

Exterior Surfaces

Study of the exterior specimen surfaces by a number of researchers revealed that specimen surfaces which were initially smooth became visibly roughened after testing in vacuum, whereas the surfaces of specimens tested in air generally remained smooth. In addition, specimens tested in vacuum generally contained a larger number of cracks than similar specimens tested in air. Figure 3 illustrates the advanced degree of surface cracking which occurs in specimens tested in vacuum.

The manner in which cracks developed in the vacuum environment was apparently different for different materials. For example, Wadsworth (1959) and Wadsworth and Hutchings (1958) found in fatigue tests on copper that fatigue cracks initiated in the same number of cycles in both air and vacuum tests. However, the rate of fatigue-crack propagation was significantly lower in vacuum than in air. This lower rate of crack propagation allowed more time for other cracks to form, and as a consequence, at the end of a test in vacuum, many more cracks were present.

On the other hand, Ham and Reichenbach (1962) in fatigue tests on 1100-H14 aluminum found that no cracks formed in his vacuum-tested specimens until the total fatigue life of his air-tested specimens was exceeded. In observing the fatigue-crack propagation which eventually occurred in vacuum-tested specimens, Ham and Reichenbach found that the fatigue cracks would initially propagate a short distance and then stop.

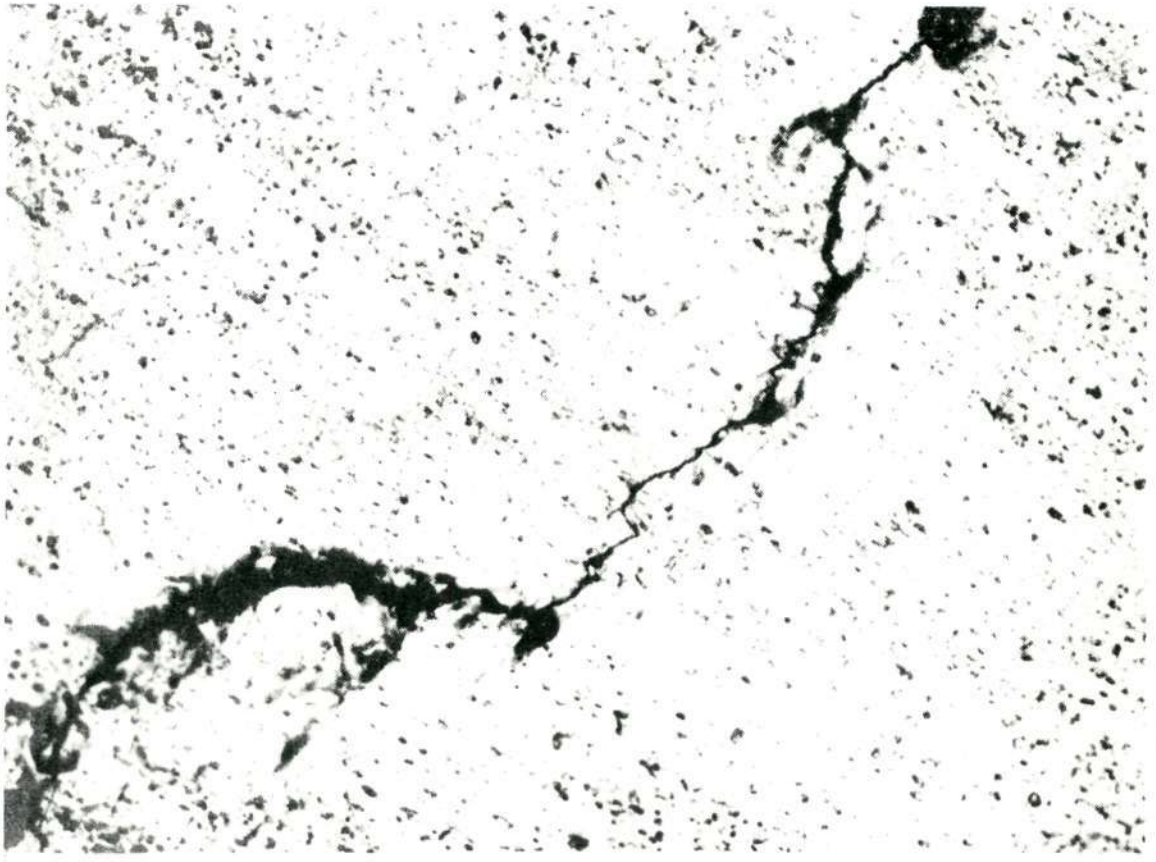

(a) Tested in air. Nominal strain = 0.087 percent. Cycles to failure, 678,000.

Figure 3.- Surfaces of fatigued aluminum specimens (from Ham 1963)).

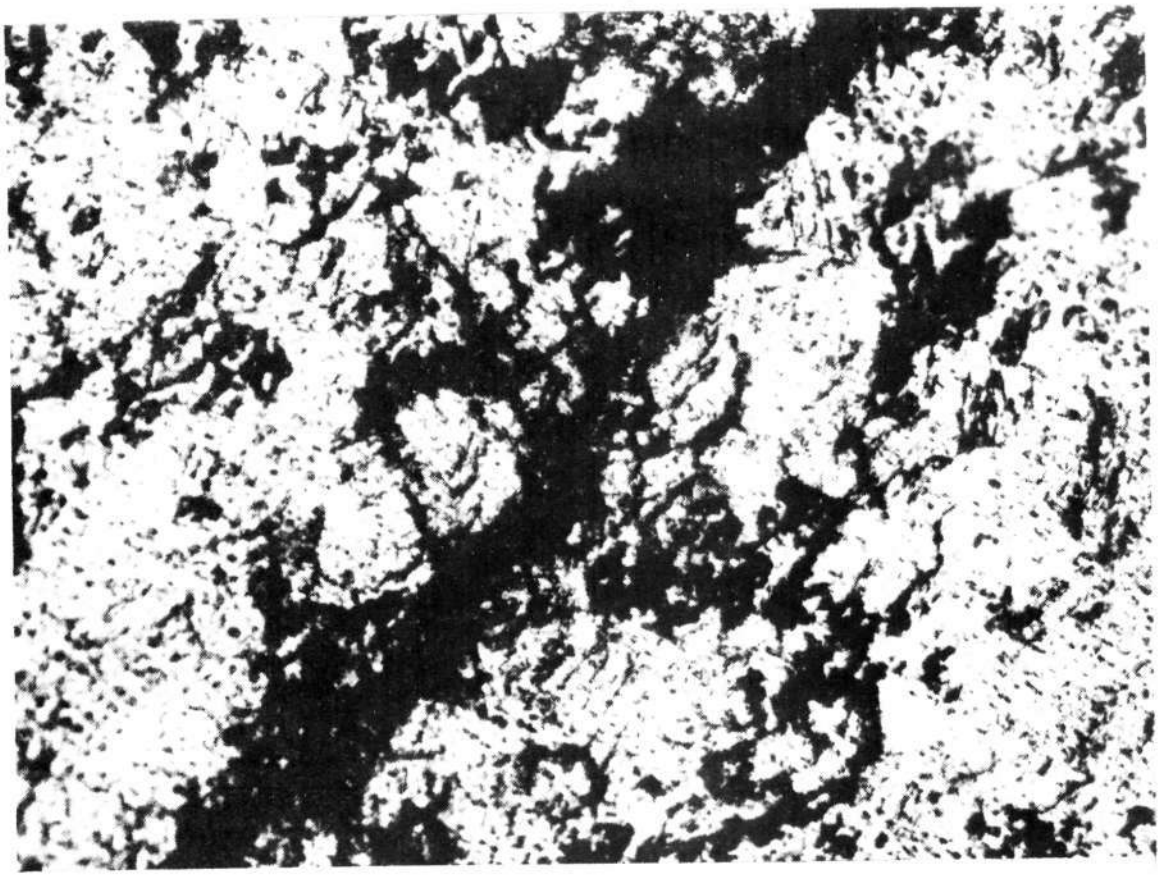

(b) Tested in vacuum. Nominal strain = 0.081 percent. Cycles to failure, 3,880,000.

Figure 3.– (continued).

A second crack would then initiate and repeat the process. Eventually, either one crack would propagate to failure, or a network of partially propagated cracks would become so extensive that the specimens became too flexible to test.

Similarly, Snowden and Greenwood (1958) in fatigue tests on pure lead found that specimens tested in air at a given stress level and for a given number of cycles contained fatigue cracks. However, identical specimens tested in vacuum at the same stress level and for the same number of cycles contained no cracks.

Thus it appears the development of fatigue cracks in vacuum and air is a function of the material being investigated.

The increased surface roughening which occurred in vacuum was usually attributed to increased slip. Here again though, the various researchers found that surface slip developed in different manners. Snowden and Greenwood (1958), in tests on pure lead, examined the surface deformation of specimens tested in air and in vacuum after a given number of loading cycles had been applied. Their examination showed that the surface deformation was greater in vacuum than in air.

Similarly, Wilkov and Applewhite (1967) in tests on pure aluminum, found that for a given number of cycles, slip lines formed faster in vacuum than in air. Surface intrusions were also observed to form in both air- and vacuum-tested specimens. The intrusions which developed in vacuum-tested specimens were longer than those which developed in air-tested ones, and the rate at which these intrusions formed was higher in vacuum-tested specimens. Formation of these intrusions is usually

associated with the escape of dislocations from the body of the metal grains. Consequently, the greater rate of intrusion formation in vacuum is indicative of higher dislocation mobility in vacuum.

Wadsworth (1959) and Wadsworth and Hutchings (1958), in tests on copper, found that slip bands developed at approximately the same rate in vacuum and air. However, the vacuum-tested specimens had longer fatigue lives than the air-tested specimens. Therefore the vacuum-tested specimens experienced more fatigue cycles, and consequently more slip roughening prior to final failure.

Grosskruetz (1967), on the other hand, investigated the very early stages of fatigue-damage accumulation, (i.e., the first 300 cycles), in single crystals of pure aluminum and found that the entire surfaces of the air-tested crystals were covered with entire slip lines. However, slip was not as widespread on the specimens subjected to 300 loading cycles in vacuum. Grosskruetz's tests were not run for prolonged periods in either vacuum or air, however; therefore the total slip accumulation at failure for the two environments was not known.

Fracture Surfaces

The fracture surfaces of specimens fatigued in vacuum and in air were observed by several investigators using electron microscopic techniques. Generally, the fracture surfaces of the vacuum-tested specimens had a more ductile appearance. In addition, no fatigue striae were usually observed on the fracture surfaces of the vacuum-tested specimens, whereas such striae were usually found on the fracture surfaces of air-tested specimens.

Sumsion (1968) found, in tests on pure magnesium, and on magnesium-lithium and magnesium-thorium alloys, a marked difference in the appearance of the fracture surfaces of air-tested and vacuum-tested specimens. In the air-tested specimens, many flat, platelet-like areas were present, and the fracture surfaces appeared to resemble brittle crystallographic cleavage. In vacuum, the brittle character of the fracture surface was less apparent, evidence of plastic deformation was more pronounced, and many short cracks were apparent.

Meyn (1968) similarly found, in tests on 2024-T3 aluminum alloy, that the fracture surfaces of specimens fatigued in air were smooth and flat with numerous characteristic features. Some of these features appeared to be small scattered cleavage facets. Meyn indicated similarity to cleavage was rather complete on these facets, i.e., these facets contained forked cleavage and a high specular reflectivity. The overall appearance of the air-tested specimens was a mosaic of bright and dull patches with bright areas predominating. These bright areas contained the cleavage facets with superimposed fatigue striae.

Examination of the fracture surfaces of the specimens which were fatigued in vacuum indicated these surfaces were quite rough and ragged, indicative of a more ductile fracture mode. Like Sumsion (1968), Meyn found numerous irregular secondary cracks on the surfaces of the vacuum-tested specimens.

Meyn also found there were generally no fatigue striae on the fracture surfaces of the vacuum-tested specimens. A similar absence of fatigue striae on the fracture surfaces of vacuum-tested specimens was reported by Pelloux (1969) in tests on 2024-T3 aluminum alloy.

Subsurface Dislocation Behavior

Several investigators have studied the arrangement of dislocations in the base metal near the oxide-base metal interface using transmission electron fractography. Both studies indicated that the dislocation arrangement immediately below the interface contained dislocation dipoles and tangled and jogged dislocations. Differences were noted in the arrangement of dislocations in vacuum- and air-tested specimens, however.

Wilkov and Applewhite (1967) found, in experiments on pure aluminum, that for air-tested specimens, there were numerous dislocations in the immediate vicinity of the surface-slip steps. For vacuum-tested specimens, there were considerably fewer dislocations in the immediate vicinity of the slip lines.

Grosskruetz (1967) similarly found, in air tests on single crystals of aluminum, that dense clusters of dislocation dipoles formed in the base metal in the vicinity of well-developed slip bands. In vacuum tests, the dislocations were evenly spaced, and heavy patches of dislocation dipoles were rarely found.

The Phase of the Fatigue Phenomenon Affected by Vacuum Environment

The fatigue phenomenon can be divided into three sequential phases, each of which has a significant effect on the overall fatigue behavior of a material. These three phases include (a) fatigue-crack initiation, (b) fatigue-crack propagation, and (c) residual static strength. The fatigue-crack-initiation phase begins with the application of the first

load cycle and is generally thought to continue until a macroscopic crack develops in the test specimen. The fatigue-crack-propagation phase begins with the development of this macroscopic crack and ends immediately before the application of the final load cycle (i.e., the one causing failure) in the fatigue test. The residual static-strength phase includes only the loading cycle which causes final failure of the test specimen.

The effects of vacuum environment on the fatigue-crack-initiation and fatigue-crack-propagation phases have been studied by a number of investigators. The effects of vacuum environment on the residual static-strength phase has generally been overlooked and this phase will be studied in the investigation reported in this dissertation.

Fatigue-crack-propagation studies were conducted in at least eleven investigations. It was found in all eleven investigations that fatigue-crack growth was generally slower in vacuum than in air. In three of these investigations, however, the rate of fatigue-crack propagation in air approached the rate of fatigue-crack propagation in vacuum at high crack-propagation rates, i.e., very near the end of the tests. In the remaining eight investigations, the fatigue-crack-propagation rates which occurred during the vacuum and air tests were not compared.

Fatigue-crack-initiation studies were conducted in at least five investigations. In two of these investigations, fatigue cracks initiated in the same number of cycles in both vacuum and air. In the remaining three investigations, fatigue cracks initiated more rapidly in air than in vacuum.

Table 1. Summary of findings on the phase of fatigue affected by a vacuum environment.

Investigator(s)	Year	Materials Tested	Nominal Minimum Gas Pressure, torr	Fatigue-Crack Initiation	Fatigue-Crack Propagation
Ishii and Weertman	1969	1100-H14 aluminum	1×10^{-4}	Not considered	Fatigue cracks propagated about fifteen times faster in vacuum than in laboratory air.
Hordon and Wright	1968	1100-H14 aluminum	8×10^{-7}	Not considered	Fatigue cracks propagated six times faster in vacuum than in laboratory air.
Nelson and Williams	1967	Pure magnesium	1×10^{-8}	Not considered	Fatigue-crack-propagation stage was influenced by vacuum environment, i.e. cracks propagated more slowly in vacuum than in laboratory air.
Wright and Argon	1970	Fe - 3-1/2 percent Si iron	0.05	Not considered	Fatigue-crack-propagation rates were twice as high in laboratory air as in vacuum. Tests in both air and vacuum were conducted at 200°C.
Grosskreutz	1960	Pure aluminum	1×10^{-5}	Fatigue-crack initiation in vacuum not considered	Fatigue-crack-propagation rates were considerably lower in vacuum than in air.

Table 1 (continued).

Investigator(s)	Year	Materials Tested	Nominal Minimum Gas Pressure, torr	Fatigue-Crack Initiation	Fatigue-Crack Propagation
Meyn	1968	2024-T3 aluminum alloy	2×10^{-6}	Not considered	At low crack-propagation rates, fatigue cracks propagated about three times faster in air than in vacuum. At high crack-propagation rates, fatigue cracks propagated at about the same rates in vacuum and laboratory air.
Mabberley	1966	Overaged Al-7 percent Zn-5 percent Mg-1 percent Mn aluminum alloy	1×10^{-8}	Not considered	At low crack-propagation rates, fatigue cracks propagated about twice as fast in laboratory air as in vacuum. At high crack-propagation rates, fatigue cracks propagated at about the same rates in laboratory as in vacuum.
		Peak aged Al-7 percent Zn-5 percent Mg-1 percent Mn aluminum alloy	1×10^{-8}	Not considered	At low crack-propagation rates, fatigue cracks propagated 250 times faster in laboratory air than in vacuum. At high crack-propagation rates, fatigue cracks propagated at about the same rates in vacuum as in laboratory air.

Table 1 (continued).

Investigator(s)	Year	Materials Tested	Nominal Minimum Gas Pressure, torr	Fatigue-Crack Initiation	Fatigue-Crack Propagation
Bradshaw and Wheeler	1965	DTD 5070A aluminum alloy	3×10^{-8}	Analysis of data indicated crack initiation was relatively insensitive to environment	At low crack-propagation rates, fatigue cracks propagated about six times faster in laboratory air than in vacuum. At high crack-propagation rates, fatigue cracks propagated at about the same rates in vacuum and laboratory air.
		Al-2.2 percent Cu-1.6 percent Mg aluminum alloy	4×10^{-8}	Analysis of data indicated crack initiation was relatively insensitive to environment	At low crack-propagation rates, fatigue cracks propagated about five times faster in laboratory air than in vacuum At high crack-propagation rates, fatigue cracks propagated at about the same rates in vacuum and laboratory air.
Wadsworth	1959	OFHC copper	3×10^{-6}	Fatigue cracks in vacuum and laboratory air tests formed in the same number of cycles	Fatigue cracks propagated faster in laboratory air than in vacuum.
		Pure aluminum	3×10^{-6}	Fatigue cracks in vacuum and laboratory air tests formed in the same number of cycles	Fatigue cracks propagated faster in laboratory air than in vacuum.

Table 1 (continued).

Investigator(s)	Year	Materials Tested	Nominal Minimum Gas Pressure, torr	Fatigue-Crack Initiation	Fatigue-Crack Propagation
Broom and Nicholson	1961	Al-4 percent Cu aluminum alloy	2×10^{-6}	The absence of a deleterious environment slowed crack initiation.	Fatigue cracks propagated faster in laboratory air than in vacuum.
Ham and Reichenbach	1962	1100-H14 aluminum	7×10^{-7}	A fatigue specimen tested in vacuum developed no cracks after being cycled a sufficient number of times to cause failure in an air-tested specimen. Therefore, the vacuum environment delayed crack initiation.	In air, a single fatigue crack initiated and propagated to failure. In vacuum, a crack would start, propagate awhile, and stop. Another crack would then start and the process repeated. Eventually, one crack grew to failure, or the specimen developed a network of cracks and became too flexible to test.
Snowden and Greenwood	1958	Pure lead	5×10^{-3}	Air-tested specimens developed fatigue cracks well before complete fracture of the specimen. Vacuum-tested specimens showed no evidence of fatigue cracking after the same number of cycles.	Not considered

A summary of the findings in these investigations is given in Table 1.

Effect of Prolonged Exposure to Vacuum on Fatigue Life

In one of the earlier vacuum-fatigue investigations, Christensen (1963) reported that the fatigue lives of aluminum-alloy specimens increased by a factor of about two after short-time exposure to vacuum environment. Christensen also found, however, that the longer the vacuum-exposure time prior to testing (up to 161 hours), the smaller the increase in fatigue life in vacuum. Christensen suggested that if the specimens were subjected to the vacuum environment for a sufficiently long time, the vacuum-fatigue life would approach the fatigue life in air.

Christensen's findings prompted several other investigations into the effects of long-time exposure to vacuum prior to testing. Sumsion (1968), Meyn (1968), and Bradshaw and Wheeler (1965) found in experiments on aluminum and magnesium alloys that prolonged exposure to vacuum prior to testing (up to 282 hours) had no detrimental effects on vacuum-fatigue behavior. Further, Hoeppner and Hyler (1966) found the fatigue lives of two aluminum alloys actually increased with increasing vacuum-exposure time (up to 160 hours).

Effect of Composition of Environment on Fatigue

One of the greatest contributions of research in vacuum-fatigue may be the identification of constituents in the atmosphere which have a detrimental effect on fatigue life. Experimental evidence already

indicates that it is the absence of deleterious constituents rather than low gas pressure which is responsible for the increased fatigue life found in vacuum. A number of fatigue investigations have been conducted in different gas environments, and the results indicate strongly that water vapor significantly reduces the fatigue resistance of a wide range of materials. In contrast, the fatigue resistance of these materials is considerably higher in pure oxygen, hydrogen, nitrogen, and argon than in laboratory air (which, of course, contains water vapor). The effects of various constituents on fatigue life and fatigue-crack propagation are summarized in Table 2.

Gas Evolution During the Fatigue Process

In one of the earlier investigations into the effects of environment on the fatigue phenomenon, Bennett, Holshouser, and Utech (1961) coated their aluminum-alloy specimens with transparent pressure-sensitive tape to protect the specimens from the atmosphere. Bennett et al. found in this investigation that the fatigue lives of the taped specimens were significantly longer than the lives of the untaped specimens. They also found that gas bubbles formed under the tape during the latter portions of their fatigue tests.

In a subsequent report, Bennett (1964) stated that mass spectrometric analysis of the gas under the tape indicated that the gas was hydrogen. Bennett also reported that metallographic examination of the test specimens during testing indicated that bubble development and fatigue-crack development began at approximately the same time. The development of these bubbles was also found to be a function of the

Table 2. Summary of effects of composition of environment on fatigue.

(a) Constituent - Water Vapor

Investigator(s)	Year	Materials Tested	Baseline Environment	Relative Humidity, % Moist	Relative Humidity, % Dry	Findings
1. Fatigue Life Investigations						
Ham and Reichenbach	1962	1100-H14	air	not given	not given	Fatigue lives were approximately three times longer in dry air than in moist air.
Shives and Bennett	1968	composition 22 brass	air	85	3	Fatigue strength was three percent lower in moist air than in dry air.
		AZ61A magnesium alloy	air	85	3	Fatigue lives were approximately three times longer in dry air than in moist air.
		Ti-4Al-4Mn titanium alloy	air	85	3	Fatigue lives were approximately three times longer in dry air than in moist air.
		4340 steel	air	85	3	Fatigue limit was two percent lower in moist air than in dry air.
Bennett	1964	6061-T6 aluminum alloy	air	90	5	Fatigue lives were three times longer in dry air than in moist air.
Wadsworth	1959	copper	air	not given	not given	Fatigue lives were not affected by moisture.
Gough and Sopwith	1946	copper	air	not given	not given	Fatigue lives were not affected by moisture.

Table 2 (continued).

(a) Constituent - Water Vapor

Investigator(s)	Year	Materials Tested	Baseline Environment	Relative Humdiity, % Moist	Dry	Findings
2. Fatigue-Crack-Propagation Investigations						
Hartman et al.	1967	7075-T6 aluminum alloy	air	100	0.05	Fatigue cracks propagated approximately eight times faster in moist air than in dry air.
		2024-T3	air	100	0.05	Fatigue cracks propagated approximately eight times faster in moist air than in dry air.
Spitzig and Wei	1967	0.45C-Ni-Cr-Mo steel	Argon	100		Fatigue-crack-propagation rates in moist Argon were nearly twice as high as the rates in dry Argon.
Shives and Bennett	1968	AZ61A magnesium alloy	air	85	3	Fatigue cracks propagated approximately three times faster in moist air than in dry air.
Feeney, McMillan, and Wei	1969	2024-T3 aluminum alloy	air	90	10	Fatigue cracks propagated about ten percent faster in moist air than in dry air.

Table 2 (continued).

(a) Constituent - Water Vapor

Investigator(s)	Year	Materials Tested	Baseline Environment	Relative Humidity, % Moist	Relative Humidity, % Dry	Findings
2. Fatigue-Crack-Propagation Investigations - continued						
Feeney, McMillan, and Wei	1969	7075-T6	air	90	10	Fatigue cracks propagated about ten percent faster in moist air than in dry air.
		7178-T6	air	90	10	Fatigue cracks propagated approximately ten percent faster in moist air than in dry air.
Bradshaw and Wheeler	1965	DTD 5070A aluminum alloy	air	not given	not given	Fatigue cracks propagated approximately three times faster in moist air than in dry air.
Hartman et al.	1967	2024-T3	air	100 to 25		Fatigue-crack-propagation rates did not vary with relative humidity over the range 100 to 25 percent.
		7075-T6	air	100 to 25		Fatigue-crack-propagation rates did not vary with relative humidity over the range 100 to 25 percent.

Table 2 (continued).

(b) Constituent - Oxygen

Investigator(s)	Year	Material(s) Tested	Environments	Findings
		1. Fatigue Life Investigations		
Broom and Nicholson	1961	Al-4 percent Cu aluminum alloy	pure oxygen and laboratory air	Fatigue lives were approximately eight times longer in pure oxygen than in laboratory air.
		B.S. L65 aluminum alloy	pure oxygen and laboratory air	Fatigue lives were approximately four times longer in pure oxygen than in laboratory air.
		D.T.D. 683 aluminum alloy	pure oxygen and laboratory air	Fatigue lives were approximately twice as long in pure oxygen as in laboratory air.
Nelson and Williams	1967	pure magnesium	pure oxygen and laboratory air	Fatigue lives were approximately eight times longer in pure oxygen than in laboratory air.
Achter, Danek, and Smith	1963	nickel	pure oxygen, nitrogen, and Argon	Fatigue lives were about the same in oxygen as in the inert gasses nitrogen and Argon.

Table 2 (continued).

(b) Constituent - Oxygen

Investigator(s)	Year	Material(s) Tested	Environments	Findings
		2. Fatigue-Crack-Propagation Investigations		
Bradshaw and Wheeler	1965	D.T.D. 5070A aluminum alloy	pure oxygen and laboratory air	Fatigue cracks propagated about three times faster in laboratory air than in pure oxygen.
Mabberley	1966	Overaged Al-7 percent Zn-5 percent Mg-1 percent Mn aluminum alloy	pure oxygen and laboratory air	Fatigue cracks propagated about two times faster in laboratory air than in pure oxygen.
		Peak aged Al-7 percent Zn-5 percent Mg-1 percent Mn aluminum alloy	pure oxygen and laboratory air	Fatigue cracks propagated about eight times faster in laboratory air than in pure oxygen.

Table 2 (continued).

(c) Constituent - Nitrogen

Investigator(s)	Year	Material(s) Tested	Environments	Findings
Thompson, Wadsworth, and Louat	1956	pure copper	pure nitrogen and laboratory air	Fatigue lives were five to six times longer in nitrogen than in laboratory air.
Wadsworth	1959	OFH copper	pure nitrogen and laboratory air	Fatigue lives were about ten times longer in nitrogen than in laboratory air.
Broom and Nicholson	1961	Al-4 percent Cu aluminum alloy	pure nitrogen and laboratory air	Fatigue lives were approximately six times longer in nitrogen than in laboratory air.
		B.S. L65 aluminum alloy	pure nitrogen and laboratory air	Fatigue lives were approximately ten times longer in nitrogen than in laboratory air.
		D.T.D. 683 aluminum alloy	pure nitrogen and laboratory air	Fatigue lives were approximately seven times longer in nitrogen than in laboratory air.
Nelson and Williams	1967	pure magnesium	pure nitrogen and laboratory air	Fatigue lives were about eight times longer in nitrogen than in laboratory air.

Table 2 (continued).

(d) Constituent - Hydrogen

Investigator(s)	Year	Material(s) Tested	Environments	Findings
Broom and Nicholson	1961	Al-4 percent Cu aluminum alloy	pure hydrogen and laboratory air	Fatigue lives were about three times longer in hydrogen than in laboratory air.
		B.S. L65 aluminum alloy	pure hydrogen and laboratory air	Fatigue lives were about three times longer in hydrogen than in laboratory air.
		D.T.D. 683 aluminum alloy	pure hydrogen and laboratory air	Fatigue lives were about the same in hydrogen and laboratory air.
Bradshaw and Wheeler	1965	D.T.D. 5070A aluminum alloy	pure hydrogen and laboratory air	Fatigue cracks propagated about five times faster in laboratory air than in hydrogen.

Table 2 (continued)

(e) Constituent - Argon

Investigator(s)	Year	Material(s) Tested	Environments	Findings
Wadsworth	1959	OFHC copper	pure Argon and laboratory air	Fatigue lives were approximately eight times longer in Argon than in laboratory air.
Nelson and Williams	1967	pure magnesium	pure Argon and laboratory air	Fatigue lives were approximately eight times longer in Argon than in laboratory air.

environment in which the fatigue tests were conducted. No bubbles formed during tests in dry air, whereas the bubbles did form in tests in moist laboratory air. Bennett concluded therefore that the hydrogen-gas evolution resulted from a reaction between the moisture in the air and the metal.

Discussion

The most universal conclusion to be drawn from this Literature Review is that the fatigue resistance of a wide variety of materials is significantly higher in vacuum than in air. It further appears that it is the exclusion of atmospheric water vapor from the environment surrounding the test specimen which is responsible for this increased fatigue life in vacuum. The mechanisms proposed by various investigators to explain this increased fatigue life can be classified into three general categories: (1) coldwelding, (2) oxide-layer formation, and (3) hydrogen embrittlement. No definite conclusions can be drawn as to whether any or all of these three types of mechanisms contribute to the increased fatigue life in vacuum. However, some comparisons between the proposed mechanisms and the experimental results are warranted.

The conditions necessary for coldwelding are certainly satisfied in a vacuum-fatigue test. In such a test, a fatigue crack develops creating two uncontaminated metal surfaces which are brought back into contact during the unloading portion of the loading cycle. Elber (1970) has shown that regardless of the stress ratio, R, used in the test, these freshly created crack surfaces will be brought back into contact on

unloading. (The stress ratio R is the ratio of the minimum applied stress to the maximum applied stress.) And indeed, coldwelding may contribute to some extent in increasing fatigue life in vacuum. However, there is evidence that increased fatigue life in vacuum can occur in materials which will not coldweld. For example, Martin (1965) found the fatigue lives of 1018 and 1113 carbon steels about a factor of two higher in vacuum than in air. Both of these steels showed very low reweldment ability in coldwelding tests in vacuum, however.

Another indication that coldwelding is not the only mechanism responsible for increased fatigue life in vacuum may be drawn from the oxygen-fatigue-test results. Fatigue lives in dry oxygen were considerably longer than fatigue lives in laboratory air. (In some instances, fatigue lives in dry oxygen were as long as fatigue lives in vacuum.) Yet coldwelding could occur in neither dry oxygen nor laboratory air, since freshly exposed metal surfaces would be readily oxidized in both environments. Obviously, some mechanism other than coldwelding must be responsible for the longer fatigue lives in dry oxygen.

The oxide-formation mechanisms proposed by a number of different investigators may also be questioned in light of the finding that the fatigue lives of some materials is considerably longer in dry oxygen than in laboratory air. Since the oxide layers form as readily in dry oxygen as in laboratory air, there should be no difference in these fatigue lives if oxide-layer formation significantly affected fatigue behavior. Again, there must be some additional mechanism active which increases fatigue lives in dry oxygen.

The increased ductility in vacuum environment suggested in a number of these oxide-formation mechanisms is substantiated by experimental results, however, and will be discussed subsequently.

The hydrogen-embrittlement mechanism suggested by several investigators could quite possibly be responsible for the increased fatigue life in vacuum. Water vapor obviously is the primary constituent responsible for decreased fatigue life in air. When this water vapor combines with a freshly formed surface to form a metal oxide, a hydrogen ion is given off. Bennett's (1964) determination that hydrogen gas is given off during fatigue testing supports this reaction. This ion may then drift off in the surrounding air to combine with another hydrogen ion to form a hydrogen molecule, or may penetrate into the specimen where it may embrittle the metal or otherwise decrease the fatigue resistance of the specimen (as suggested by Broom and Nicholson). No explanation has ever been offered as to why the hydrogen ions would preferentially enter the specimen, however.

Although the entire mechanism responsible for increased fatigue life in vacuum is not known, there is experimental evidence indicating that dislocation movement occurs more freely in the vacuum environment. For example, slip-step development appears to be accelerated in vacuum as evidenced by the increased surface roughening. Further, the fatigue-fractured surfaces of vacuum-tested specimens show evidence of more ductile failure than do the fracture surfaces of air-tested specimens. Finally, there are fewer dislocation pileups near the surfaces of

vacuum-tested specimens indicating easier dislocation egress through the specimen surface. These three findings are evidence of greater dislocation mobility and consequently, greater ductility is most probably responsible for the greater fatigue life in vacuum.

Fatigue-crack propagation appears to be slower in vacuum than in air for all of the materials covered in this review. Contradictory findings on the effect of vacuum on the fatigue-crack-initiation phase may be attributable to differences in the materials tested and/or difficulties in determining exactly when a fatigue crack has initiated.

The preponderance of evidence indicates that prolonged exposure to vacuum prior to testing causes no decrease in vacuum-fatigue resistance. Perhaps, as suggested in Meyn's paper (1968), backstreaming oil vapors from the diffusion pump collected on Christensen's specimens and had a detrimental effect. Christensen's vacuum system contained no cold trap to keep backstreaming oil vapors from reaching the inside of the test chamber.

MATERIALS

The material used in this investigation was taken from a special stock of 7075-T6 aluminum alloy retained at Langley Research Center for fatigue testing. This material has a nominal thickness of 0.090-inch. The fatigue properties of this material are described in a report by Grover, Bishop, and Jackson (1951). The chemical properties of this material, which were determined by the material producer, are shown in Table 3. The nominal tensile properties of this 7075-T6 were obtained using standard American Society for Testing and Materials (ASTM) tensile specimens and are listed in Table 4. This material was fabricated and heat-treated according to normal commercial practices and under close metallurgical supervision to maintain uniformity. The sheets from which the test specimens were made were from two consecutive mill heats.

Table 3. Nominal chemical composition of the 7075-T6 aluminum alloy tested.

Element	Si	Fe	Cu	Mn	Mg	Cr	Ni	Zn	Pb	Sn	Ti	Al
Percent	0.07	0.22	1.58	0.16	2.56	0.24	0	5.68	0	0	0.07	Remainder

Table 4. Average tensile properties of the 7075-T6 aluminum alloy tested.

Ultimate tensile strength, ksi	Yield strength, ksi (0.2-percent offset)	Young's modulus of elasticity, ksi	Elongation in 2-inch gage length, percent	No. tests
83.2	75.9	10,100	12	20

SPECIMENS

Fatigue Life

The fatigue-life specimens had the configuration shown in figure 4. These specimens were fabricated by first shearing oversized specimen blanks from the base-sheet material which was 35 inches long and 12 inches wide. These specimen blanks were approximately 0.1 inch larger than the finished dimensions of the specimens. The specimen blanks were marked for identification and these markings are used to identify the test specimens in the tables of results.

All specimen blanks were initially machined along the straight edges. Machining speeds were selected to produce a clean-cut surface with a minimum amount of burrs. Throughout the machining process, efforts were made to keep the flat sections of the specimen surface unmarred.

The specimen blanks were stacked approximately eight at a time and mounted in the headstock of a lathe. The 7.5-inch radius was cut at approximately 20 rpm. The final cut in the radius was 0.001 inch deep. The finish on the machined radius was 64 rms. The specimens were then hand-polished on all sides, machined and flat, first with number 600 silicon-carbide polishing paper, then with number 600 aluminum-oxide polishing powder, and finally with 5 micron-aluminum-oxide polishing powder to remove all burrs, scratches, and tool marks. All polishing was done in the longitudinal direction on the specimen in order to insure that no transverse polishing marks would be left on the

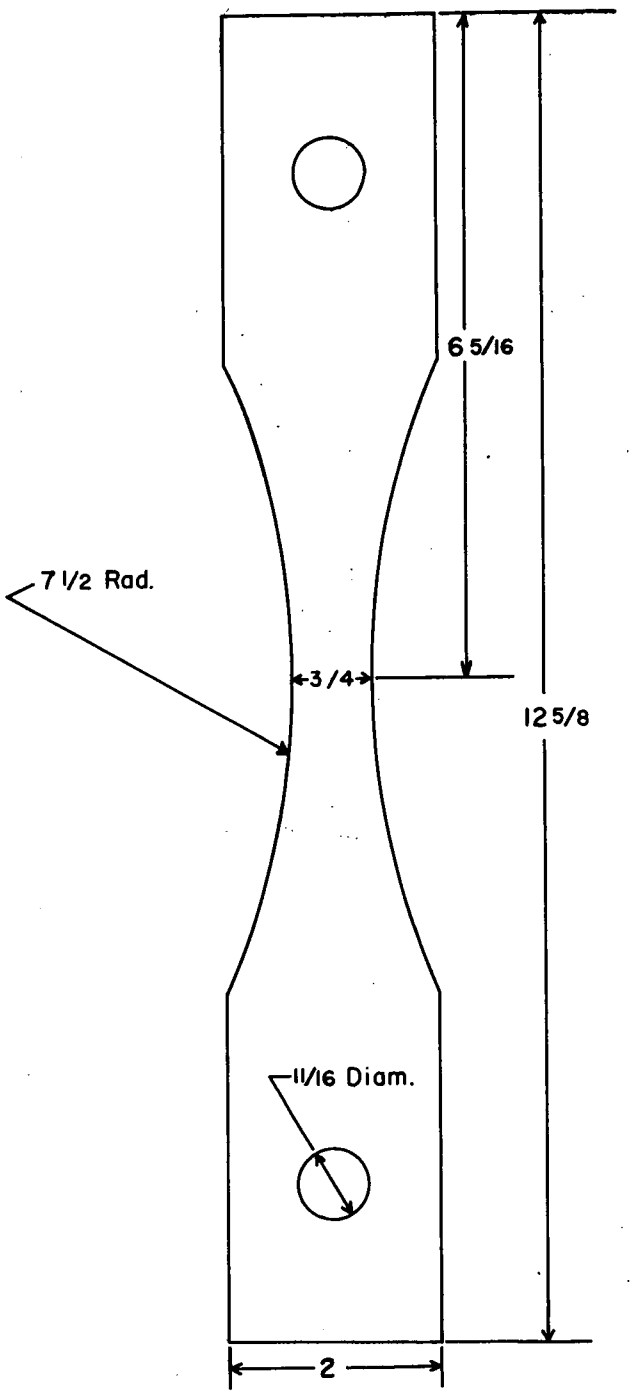

Figure 4.- Configuration of fatigue-life specimens. All dimensions are in inches.

specimen. Such marks could act as microscopic stress concentrations and reduce the overall fatigue resistance of the specimens. After polishing, the average surface roughness on the test specimens was 16 rms. An average of two hours was required to polish each specimen. Following polishing, the residual stresses in the surfaces of selected specimens were measured using X-ray diffraction techniques. A discussion of these techniques is given in Appendix A. The test specimens were then ready for fatigue testing.

All fatigue-life specimens were made with the longitudinal axis of the specimen parallel to the rolling direction of the sheet.

Fatigue-Crack Propagation and Fracture Toughness

The fatigue-crack-propagation and fracture-toughness specimens had the configuration shown in figure 5. These specimens were sheared directly to size from the 12-inch by 35-inch basic sheets of material. No machining was done on the sheared edges of the specimens. A 0.1-inch notch was cut into the center of each specimen using electrical-discharge machining. The width of the central notch was 0.010 inch. Very localized heating occurs in making notches in this manner. Thus, virtually all of the material through which the fatigue crack propagates is unaltered by the cutting process. This 0.1-inch notch serves as a stress concentration at which fatigue cracks initiate readily.

All fatigue-crack-propagation and fracture-toughness specimens were made with the longitudinal axis of the specimen parallel to the rolling direction of the sheet.

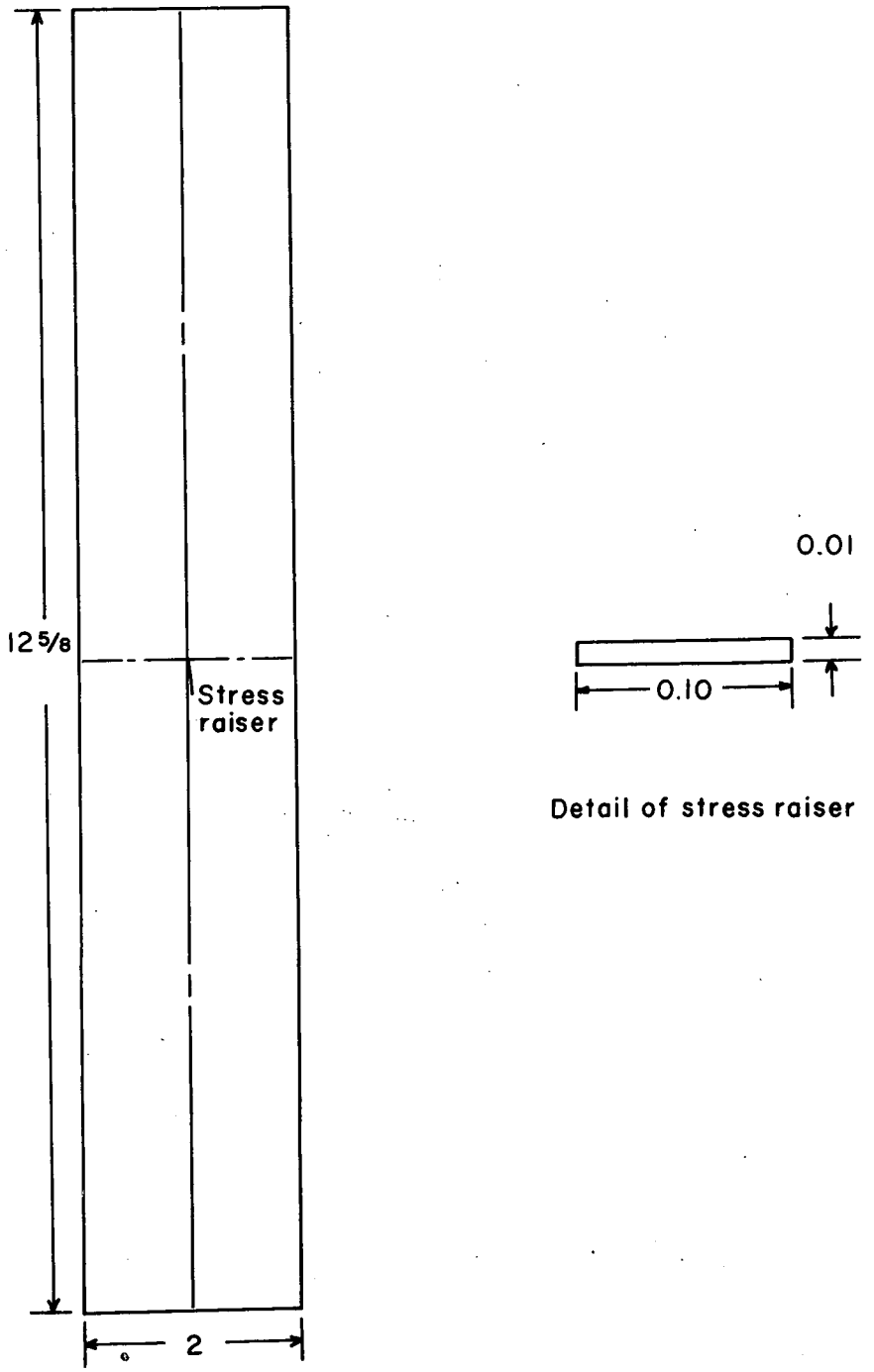

Figure 5.- Configuration of fatigue-crack propagation and fracture-toughness specimens. All dimensions are in inches.

A reference grid was photographically printed on the surface of each specimen to mark intervals in the path of the crack. This reference grid afforded ready observation of the crack front and provided a crack-propagation path free of mechanical defects which might affect normal crack propagation. Before adopting the photographic reference grid, it was determined by metallographic examinations and tensile tests on specimens bearing the grid that the grid had no detrimental effects on the material. The procedure used in applying the reference grids is shown in Table 5.

Table 5. Materials and procedures for applying the reference grid to fatigue-crack-propagation and fracture-toughness specimens.

1. The photographic materials used are described in the anonymously written report, Kodak Industrial Data Book P-7 (1962).

2. The emulsion is spread over the area to which the grid is to be applied, and allowed to cure in air for 16-20 hours.

3. The area containing the emulsion is covered with a negative containing the desired grid. This negative is held to the specimen by vacuum to insure good contact. This covered area is then exposed to an arc-light flux for two minutes.

4. The exposed area is dipped in black dye for one minute.

5. The exposed area is washed in a warm water spray to remove the dye.

6. The exposed area is then dried using a stream of compressed air.

TESTING EQUIPMENT

Fatigue

All experiments were carried out in the three vacuum-fatigue testing systems shown in figure 6. All three of these systems apply axial loads to the test specimen. Two of these systems have closed-loop hydraulic-loading systems. The third has a subresonant loading system.

A schematic diagram of the closed-loop hydraulic-loading system is shown in figure 7. To operate this system, the mean load is first applied to the test specimen by adjusting the variable mean-load potentiometer until the desired mean load is observed on the calibrated load-readout unit. The variation from the mean load required to give the desired maximum load is then dialed into the closed-loop system using the (+) variable alternating-load potentiometer. Here again, the calibrated load-readout unit is used to determine when the desired dial setting is obtained. The minimum load is similarly dialed into the closed-loop system using the (-) variable alternating-load potentiometer. The voltages from these potentiometers are fed into the servoloop summing point which also receives the voltage from the load cell in the system's loading train. The combined voltage from the summing point is routed into the carrier amplifier where the incoming voltage is compared with a reference voltage to determine the magnitude and sign of the signal sent to the d-c amplifier. The d-c amplifier uses this signal to drive the servovalve which directs oil to the appropriate side of the load ram, thus loading the specimen and consequently changing the

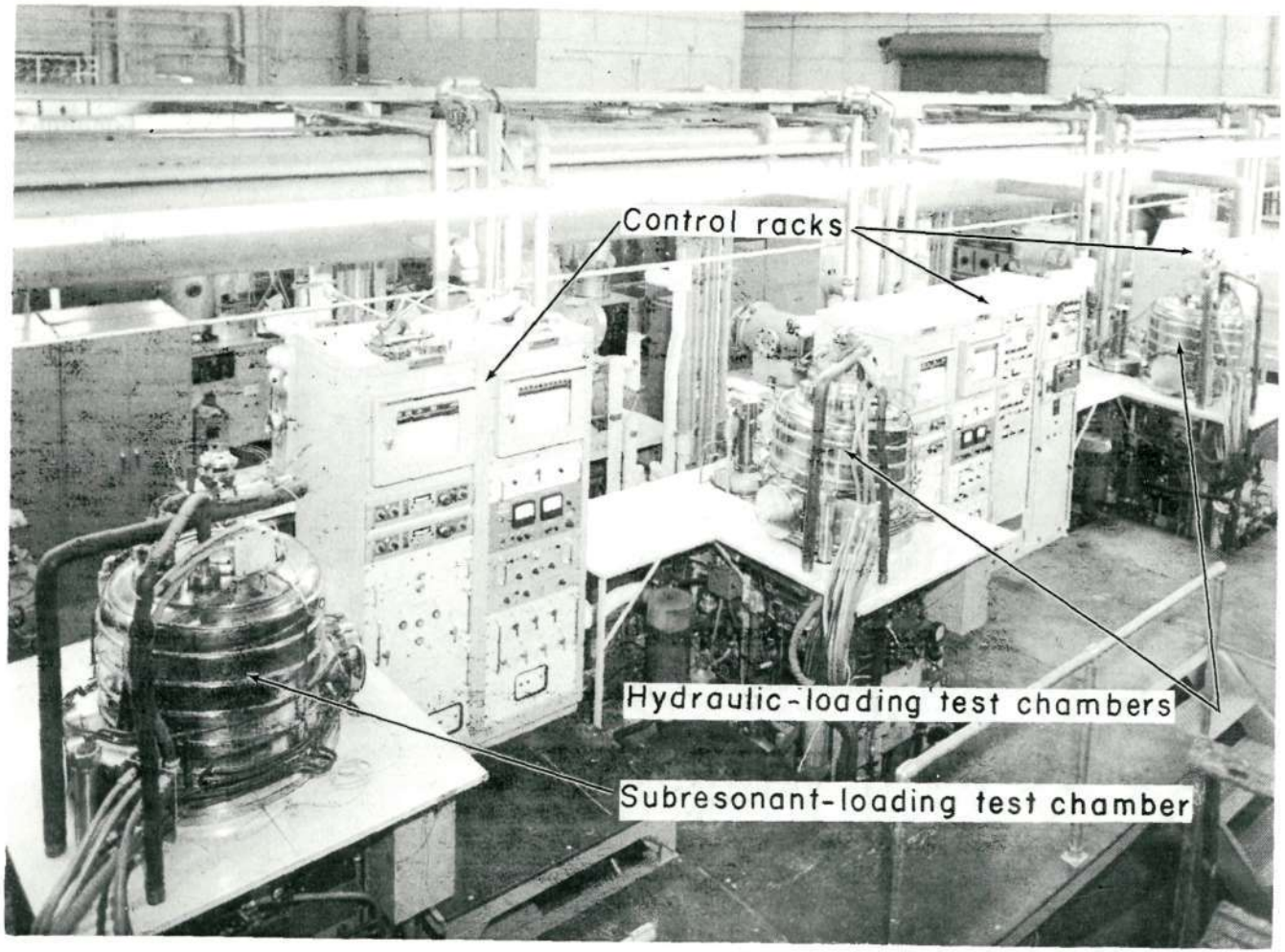

Figure 6.- Vacuum-fatigue testing systems.

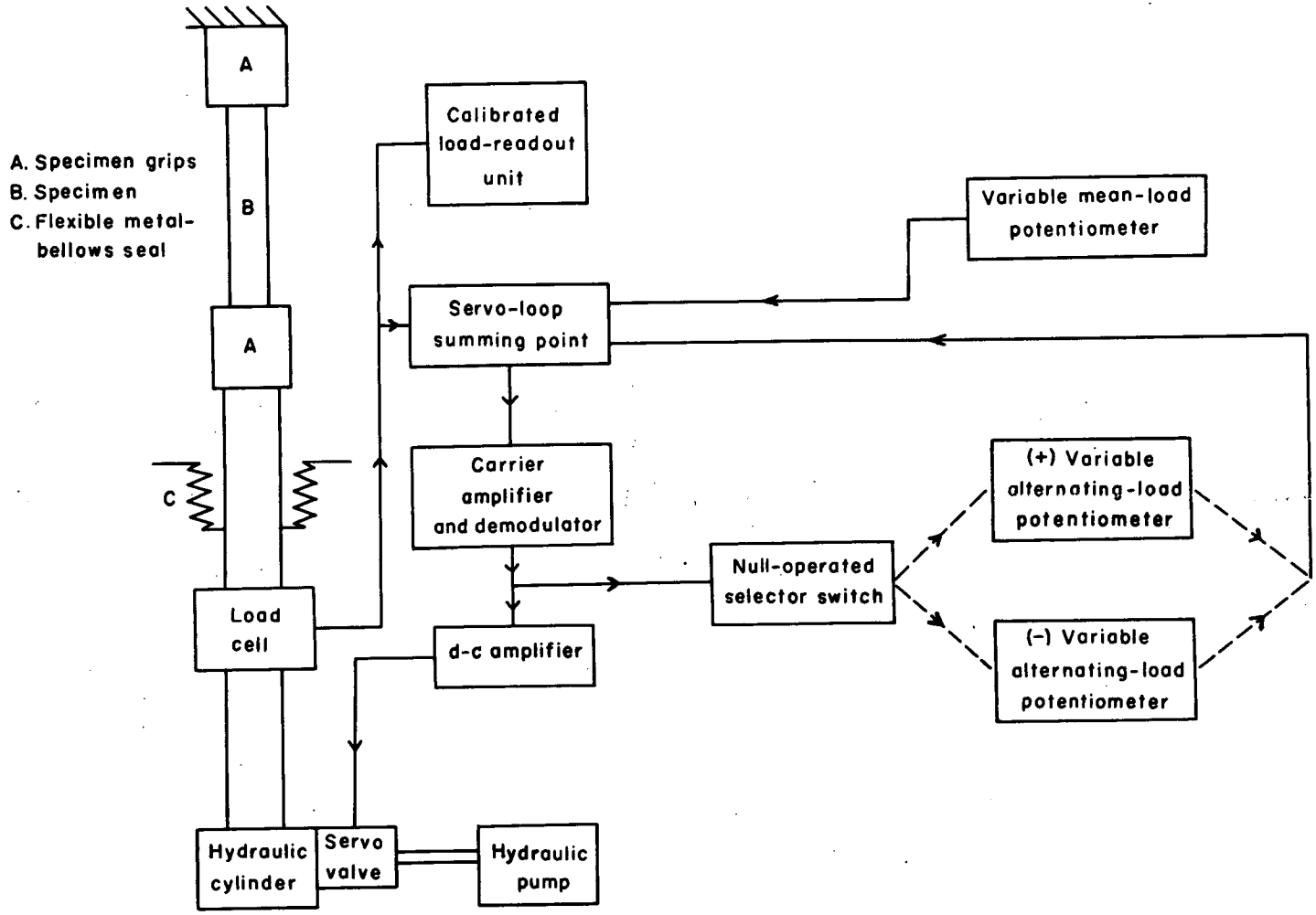

Figure 7.- Schematic diagram of the closed-loop hydraulic-loading system.

output from the load cell. As the applied load approaches the desired load, the flow of oil is proportionately slowed such that the applied load approaches the desired load slowly. When the applied load equals the desired load, a signal is generated by the null-operated selector switch which commands the system to load in the opposite direction. This sequence is continuously repeated at the maximum and minimum load points.

Specimen failure, error detection in the closed-loop system itself, or loss of command signal to the servovalve will all cause the servovalve to be deenergized and consequently stop the testing machine.

The calibrated load-readout unit consisted of a null-indicating bridge. Null was obtained when the difference between the signal from the load cell and a calibrated variable resistor was zero. Null was determined using an oscilloscope. The whole system was calibrated periodically, and the loading accuracy found to be ±24 pounds.

The load capacity of the two closed-loop hydraulic fatigue testers is ±20,000 pounds, and the operating frequencies varied between 800 and 1400 cycles per minute, depending upon the magnitude of the applied load.

Forces were transferred inside the vacuum chamber through a flexible metal-bellows seal in the bottom of the vacuum chamber.

A schematic diagram of the subresonant loading system is shown in figure 8. A vibrating beam is supported by flexure plates, the specimen, and two preload springs which are used to apply the desired mean load. The natural frequency of vibration of the beam in the vertical

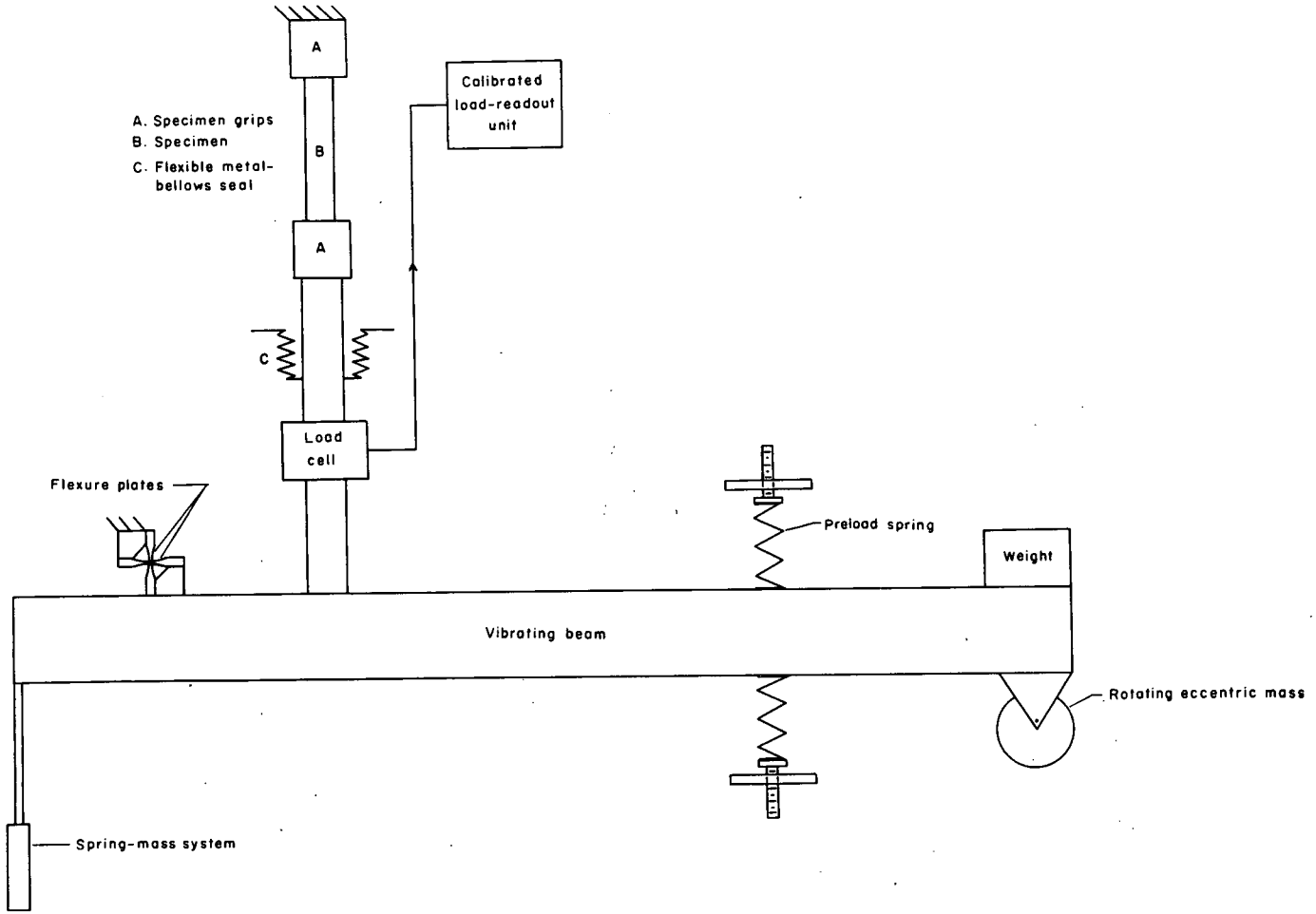

Figure 8.- Schematic diagram of the subresonant-loading system.

plane is adjusted to about 1850 cycles per minute by adjusting the amount of weight on the free end of the beam. The beam is excited to vibrate near resonance by a rotating eccentric mass driven at 1800 cycles per minute by a 3/4 horsepower electric motor. The vibrating beam imparts a sinusoidually varying axial load to the specimen which acts as one of the supports to the vibrating beam.

There are three basic methods of controlling the amplitude of the alternating load applied to the test specimen: (1) adjustment of the degree of eccentricity on the rotating eccentric mass, (2) adjustment of the natural frequency of the machine, and (3) adjustment of the natural frequency of a small spring-mass system which is coupled to and vibrates with the vibrating beam. The first two methods are employed to make large changes in the alternating load and are used before the loading system is started. The third method is used to make small changes in the alternating load and is used while the loading system is running. In order to make these small changes, the length of the spring is changed by a lead screw which is driven by a small electric motor located inside the vibrating beam. The entire system is mounted on a concrete block which is in turn supported by coil springs to provide a seismic mount.

Limit switches are positioned above and below the vibrating beam such that when the test specimen fails, a switch is tripped and the electric drive motor shut off.

The loads on the specimen are measured by a load cell whose signal is fed into the calibrated load-readout unit used with the closed-loop

hydraulic system. A three-position switch in the wiring leading to the load-readout unit allows the operator to select the desired system on which he wishes to monitor the load. Here again, the whole system was calibrated periodically, and the loading accuracy found to be ±36 pounds. (The loading accuracies of the hydraulic and subresonant loading systems are different because different load cells are used in the two systems.)

The load capacity of the subresonant fatigue tester is ±20,000 pounds, and as stated previously, the loading frequency was fixed at 1800 cycles per minute.

A schematic diagram of the vacuum pumping system is shown in figure 9. This system is capable of pumping the chamber pressure down to 8×10^{-10} torr (1 torr equals 1 millimeter of Mercury). A 10-inch diffusion pump having a pumping speed of approximately 4200 liters per second when operating at a pressure of 1×10^{-3} torr was used for high-vacuum evacuation of the chamber (i.e., from 1×10^{-3} to 8×10^{-10} torr). An optically dense water-cooled baffle was mounted on top of the diffusion pump to prevent backstreaming of the diffusion pump oil into the chamber. An optically dense liquid-nitrogen (LN_2) baffle was mounted on top of the water-cooled baffle to further inhibit backstreaming.

The diffusion pump could be backed by either a mechanical roughing pump having a capacity of 1500 liters per minute at 760 torr, or by a mechanical holding pump having a pumping capacity of 65 liters per minute at 760 torr.

Gas pressures inside the chamber were measured using thermocouple and ionization gages in conjunction with a gage controller. Pressures

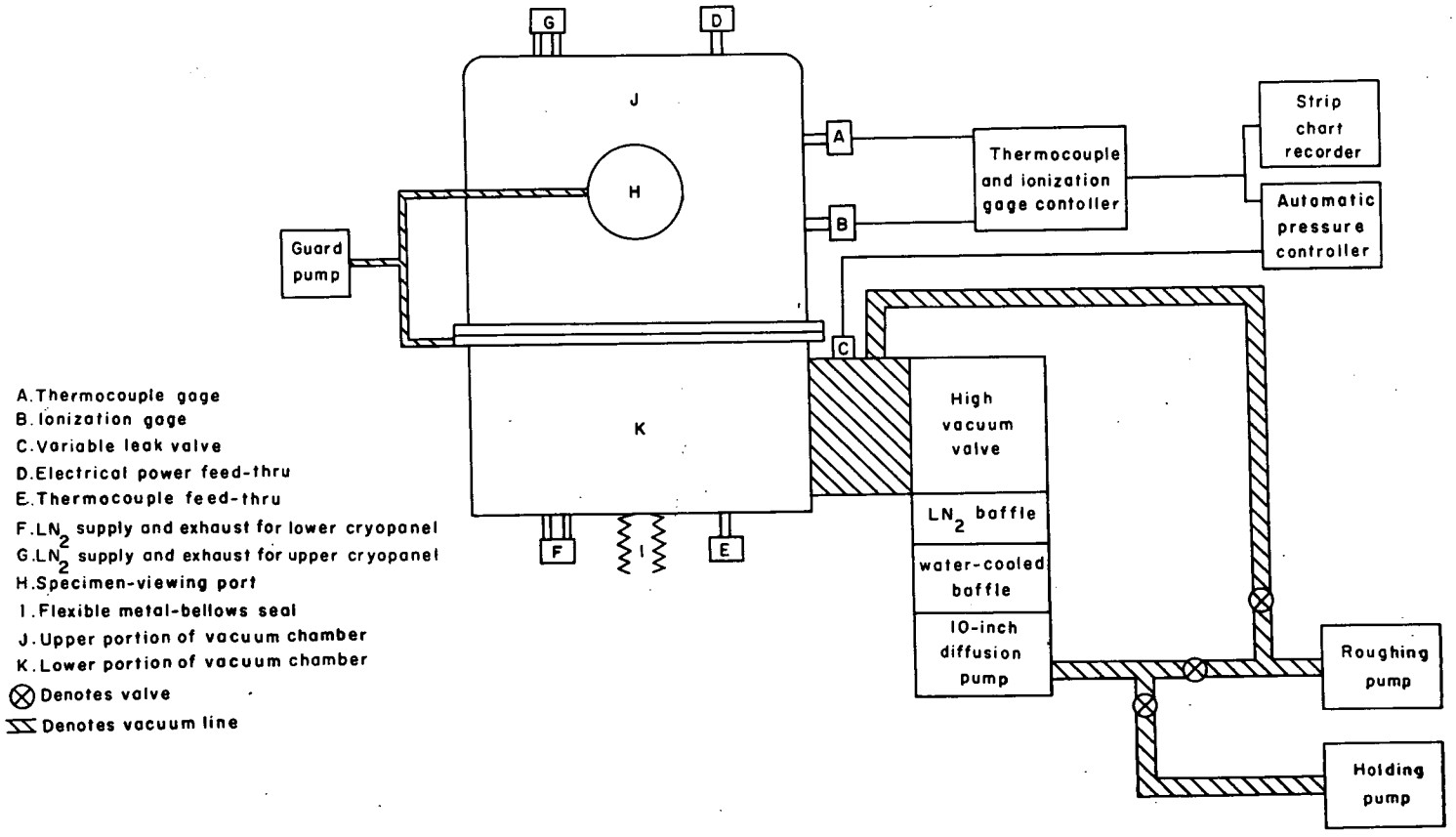

Figure 9.- Schematic diagram of the vacuum-pumping system.

between 1 torr and $1x10^{-3}$ torr were measured using the thermocouple gage. Pressures between $1x10^{-3}$ torr and $8x10^{-10}$ torr were measured using the ionization gage. Pressures between 760 and 1 torr were not measured.

The pressure inside the chamber was controlled by an automatic pressure controller which actuated a variable leak valve which in turn admitted dry air into the vacuum chamber. The chamber pressure could be controlled anywhere within the range 1 torr to $8x10^{-10}$ torr. The pressure controller was accurate to ±1 percent full scale of the input voltage to the automatic pressure controller from the pressure transducer. The chamber pressure was recorded on a strip chart recorder.

There were two specimen-viewing ports on the upper half of the chamber which were located 180 degrees apart. The seals on these ports and on the main flange of the vacuum systems consisted of two concentric "0" rings. The area between these two "0" rings was evacuated using a guard pump in order to decrease the pressure differential between the inside of the chamber and the area outside the interior "0" ring. The pressure in the evacuated area between the "0" rings was nominally $5x10^{-2}$ torr.

Feed-thrus through the chamber walls were provided in order to get electrical power, liquid nitrogen, and thermocouples inside the chamber, and to expose the sensing elements of the ionization and thermocouple gages to the vacuum environment. Copper gaskets were used to seal all of these feed-thrus and the feed-thrus for the variable leak valve and the metal bellows.

A schematic diagram of the temperature-control system is shown in figure 10. This system can control the specimen temperature within the range $-100^{\circ}F$ to $+200^{\circ}F$. The test specimen is heated by radiation using eight quartz-line heating lamps. Two banks of four lamps each are mounted on each side of the test specimen. These lamps are mounted in polished plano-parabolic reflectors which concentrate the radiant energy from the lamps on the test specimen. There are separate temperature controllers for the two banks of heating lamps. Thermocouples attached to a tab mounted next to the test specimen were used to control specimen temperature. The relationship between tab temperature and specimen temperature was carefully studied so that experiments were conducted at the proper temperature.

The test specimen was cooled by radiation using two OFHC copper cryopanels which encircle the specimen and the load trains. This cryopanel is filled with liquid nitrogen (LN_2) having a temperature of $-320^{\circ}F$. An example of the upper cryopanel is shown in figure 11. This cryopanel is a double-embossed header type. The inward facing side of the cryopanel is painted with black paint having a minimum emmisivity of 0.9 to make it highly absorptive. The outward facing side of the cryopanel is chrome plated to make it highly reflective.

In addition to cooling the test specimen, the cryopanels help with the vacuum pumping of the system by condensing gasses which have a dew point above $-320^{\circ}F$ onto the sides of the cryopanel. These condensed gasses then remain on the side of the cryopanel until the fatigue experiment is completed and the cryopanel warmed prior to opening the chamber.

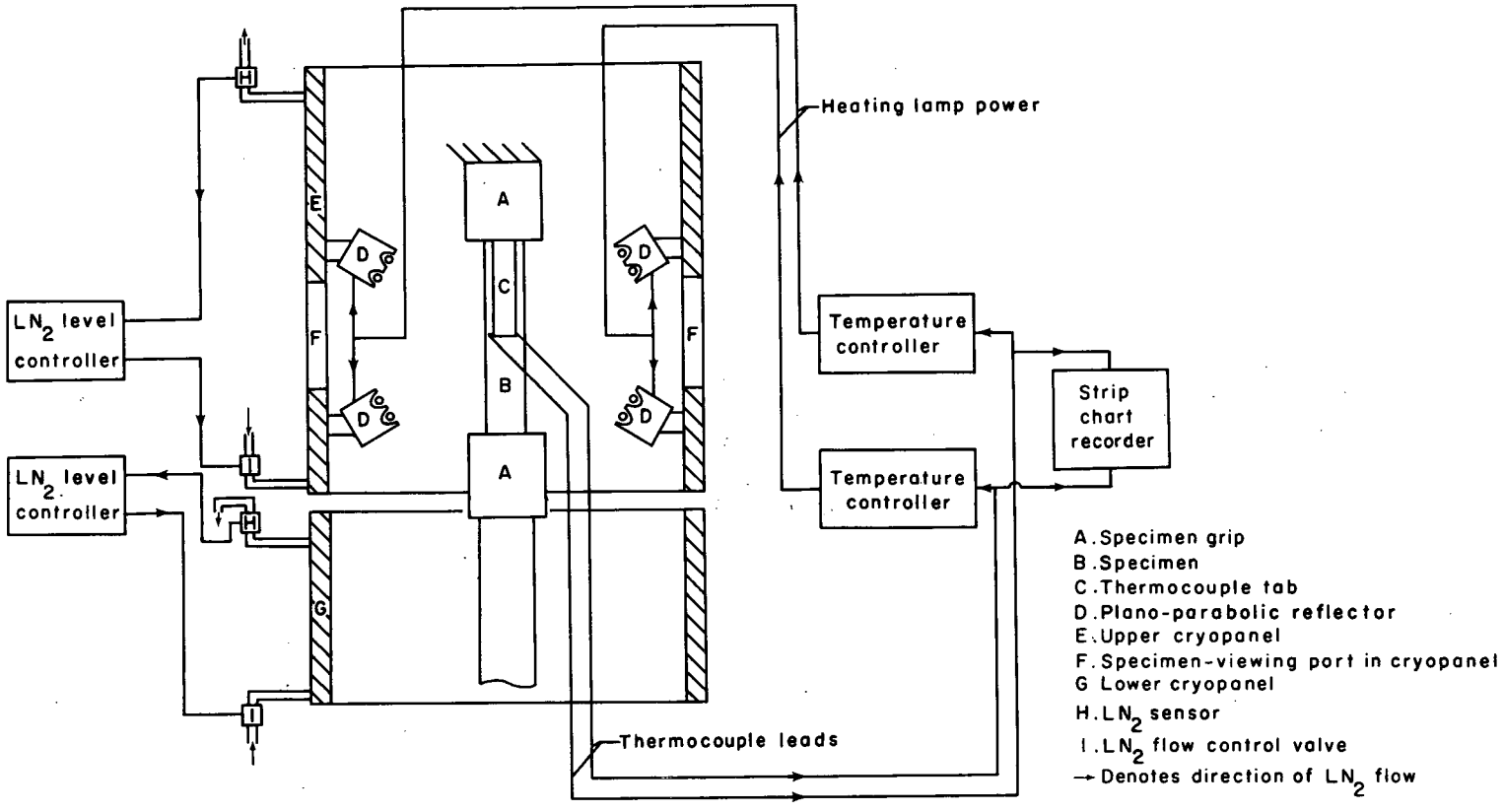

Figure 10.- Schematic diagram of the specimen temperature-control system.

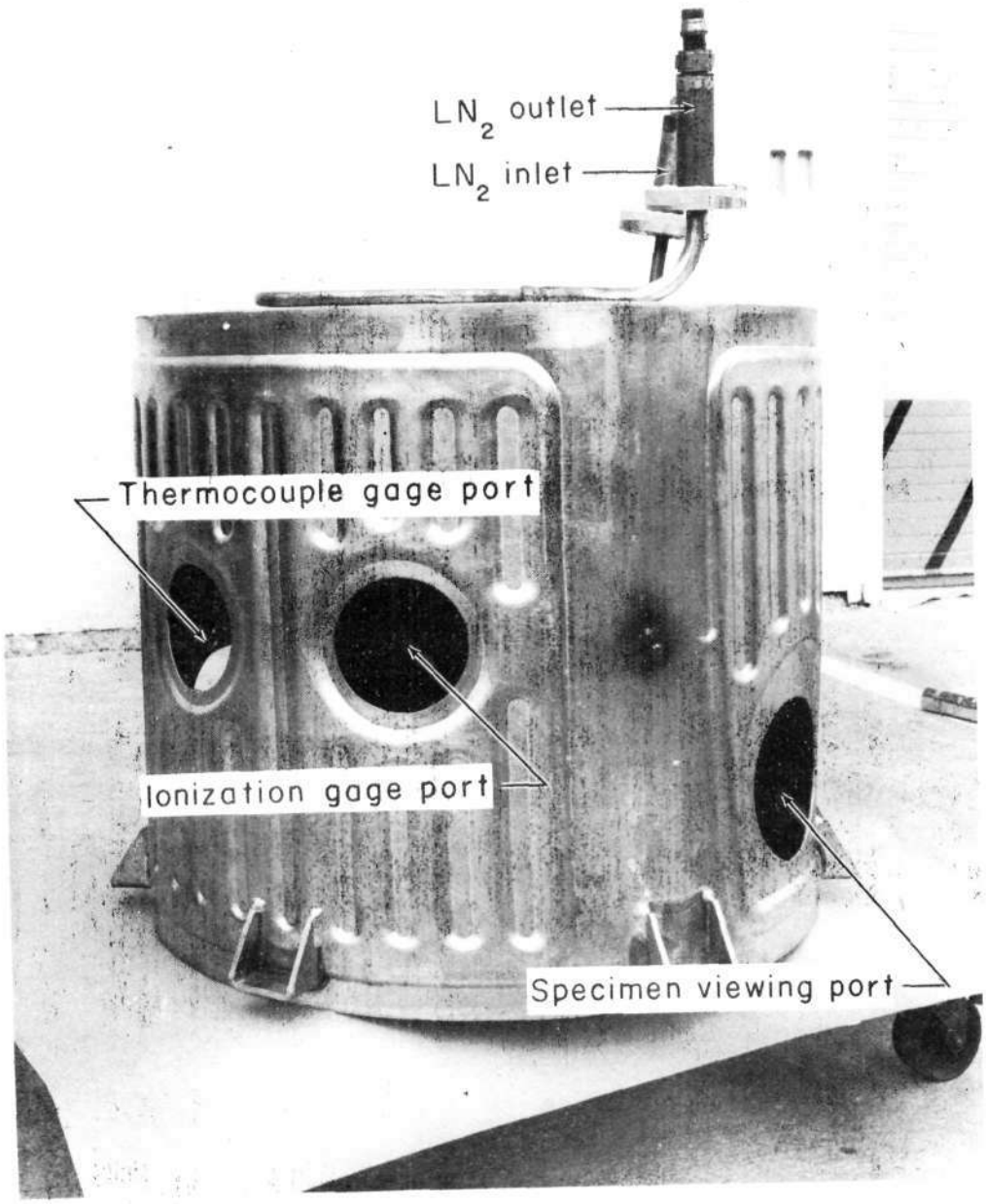

Figure 11.- Upper cryopanel.

Liquid-nitrogen level controllers are used to keep the cryopanels filled with liquid nitrogen during testing. Specimen temperatures are recorded on a strip chart recorder.

In order to evacuate the vacuum chamber into the high-vacuum range, i.e., 10×10^{-4} to 1×10^{-9} torr, the diffusion and roughing pumps are turned on simultaneously. The high-vacuum valve is closed such that the diffusion pump pumps against this valve. The roughing pump is used to evacuate the vacuum line between the diffusion pump and the roughing pump to a pressure of about 5×10^{-2} torr. Once this pressure is reached, the holding pump is energized and used to back the diffusion pump while the roughing pump is switched to pump on the vacuum chamber. Once the chamber pressure reaches about 5×10^{-2} torr, the high-vacuum valve is opened and the diffusion pump used to pump the chamber. Once a pressure of 1×10^{-4} torr is reached inside the chamber, liquid nitrogen can be introduced into the cryopanels. As explained previously, these cold cryopanels effectively pump the chamber environment by condensing gasses on the cryopanel walls.

The chamber is then pumped to a pressure below that at which the fatigue experiment is to be conducted, and the pressure controller used to bring the pressure back up to the desired level using dry air. A typical plot of time versus chamber pressure is shown in figure 12.

Electron Microscopes

The fatigue-fractured surfaces of selected specimens were inspected in this investigation using both a Hitachi transmission electron

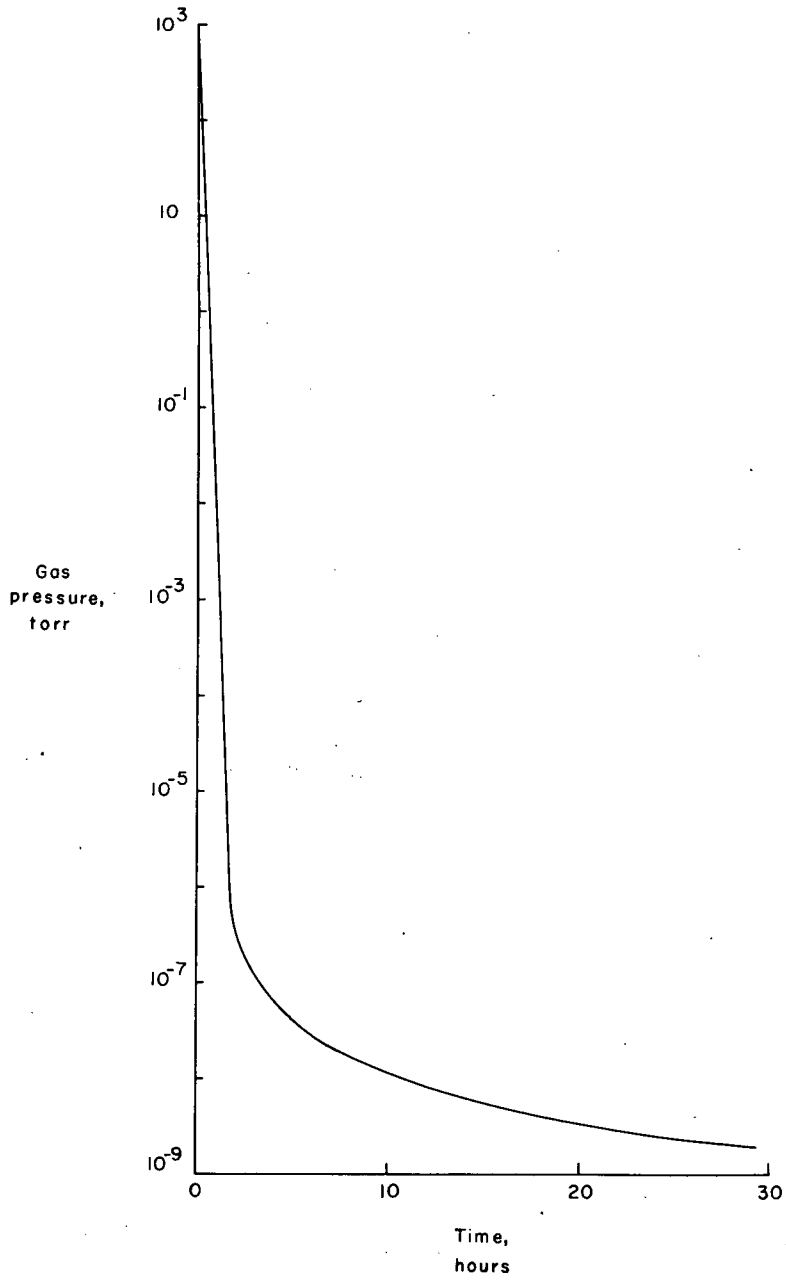

Figure 12.- Typical plot of time versus chamber pressure.

microscope (figure 13) and a Cambridge scanning electron microscope (figure 14). The procedures used in preparing the replicas for use in the transmission electron microscope are listed in Table 6. This transmission microscope was calibrated immediately before it was used in this investigation.

The fatigue-fractured sections of the specimens were mounted inside the specimen chamber of the scanning electron microscope where these sections could be observed directly.

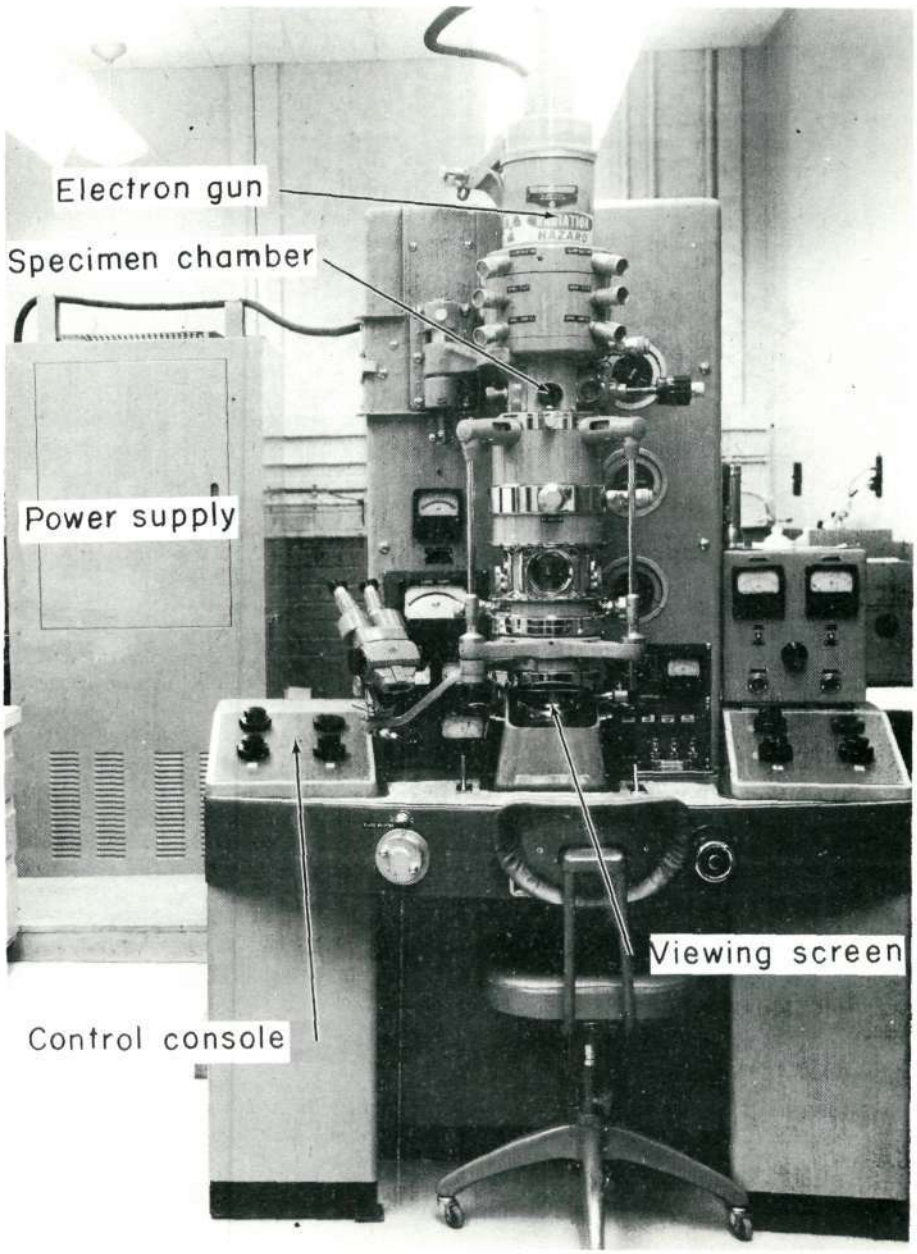

Figure 13.- Hitachi transmission electron microscope.

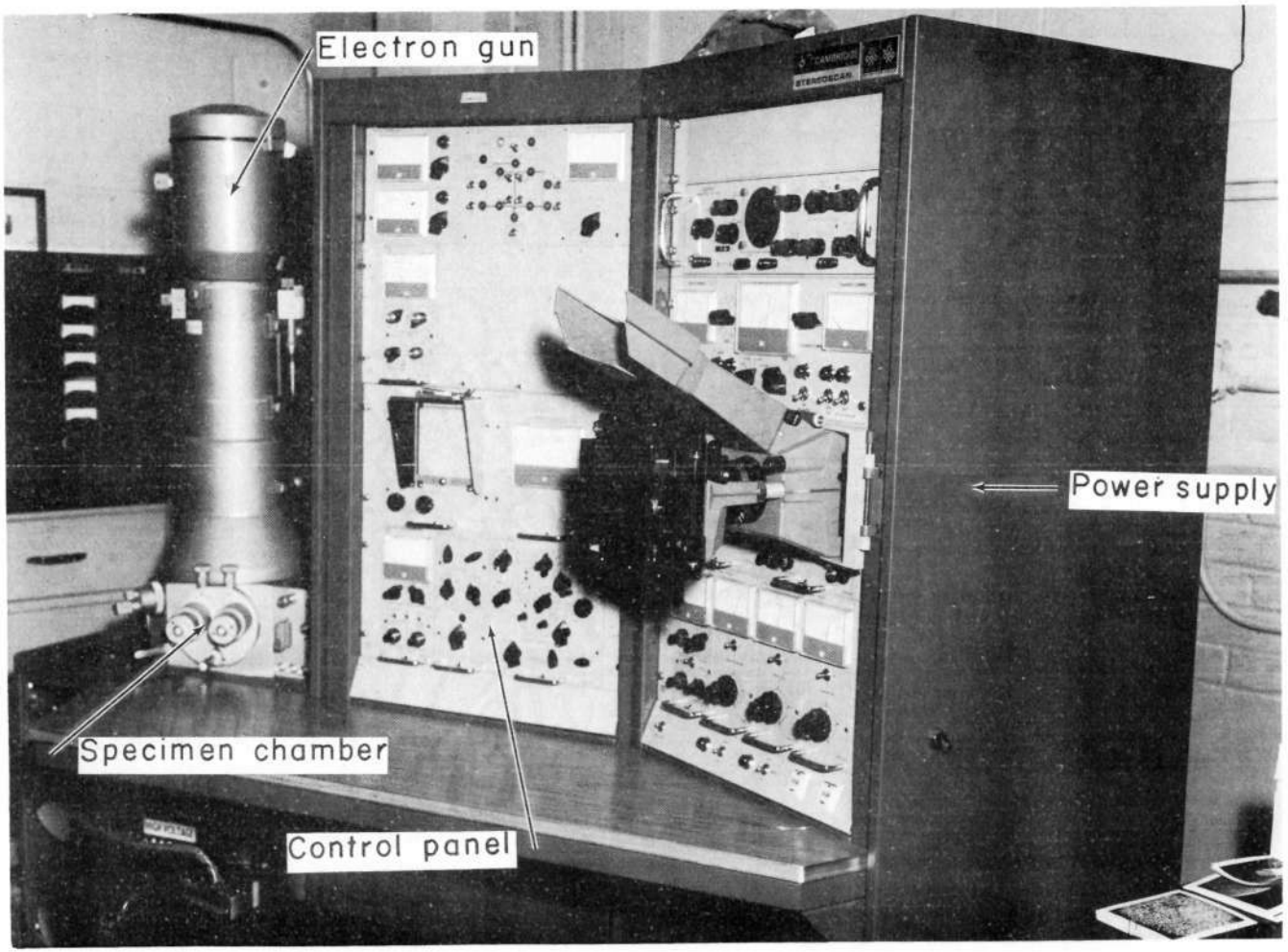

Figure 14.- Cambridge scanning electron microscope.

Table 6. Procedures for preparation of two-stage carbon-platinum replicas.

1. A sheet of acetyl cellulose film having a nominal thickness of 0.001 inch was softened in acetone and placed on the fatigue-fractured surface of the specimen. This specimen surface was also wetted with acetone.
2. On drying, the film was carefully peeled from the fracture surface and mounted in a High-Vacuum Equipment Corporation vacuum evaporator where the film was shadowed at a 45-degree angle using carbon and platinum. A pure carbon backing was then deposited on the carbon-platinum shadow material.
3. The areas to be inspected in the microscope were then sectioned out of the film. These sectioned areas were then mounted on glass slides using softened (heated) paraffin as an adhesive.
4. The glass slides were placed in a room-temperature acetone bath and left there until the acetyl cellulose film dissolved leaving the replica on the paraffin.
5. The glass slides were then placed in a warm acetone bath and the bath heated until the paraffin softened and the replica drifted free.
6. The replicas were then caught on a circular copper grid and placed in a room-temperature acetone bath for final cleaning.
7. After cleaning, the replicas were caught on the circular copper grid and dried in still air. The replicas were then ready for inspection in the transmission electron microscope.

TEST PROCEDURE

Fatigue-Life Tests

Axial-load fatigue-life experiments were conducted on all unnotched specimens at a stress ratio (i.e., the ratio of the minimum applied stress in the cycle to the maximum applied stress in the cycle) of 0.02. The primary experiments to determine the effects of vacuum on the fatigue behavior of 7075-T6 aluminum alloy were conducted at atmospheric pressure and 5×10^{-8} torr. The maximum stresses applied in these tests ranged from 60 ksi to 33 ksi. Normally, five duplicate tests were conducted at each stress level.

Additional fatigue-life experiments were conducted at gas pressures of 5×10^{-1}, 5×10^{-2}, 5×10^{-4}, and 5×10^{-8} torr to determine the variation of fatigue life with decreasing gas pressure. The stress levels in these experiments ranged from 60 ksi to 40 ksi. Generally, three tests were conducted at each stress level in these additional experiments.

The loading frequencies in the fatigue-life experiments were 1800 cpm using the subresonant loading system, and ranged from approximately 1000 cpm to 1400 cpm in the two hydraulic loading systems.

The grip jaws in the three testing systems are made of stainless steel and are serrated. When the grips are tightened directly against the softer aluminum specimens, the serrations dig into the specimens introducing severe stress concentrations. The specimens occasionally failed at these stress concentrations during testing, rather than at their critical section. To preclude such failures, lead liners were

placed between the test specimens and the grip jaws. These lead liners provided sufficient friction for gripping the test specimen when the grip bolts were torqued to 90-foot-pounds, and introduced no stress concentrations into the test specimens.

The loads on the specimens were checked periodically during each test and adjusted when necessary. Variations in load seldom exceeded one percent of the maximum load during the experiment.

In order to accelerate the pumping of the vacuum chamber, the cryopanels were filled with liquid nitrogen for tests at pressures of 5×10^{-8} torr. These cryopanels would then, of course, cool the test specimen by radiant-heat transfer. The quartz-line heating lamps were then used to raise and to keep the specimen temperature at 75°F during the course of the tests. In all tests at other gas pressures, i.e., 760 torr to 5×10^{-4} torr, experiments were conducted at approximately 70°F to 85°F.

Fatigue-Crack-Propagation Tests

Axial-load fatigue-crack-propagation experiments were conducted on the center-notched specimens at a stress ratio of 0.02. These experiments were conducted at the two primary pressures used in the fatigue-life experiments, i.e., atmospheric pressure and 5×10^{-8} torr. The maximum stress applied in these experiments ranged from 10 ksi to 40 ksi. Duplicate experiments were conducted at each stress level.

Fatigue-crack propagation was observed through the specimen-viewing ports using 10-power microscopes. The test specimen inside the

chamber was illuminated with a flashlight. The number of cycles required to propagate the crack to each grid line was recorded so that crack-propagation rates could be determined. All tests were terminated when the fatigue cracks reached a predetermined crack length. These cracked specimens were then used for the fracture-toughness portion of the investigation.

The loading frequencies in these experiments were again 1800 cpm for the subresonant loading system, and 1000 to 1400 cpm for the two hydraulic loading systems.

Lead liners were used in the testing machine grips, and the loads periodically checked on all of these crack-propagation experiments.

Liquid nitrogen was used in the cryopanels for tests at 5×10^{-8} torr, and the specimen temperature kept at 75°F.

Fracture-Toughness Tests

Axial-load fracture-toughness tests were conducted on the unfailed crack-propagation specimens. For a given specimen, the same gas pressure was used for both the fatigue-crack-propagation and the fracture-toughness experiments. The closed-loop hydraulic loading systems were used for these fracture-toughness tests. The load at failure was obtained using a calibrated Consolidated Electrodynamics Corporation recording oscillograph which read the output of the load cell at specimen failure. The length of the crack at the onset of unstable crack growth was obtained by visually observing the location of the crack tip relative to the reference grid throughout the fracture-toughness tests.

This observation was made using a 10-power microscope. The loading rate in these fracture-toughness experiments was approximately 20,000 lbf/minute.

RESULTS AND DISCUSSION

Fatigue-Life Experiments

The results of the fatigue life experiments conducted on the unnotched sheet specimens are presented in Tables 7, 8, 9, 10, and 11. These experiments were conducted at gas pressures of 760, $5x10^{-1}$, $5x10^{-2}$, $5x10^{-4}$, and $5x10^{-8}$ torr. The data are also plotted in figures 15, 16, 17, 18 and 19. An S-N curve is faired through each set of data. In these figures the maximum stress in a cycle is plotted against the number of cycles to failure. The data points in figures 15 through 19 which are surmounted by an arrow indicate tests in which the specimen reached or exceeded the fatigue limit (selected as 5,000,000 cycles in this investigation) without failing. Data points in these figures which are surmounted by numeral indicate tests in which a number of specimens had essentially the same fatigue lives.

The S-N curves faired through the data at each gas pressure are also plotted in figure 20. Inspection of this indicates that the fatigue resistance of 7075-T6 aluminum is significantly higher in vacuum than in air. This increase in fatigue resistance occurred at all gas pressures below 760 torr. Furthermore, the lower the gas pressure was, the greater the resistance to fatigue was.

Fatigue lives at $5x10^{-1}$ torr were approximately three to seven times longer (depending upon the stress level) than they were at 760 torr. The fatigue limit (which is defined in the Annual Book of ASTM Standards (1970) as "the limiting value of the median fatigue

Table 7. Results of fatigue-life tests at 760 torr.

Specimen Number	Maximum Stress Level, ksi	Mean Stress Level, ksi	Minimum Stress Level, ksi	Fatigue Life, Cycles	Remarks
B83N7-47	60	30.6	1.2	8,590	Valid test
B83N7-45	60	30.6	1.2	10,320	Valid test
B83N7-46	60	30.6	1.2	16,810	Valid test
B83N7-42	60	30.6	1.2	18,560	Valid test
B65N7-125	60	30.6	1.2	22,550	Valid test
B72N7-195	60	30.6	1.2	1,670	Specimen accidently overloaded, test invalid
B84N7-59	50	25.5	1.0	27,660	Valid test
B71N7-184	50	25.5	1.0	27,710	Valid test
B71N7-181	50	25.5	1.0	35,040	Valid test
B84N7-53	50	25.5	1.0	42,130	Valid test
B84N7-56	50	25.5	1.0	46,990	Valid test
B71N7-183	40	20.4	0.8	47,290	Valid test
B71N7-182	40	20.4	0.8	54,970	Valid test
B71N7-188	40	20.4	0.8	74,020	Valid test
B71N7-189	40	20.4	0.8	79,260	Valid test
B84N7-57	40	20.4	0.8	145,640	Valid test
B72N7-196	40	20.4	0.8	195,930	Valid test
B71N7-190	40	20.4	0.8	1,890	Specimen failed at grip line, test invalid
B84N7-54	40	20.4	0.8	Not recorded	Specimen failed at grip line, test invalid

Table 7 (continued).

Specimen Number	Maximum Stress Level, ksi	Mean Stress Level, ksi	Minimum Stress Level, ksi	Fatigue Life, Cycles	Remarks
B88N7-93	35	17.85	0.7	239,090	Valid test
B65N7-126	35	17.85	0.7	1,405,500	Valid test
B65N7-130	35	17.85	0.7	4,246,550	Valid test
B88N7-99	35	17.85	0.7	5,113,230	Runout, valid test
B84N7-52	35	17.85	0.7	5,376,110	Runout, valid test
B72N7-197	35	17.85	0.7	6,135,730	Runout, valid test
B71N7-187	35	17.85	0.7	621,410	Specimen failed at grip line, test invalid
B88N7-97	35	17.85	0.7	247,450	Specimen buckled by machine malfunction, test invalid
B69N7-168	33	16.83	0.66	134,340	Valid test
B83N7-43	33	16.83	0.66	421,500	Valid test
B65N7-123	33	16.83	0.66	440,540	Valid test
B65N7-124	33	16.83	0.66	2,337,380	Valid test
B69N7-162	33	16.83	0.66	5,000,000	Runout, valid test
B69N7-166	33	16.83	0.66	5,009,850	Runout, valid test
B83N7-44	33	16.83	0.66	5,012,250	Runout, valid test
B74N7-15	33	16.83	0.66	9,066,790	Runout, valid test

Table 8. Results of fatigue-life tests at 5×10^{-1} torr.

Specimen Number	Maximum Stress Level, ksi	Mean Stress Level, ksi	Minimum Stress Level, ksi	Fatigue Life, Cycles	Remarks
B64N7-120	60	30.6	1.2	78,220	Valid test
B88N7-92	60	30.6	1.2	94,580	Valid test
B64N7-111	60	30.6	1.2	116,360	Valid test
B83N7-49	50	25.5	1.0	101,020	Valid test
B69N7-161	50	25.5	1.0	101,070	Valid test
B65N7-129	50	25.5	1.0	140,340	Valid test
B69N7-163	50	25.5	1.0	Not recorded	Specimen buckled when machine malfunctioned
B65N7-127	50	25.5	1.0	Not recorded	Specimen buckled when machine malfunctioned
B74N7-17	45	22.95	0.9	221,740	Valid test
B56N7-5	45	22.95	0.9	844,830	Valid test
B60N7-7	45	22.95	0.9	1,159,740	Valid test
B64N7-114	40	20.4	0.8	1,264,000	Valid test
B87N7-90	40	20.4	0.8	5,004,290	Runout, valid test
B87N7-86	40	20.4	0.8	8,181,610	Runout, valid test
B87N7-193	40	20.4	0.8	Not recorded	Specimen accidently buckled

Table 9. Results of fatigue life tests at 5×10^{-2} torr.

Specimen Number	Maximum Stress Level, ksi	Mean Stress Level, ksi	Minimum Stress Level, ksi	Fatigue Life, Cycles	Remarks
B68N7-157	60	30.6	1.2	89,600	Valid test
B86N7-80	60	30.6	1.2	140,450	Valid test
B74N7-18	60	30.6	1.2	146,370	Valid test
B68N7-151	60	30.6	1.2	620	Specimen buckled when machine malfunctioned
B69N7-165	50	25.5	1.0	83,190	Valid test
B69N7-170	50	25.5	1.0	98,880	Valid test
B69N7-167	50	25.5	1.0	114,210	Valid test
B69N7-169	50	25.5	1.0	124,790	Valid test
B65N7-128	50	25.5	1.0	171,840	Valid test
B83N7-50	50	25.5	1.0	225,090	Valid test
B74N7-16	45	22.95	0.9	711,870	Valid test
B87N7-83	45	22.95	0.9	1,047,810	Valid test
B63N7-103	45	22.95	0.9	1,168,970	Valid test
B68N7-158	40	20.4	0.8	5,201,580	Runout, valid test
B86N7-74	40	20.4	0.8	7,095,840	Runout, valid test
B87N7-89	40	20.4	0.8	Not recorded	Machine malfunctioned

Table 10. Results of fatigue-life tests at 5×10^{-4} torr.

Specimen Number	Maximum Stress Level, ksi	Mean Stress Level, ksi	Minimum Stress Level, ksi	Fatigue Life, Cycles	Remarks
B74N7-14	60	30.6	1.2	180,310	Valid test
B87N7-81	60	30.6	1.2	188,740	Valid test
B49N7-7	60	30.6	1.2	379,170	Valid test
B52N7-1	50	25.5	1.0	251,960	Valid test
B74N7-19	50	25.5	1.0	359,780	Valid test
B74N7-12	50	25.5	1.0	517,600	Valid test
B87N7-84	45	22.95	0.9	340,400	Valid test
B58N7-3	45	22.95	0.9	375,000	Valid test
B52N7-9	45	22.95	0.9	5,000,300	Runout, valid test
B58N7-1	45	22.95	0.9	5,197,200	Valid test
B86N7-71	40	20.4	0.8	2,442,500	Valid test
B68N7-156	40	20.4	0.8	5,008,710	Runout, valid test
B87N7-87	40	20.4	0.8	5,049,570	Runout, valid test
B64N7-118	40	20.4	0.8	7,106,710	Runout, valid test
B68N7-160	40	20.4	0.8	2,160,300	Machine malfunctioned, invalid test

Table 11. Results of fatigue-life tests at 5×10^{-8} torr.

Specimen Number	Maximum Stress Level, ksi	Mean Stress Level, ksi	Minimum Stress Level, ksi	Fatigue Life, Cycles	Remarks
B64N7-117	60	30.6	1.2	137,790	Valid test
B88N7-98	60	30.6	1.2	155,460	Valid test
B86N7-77	60	30.6	1.2	296,560	Valid test
B72N7-192	60	30.6	1.2	364,880	Valid test
B72N7-194	60	30.6	1.2	570,870	Valid test
B64N7-119	50	25.5	1.0	583,300	Valid test
B68N7-153	50	25.5	1.0	634,310	Valid test
B72N7-191	50	25.5	1.0	874,000	Valid test
B64N7-115	50	25.5	1.0	954,680	Valid test
B88N7-100	50	25.5	1.0	1,194,830	Valid test
B63N7-104	50	25.5	1.0	1,319,420	Valid test
B86N7-75	50	25.5	1.0	1,412,010	Valid test
B64N7-112	45	22.95	0.9	625,200	Valid test
B74N7-11	45	22.95	0.9	805,020	Valid test
B63N7-107	45	22.95	0.9	1,956,270	Valid test
B86N7-79	45	22.95	0.9	2,119,710	Valid test
B64N7-113	45	22.95	0.9	2,496,230	Valid test
B87N7-88	40	20.4	0.8	5,000,000	Runout, valid test
B87N7-82	40	20.4	0.8	5,799,290	Runout, valid test
B87N7-85	40	20.4	0.8	7,992,310	Runout, valid test
B63N7-105	40	20.4	0.8	8,086,090	Runout, valid test
B63N7-106	40	20.4	0.8	8,243,700	Runout, valid test

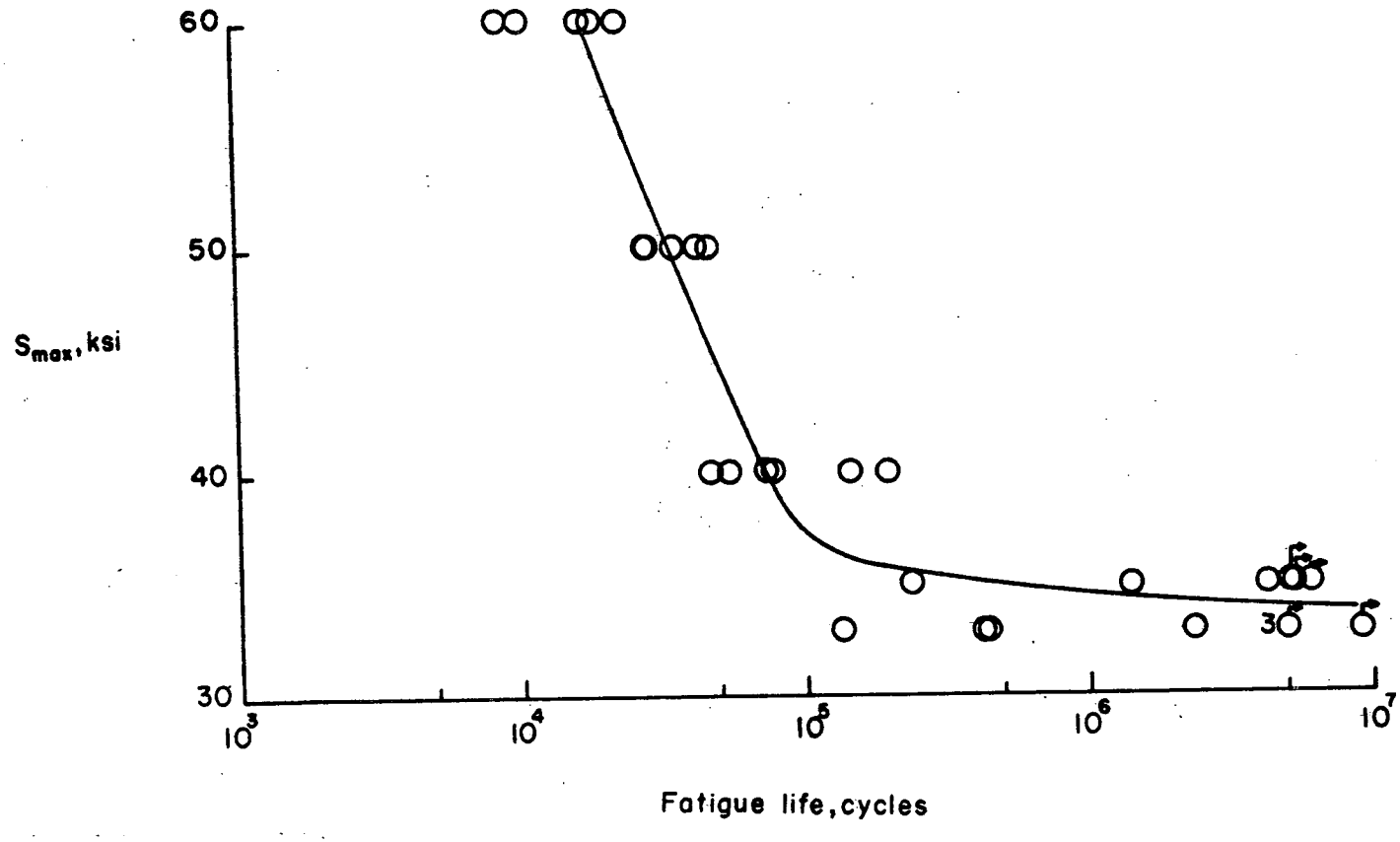

Figure 15.- Variation of fatigue life with stress for 7075-T6 at 760 torr.

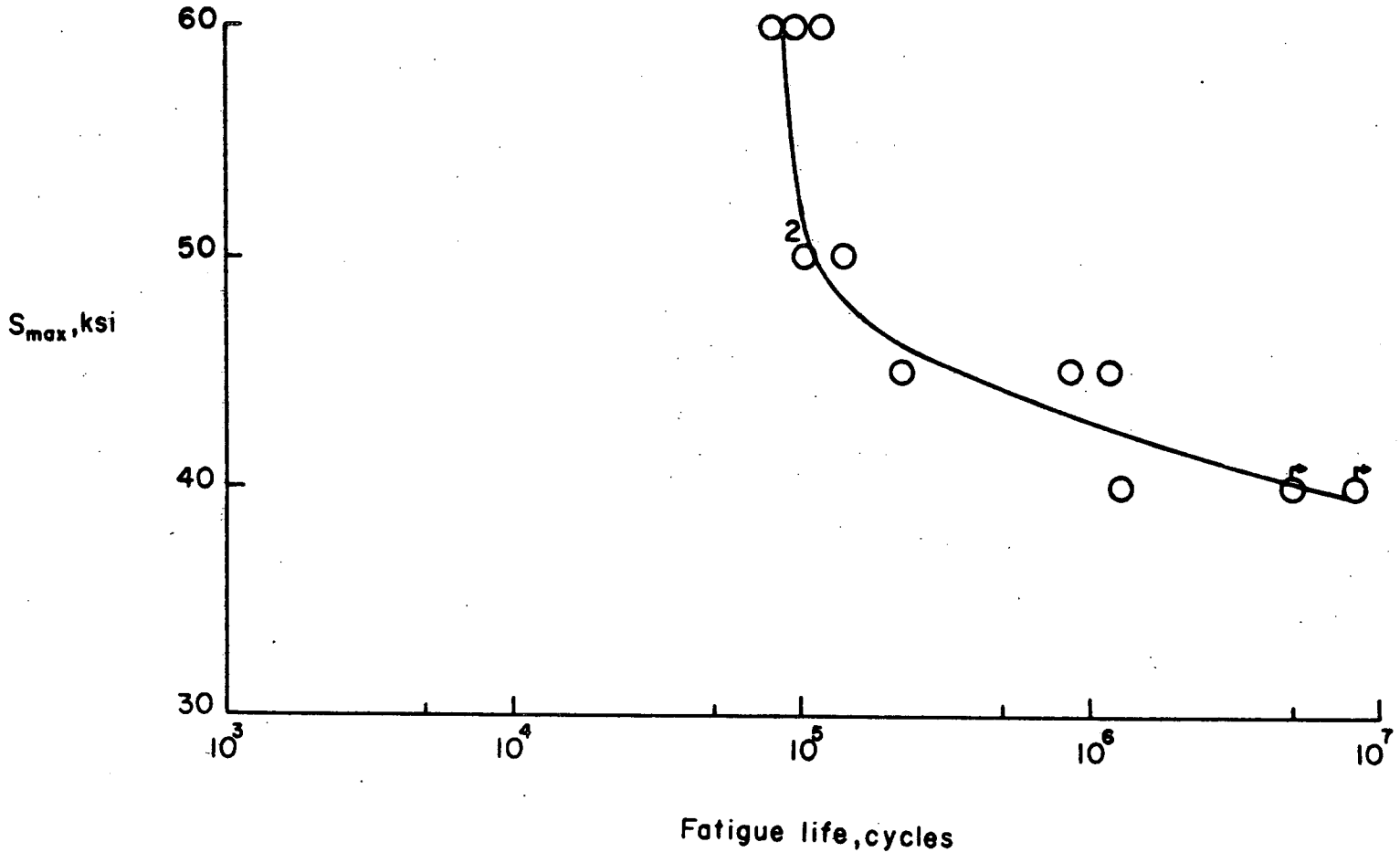

Figure 16.- Variation of fatigue life with stress for 7075-T6 at 5 X 10^{-1} torr.

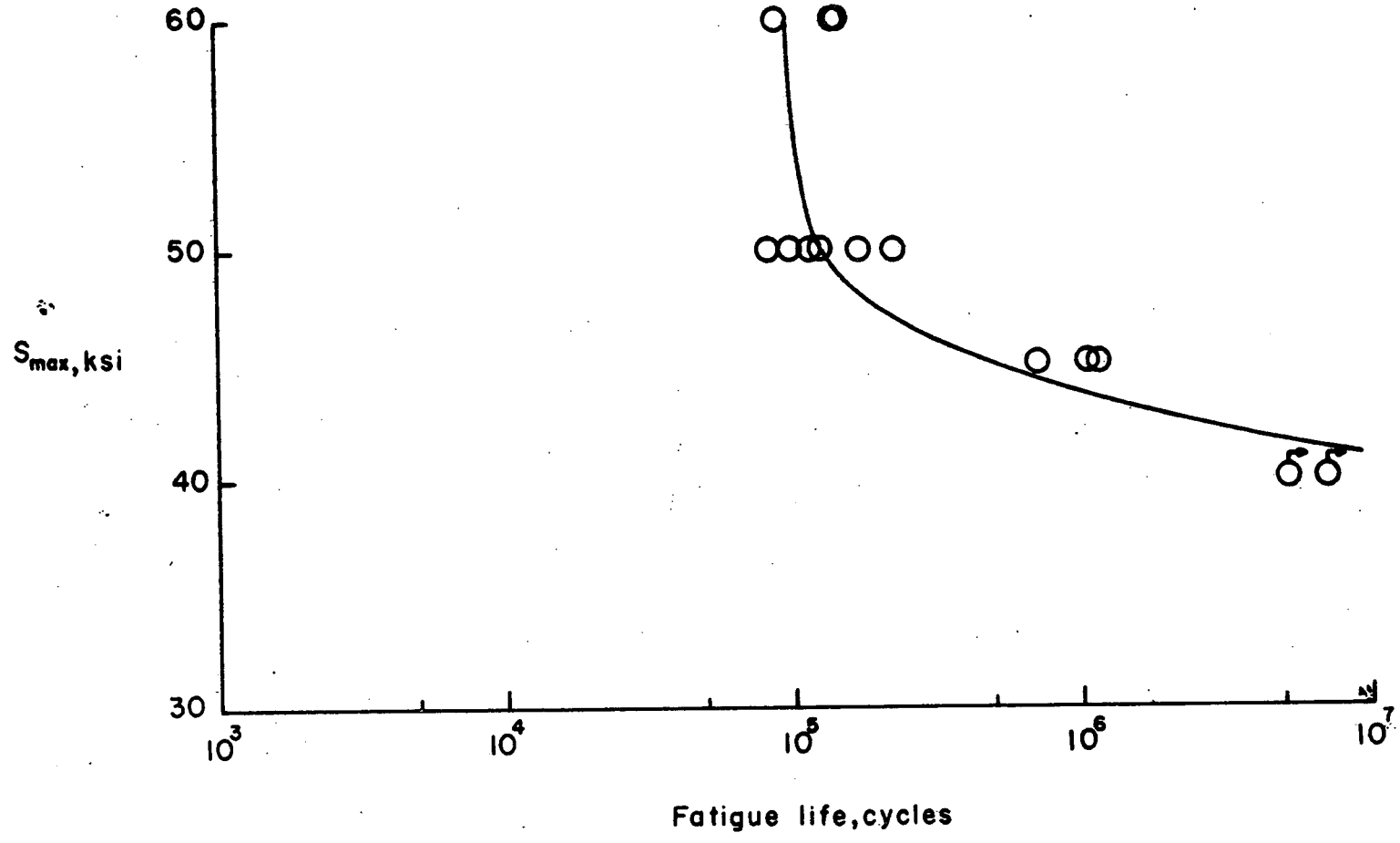

Figure 17.- Variation of fatigue life with stress for 7075-T6 at 5 X 10^{-2} torr.

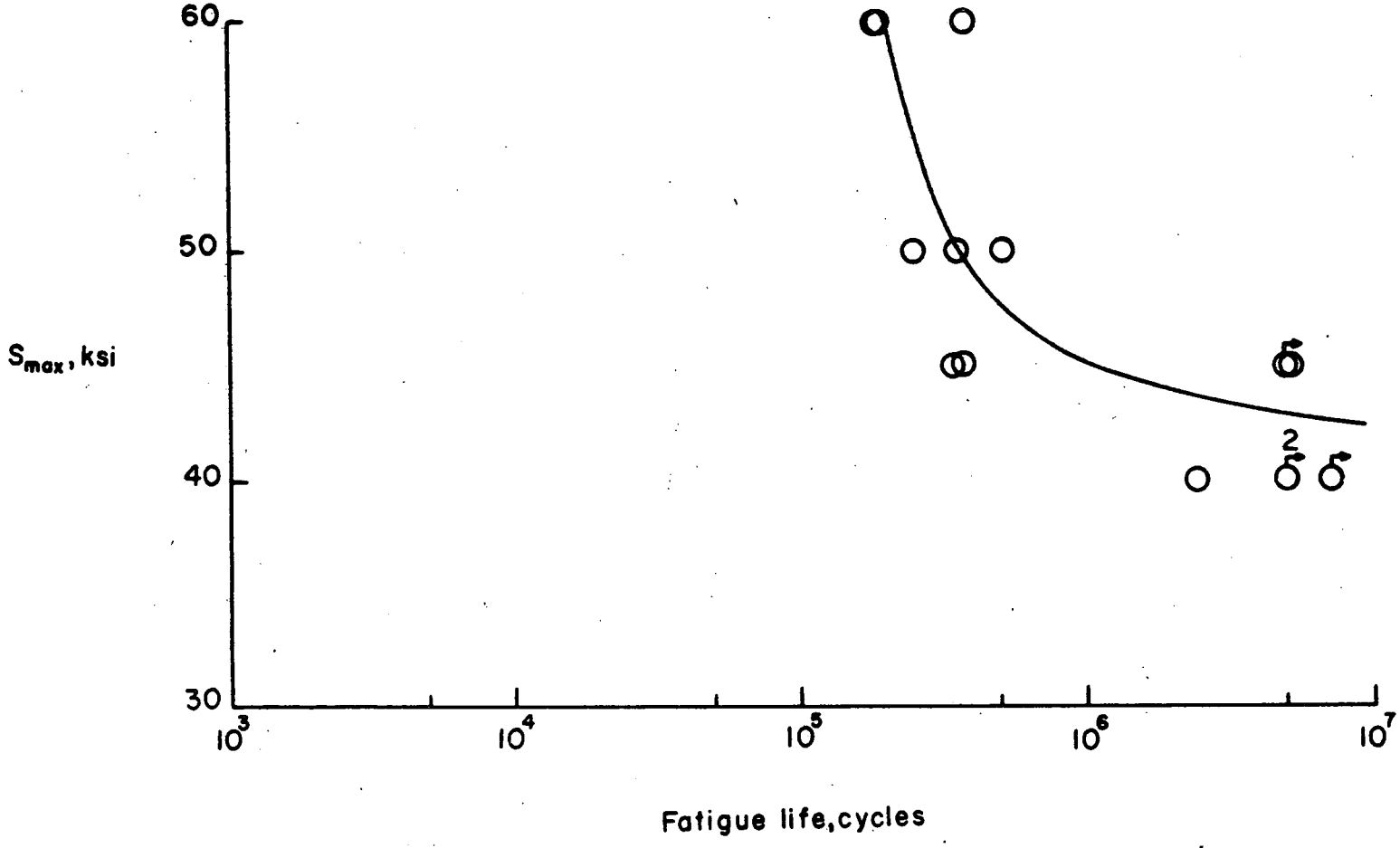

Figure 18.- Variation of fatigue life with stress for 7075-T6 at 5 X 10^{-4} torr.

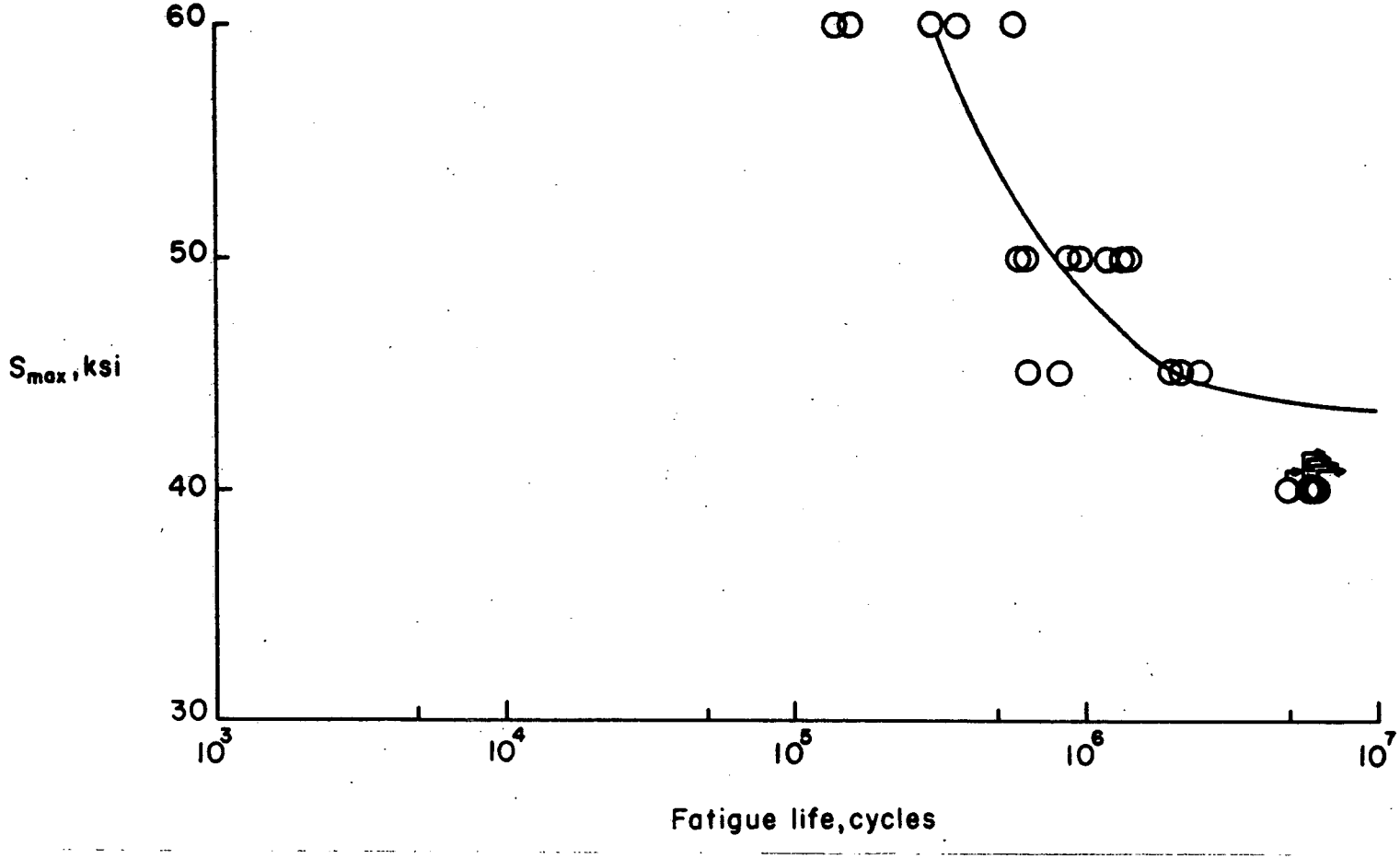

Figure 19.- Variation of fatigue life with stress for 7075-T6 at 5 X 10^{-8} torr.

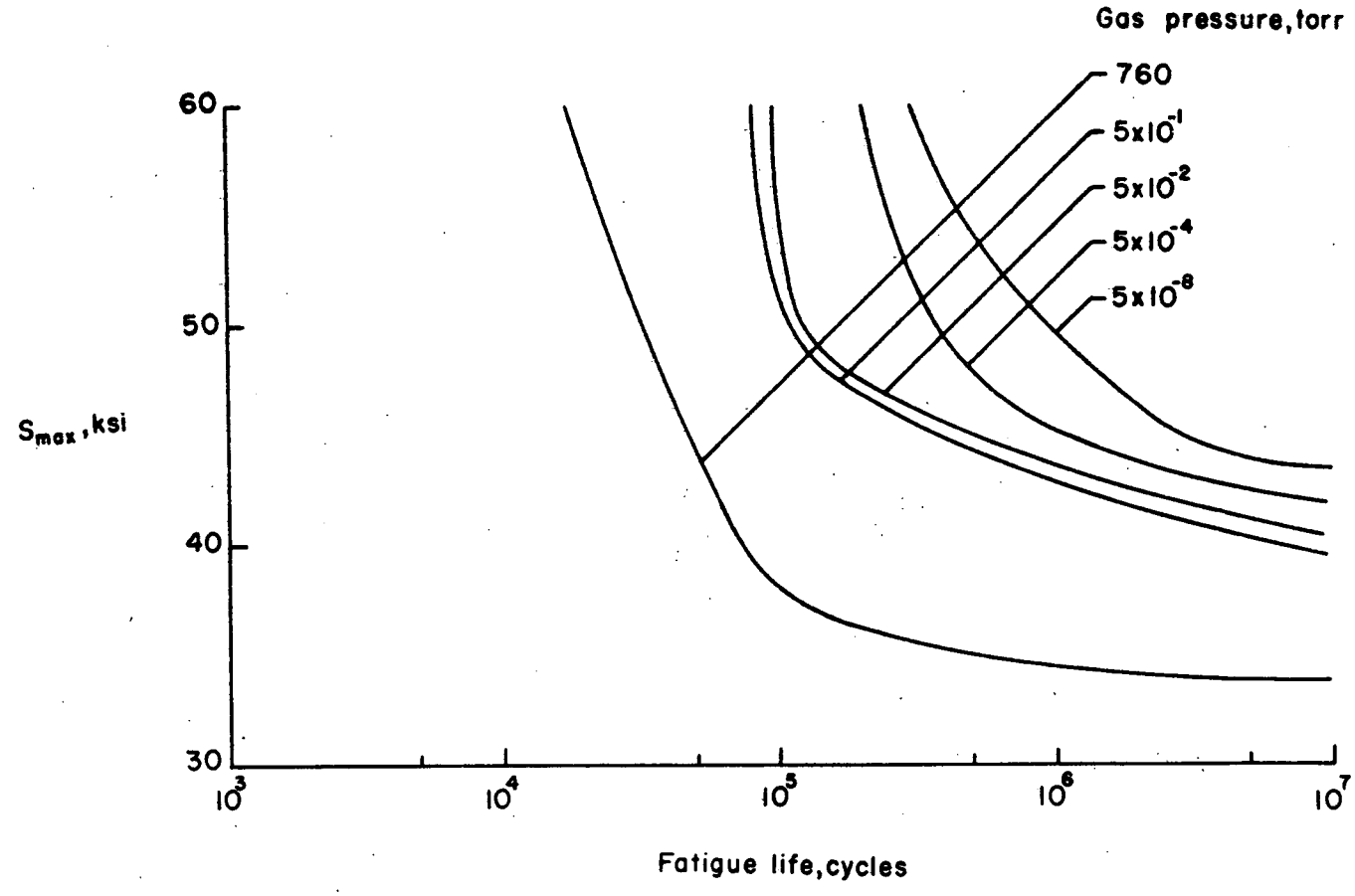

Figure 20.- Combined S-N curves for 7075-T6 obtained at various gas pressures.

strength as N becomes very large") was about 5 ksi higher at $5x10^{-1}$ torr than at 760 torr.

Fatigue lives at $5x10^{-2}$ torr were slightly longer than the fatigue lives at $5x10^{-1}$ torr, and the fatigue limit slightly higher at $5x10^{-2}$ torr than at $5x10^{-1}$ torr.

Fatigue lives at $5x10^{-4}$ torr were ten to twenty times longer than at 760 torr, and the fatigue limit approximately 8 ksi higher at $5x10^{-4}$ torr.

Fatigue lives at $5x10^{-8}$ torr were fifteen to thirty times longer than at 760 torr, and the fatigue limit about 11 ksi higher at $5x10^{-8}$ torr.

The fatigue data from tests at 760 torr are also plotted in figure 21. Included in this figure is the scatterband (crossshatched area) from fatigue tests conducted on unnotched specimens made from the same lot of 7075-T6 used in the present investigation. The fatigue tests used to generate the scatterband were conducted approximately twenty years ago (see Grover, Bishop and Jackson (1951)). These earlier tests were conducted in air and at a stress ratio of 0.02, the same environment and stress ratio used in the present investigation. Comparison of the data from the present investigation with the scatterband from the data generated twenty years ago indicates the fatigue resistance of the 7075-T6 has decreased by a factor of one and one-half to three (depending upon the stress level) and that the fatigue limit has decreased by about 3 ksi.

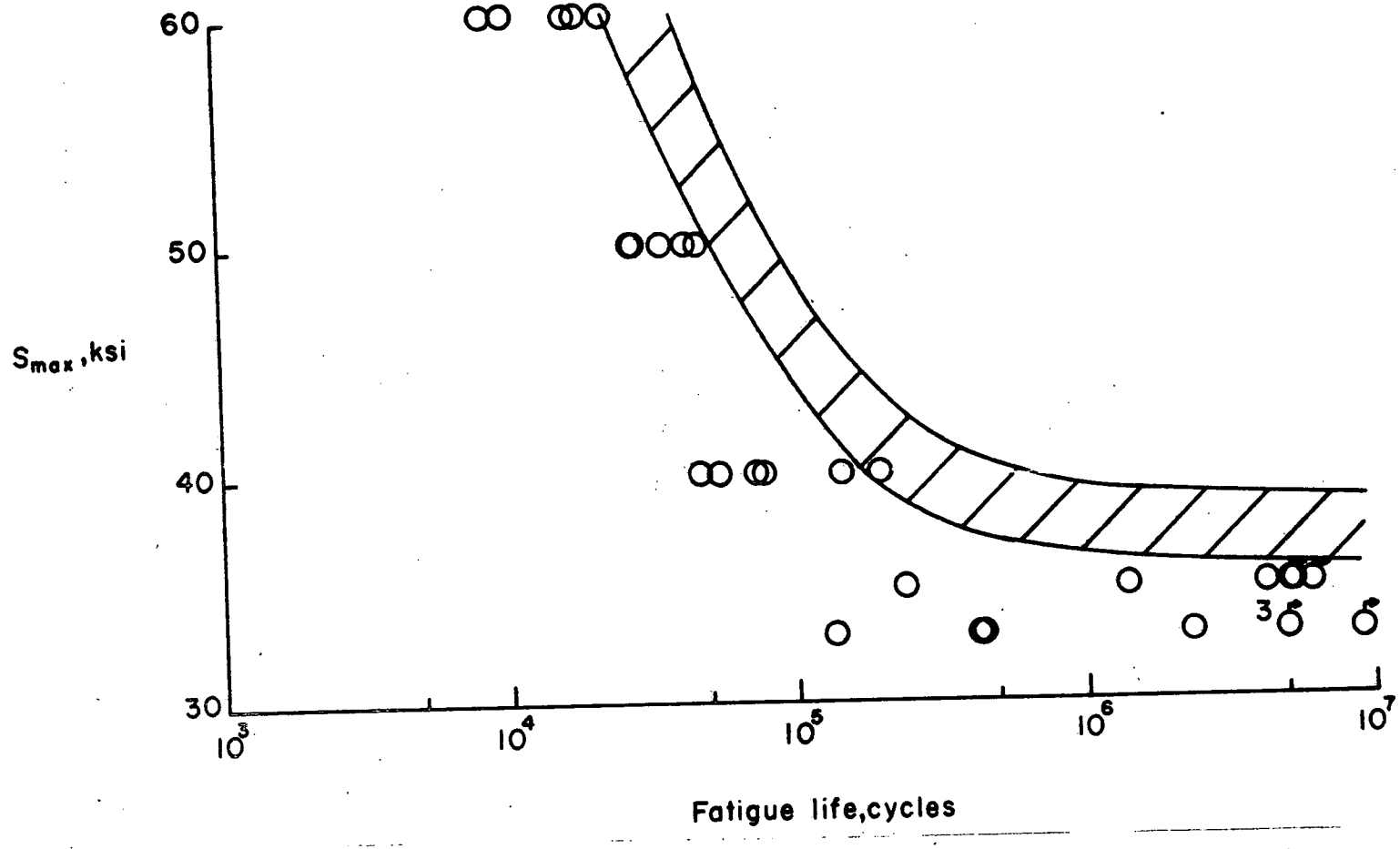

Figure 21.- Variation of fatigue life with stress for 7075-T6 at 760 torr. The crosshatched area represents the scatterband from tests conducted on the same lot of material twenty years ago.

It should be noted here however, that the tensile properties, i.e., σ_{us}, σ_{ys}, E, and e, for this lot of 7075-T6 were essentially unchanged over the twenty year period.

Fatigue-Crack-Propagation Experiments

The results of the fatigue-crack-propagation tests conducted on centrally-notched sheet specimens made of 7075-T6 aluminum alloy are listed in Tables 12 and 13. These tests were conducted at gas pressures of 760 and 5×10^{-8} torr. In these tests the fatigue cracks typically initiated at both ends of the central notch and propagated towards the edges of the specimen. (The difference in the lengths of the two cracks, measured from the centerline of the specimen, seldom exceeded 0.05 inch.) Consequently Tables 12 and 13 give the number of cycles, N_{ip}, required to initiate the fatigue cracks at each end of the central notch and to propagate them to the specified half-lengths, a, on both sides (right and left) of the centerline.

Fatigue-crack-propagation rates, da/dN, were determined graphically by taking the slopes of the half-crack length against cycles curves (plotted on a linear scale) at various crack lengths. These rates are plotted against the stress-intensity range, ΔK, in figures 22 and 23. (A discussion of the use of the stress-intensity range in correlating fatigue-crack-propagation data is given in Appendix B.) Examination of figures 22 and 23 indicates that the rate of fatigue-crack-propagation in 7075-T6 aluminum alloy at 760 and 5×10^{-8} torr is in general a single-valued function of ΔK. A composite plot, figure

Table 12. Number of cycles required to initiate and propagate fatigue cracks in air (760 torr) to the specified crack lengths.

Specimen Number B58N7-10P

S_{max}, 40 ksi		S_{mean}, 20.4 ksi	S_{min}, 0.8 ksi
a(left side), in.	N_{ip}, cycles	a(right side), in.	N_{ip}, cycles
0.10	1450	0.10	1350
.15	1930	.15	1930
.20	2110	.20	2140
.25	2270	.25	2270
.30	2360	.30	2360
.35	2400	.35	2400

Specimen Number B52N7-8P

S_{max}, 40 ksi		S_{mean}, 20.4 ksi	S_{min}, 0.8 ksi
a(left side), in.	N_{ip}, cycles	a(right side), in.	N_{ip}, cycles
0.10	1530	0.10	1350
.15	2180	.15	2060
.20	2420	.20	2360
.25	2530	.25	2490
.30	2610	.30	2610

Table 12 (continued).

Specimen Number B52N7-10P

S_{max}, 30 ksi		S_{mean}, 15.3 ksi	S_{min}, 0.6 ksi
a(left side), in.	N_{ip}, cycles	a(right side), in.	N_{ip}, cycles
0.10	3340	0.10	3190
.15	4350	.15	4350
.20	5080	.20	5080
.25	5530	.25	5530
.30	5770	.30	5770
.35	5890	.35	5890

Specimen Number B51N7-10P

S_{max}, 30 ksi		S_{mean}, 15.3 ksi	S_{min}, 0.6 ksi
a(left side), in.	N_{ip}, cycles	a(right side), in.	N_{ip}, cycles
0.10	2990	0.10	2750
.15	4320	.15	4140
.20	4920	.20	4790
.25	5260	.25	5120
.30	5510	.30	5460
.35	5680	.35	5650
		.40	5700

Table 12 (continued).

Specimen Number B59N7-110P

S_{max}, 20 ksi		S_{mean}, 10.2 ksi	S_{min}, 0.4 ksi
a(left side), in.	N_{ip}, cycles	a(right side) in.	N_{ip}, cycles
0.10	8710	0.10	9050
.15	12350	.15	12700
.20	14560	.20	14560
.25	16350	.25	16350
.30	17480	.30	17480
.35	18040	.35	18110
.40	18680	.40	18860
.45	19120	.45	19170

Specimen Number B57N7-2P

S_{max}, 20 ksi		S_{mean}, 10.2 ksi	S_{min}, 0.4 ksi
a(left side), in.	N_{ip}, cycles	a(right side), in.	N_{ip}, cycles
0.10	10020	0.10	10090
.15	13200	.15	13510
.20	15690	.20	16240
.25	17280	.25	17710
.30	18460	.30	18860
.35	19480	.35	19690
.40	19980	.40	20200
.45	20440	.45	20500
.50	20510		

Table 12 (continued).

Specimen Number B57N7-4P

S_{max}, 15 ksi		S_{mean}, 7.65 ksi	S_{min}, 0.3 ksi
a(left side), in.	N_{ip}, cycles	a(right side) in.	N_{ip}, cycles
0.09	21970	0.11	23610
.14	29980	.16	31090
.19	34640	.21	35270
.24	38630	.26	39410
.29	41420	.31	41680
.34	43460	.36	43530
.39	44960	.41	45190
.44	46160	.46	46290
.49	47030	.51	47170
.54	47750	.56	47850

Table 12 (continued).

Specimen Number B58N7-6P

S_{max}, 15 ksi		S_{mean}, 7.65 ksi	S_{min}, 0.3 ksi
a(left side), in.	N_{ip}, cycles	a(right side), in.	N_{ip}, cycles
0.10	22200	0.10	21230
.15	29440	.15	28750
.20	32950	.20	32950
.25	36730	.25	36730
.30	39330	.30	39300
.35	41230	.35	41140
.40	42780	.40	42350
.45	43900	.45	43760
.50	44750	.50	44620
.55	45320	.55	45230

Specimen Number B56N7-2P

S_{max}, 10 ksi		S_{mean}, 5.1 ksi	S_{min}, 0.2 ksi
a(left side), in.	N_{ip}, cycles	a(right side), in.	N_{ip}, cycles
0.10	157150	0.10	159440
.15	192370	.15	193570
.20	209310	.20	210430
.25	218290	.25	219000
.30	224730	.30	224960
.35	230000	.35	229680
.40	233860	.40	233310
.45	237220	.45	236610
.50	239800	.50	239410
.55	241970	.55	241380

Table 12 (continued).

Specimen Number B53N7-6P

S_{max}, 10 ksi		S_{mean}, 5.1 ksi	S_{min}, 0.2 ksi
a(left side), in.	N_{ip}, cycles	a(right side) in.	N_{ip}, cycles
0.10	118960	0.10	140600
.15	163400	.15	172030
.20	179030	.20	182870
.25	187560	.25	190780
.30	194370	.30	196410
.35	199590	.35	201650
.40	203700	.40	205430
.45	206850	.45	208250
.50	209620	.50	210570
.55	212390	.55	212890

Table 13. Number of cycles required to initiate and propagate fatigue cracks in vacuum (5×10^{-8} torr) to the specified crack lengths.

Specimen Number B53N7-10P

S_{max}, 40 ksi		S_{mean}, 20.4 ksi	S_{min}, 0.8 ksi
a(left side), in.	N_{ip}, cycles	a(right side) in.	N_{ip}, cycles
0.10	2650	0.10	2750
.15	3200	.15	3260
.20	3410	.20	3410
.25	3500	.25	3500
.30	3600	.30	3600

Specimen Number B57N7-6P

S_{max}, 40 ksi		S_{mean}, 20.4 ksi	S_{min}, 0.8 ksi
a(left side), in.	N_{ip}, cycles	a(right side) in.	N_{ip}, cycles
0.10	2340	0.10	2470
.15	3060	.15	3100
.20	3380	.20	3430
.25	3540	.25	3570
.30	3650	.30	3650

Table 13 (continued).

Specimen Number B60N7-6P

S_{max}, 30 ksi		S_{mean}, 15.3 ksi	S_{min}, 0.6 ksi
a(left side), in.	N_{ip}, cycles	a(right side) in.	N_{ip}, cycles
0.10	8160	0.10	7110
.15	10330	.15	10100
.20	11190	.20	11090
.25	11710	.25	11680
.30	12000	.30	11970
.35	12170	.35	12170

Specimen Number B57N7-10P

S_{max}, 30 ksi		S_{mean}, 15.3 ksi	S_{min}, 0.6 ksi
a(left side), in.	N_{ip}, cycles	a(right side) in.	N_{ip}, cycles
0.10	7250	0.10	8250
.15	9130	.15	9590
.20	9870	.20	10180
.25	10340	.25	10530
.30	10640	.30	10780
.35	10830		

Table 13 (continued).

Specimen Number B56N7-10P

S_{max}, 20 ksi		S_{mean}, 10.2 ksi	S_{min}, 0.4 ksi
a(left side), in.	N_{ip}, cycles	a(right side) in.	N_{ip}, cycles
0.10	39740	0.10	37510
.15	44510	.15	43460
.20	48700	.20	47810
.25	51150	.25	50740
.30	52360	.30	52610
.35	53100	.35	53490
.40	53600	.40	53950
.45	53950		

Specimen Number B55N7-6P

S_{max}, 20 ksi		S_{mean}, 10.2 ksi	S_{min}, 0.4 ksi
a(left side), in.	N_{ip}, cycles	a(right side) in.	N_{ip}, cycles
0.10	31380	0.10	30430
.15	38160	.15	38160
.20	42780	.20	42710
.25	45130	.25	45370
.30	46570	.30	46810
.35	47600	.35	48370
.40	48270	.40	48890
.45	48800		

Table 13 (continued).

Specimen Number B55N7-4P

S_{max}, 15 ksi		S_{mean}, 7.65 ksi	S_{min}, 0.3 ksi
a(left side), in.	N_{ip}, cycles	a(right side) in.	N_{ip}, cycles
0.10	367570	0.10	Not recorded
.15	382340	.15	363620
.20	391170	.20	379860
.25	398060	.25	389350
.30	402440	.30	394980
.35	404540	.35	400720
.40	406750	.40	403340
.45	407840	.45	405780
.50	408910	.50	407470
.55	409500	.55	408540
.60	409870	.60	409250
		.65	409820

Table 13 (continued).

Specimen Number B56N7-6P

S_{max}, 15 ksi		S_{mean}, 7.65 ksi	S_{min}, 0.3 ksi
a(left side), in.	N_{ip}, cycles	a(right side) in.	N_{ip}, cycles
0.10	187600	0.10	187130
.15	207720	.15	206400
.20	219040	.20	218130
.25	225540	.25	224250
.30	230260	.30	230030
.35	233410	.35	233220
.40	235860	.40	235560
.45	237030	.45	237230
.50	238230	.50	238410
.55	238960	.55	239120

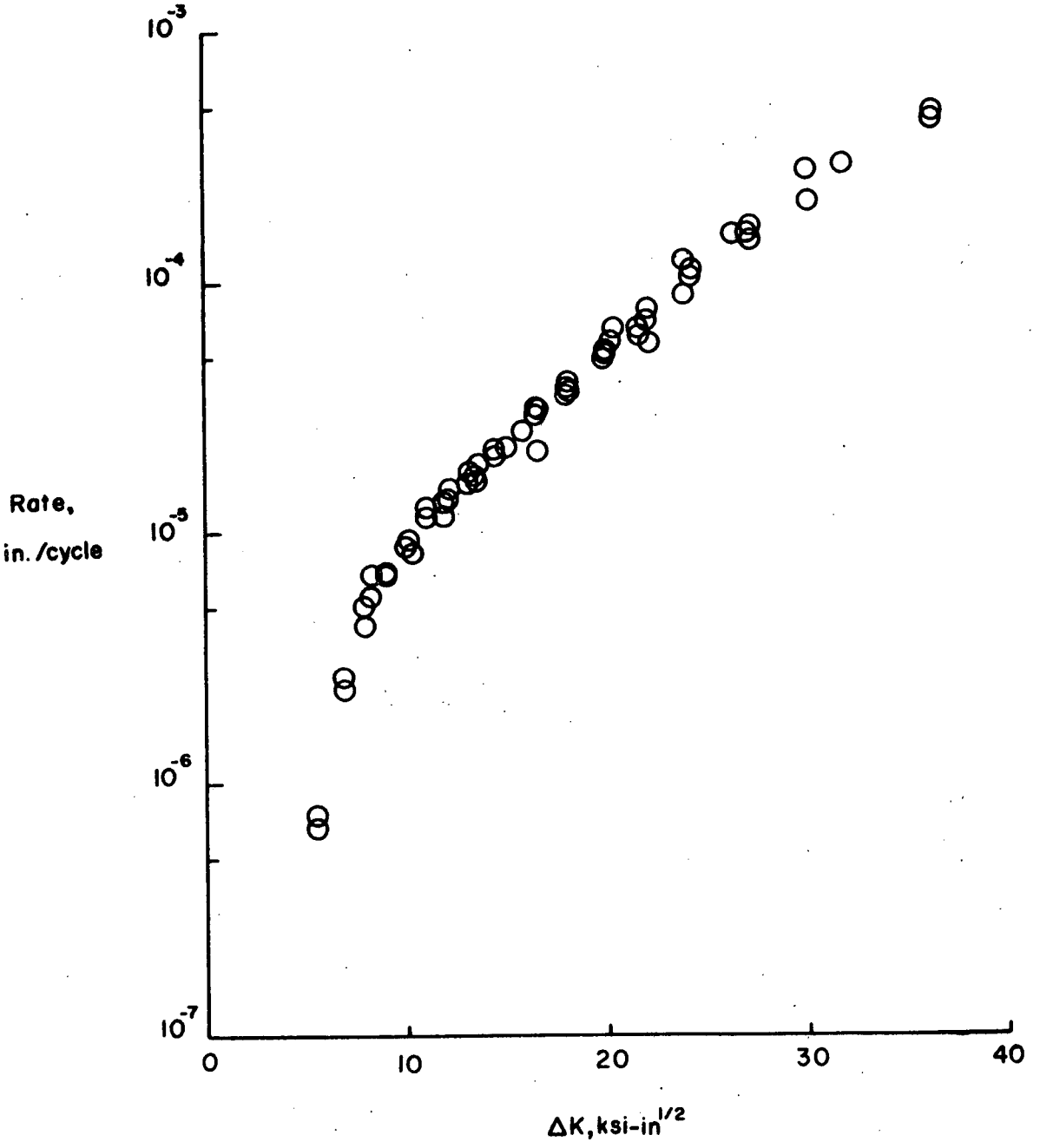

Figure 22.- Variation of fatigue-crack-growth rate with ΔK in 7075-T6 at 760 torr.

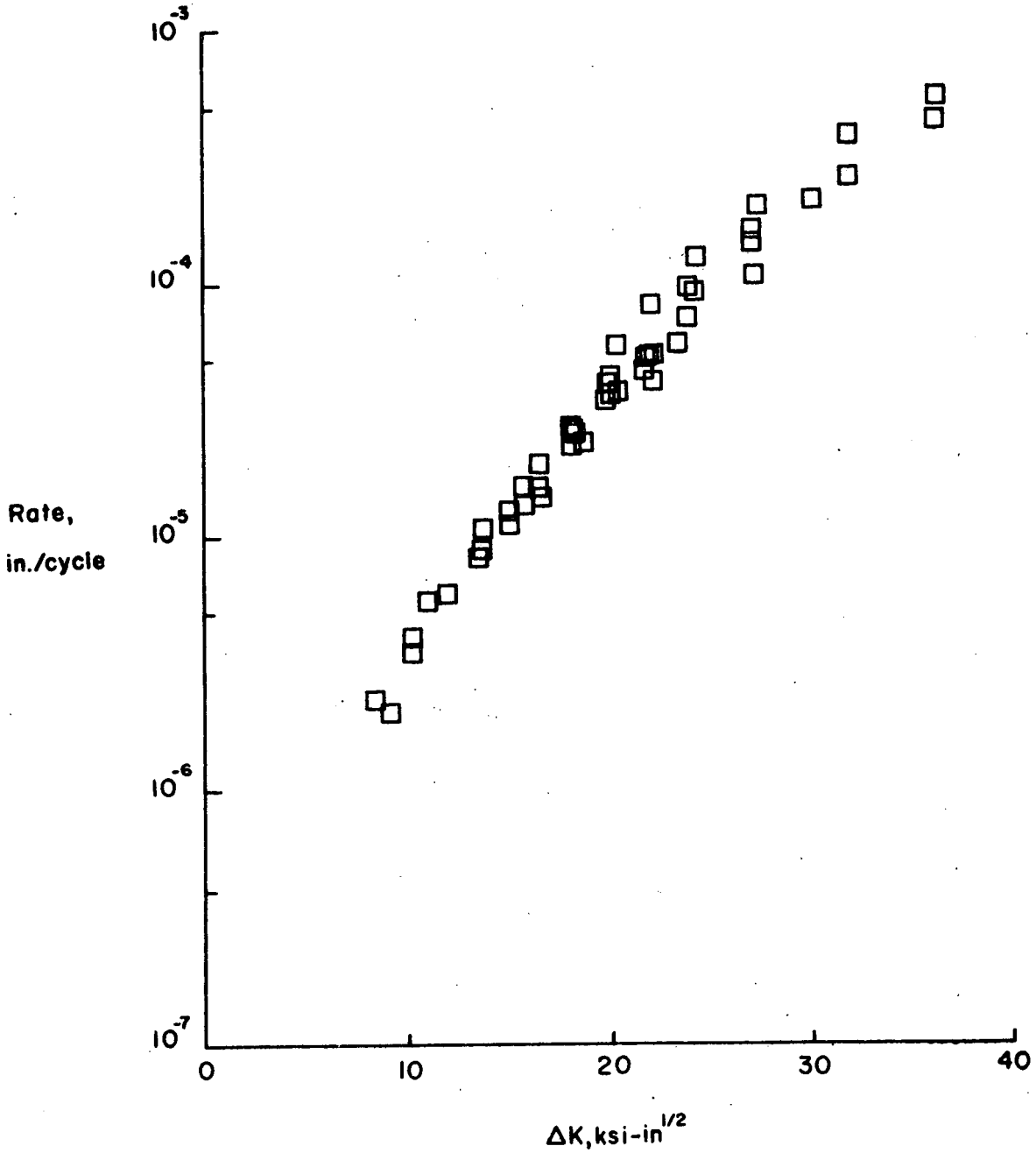

Figure 23.- Variation of fatigue-crack-growth rate with ΔK in 7075-T6 at 5 X 10^{-8} torr.

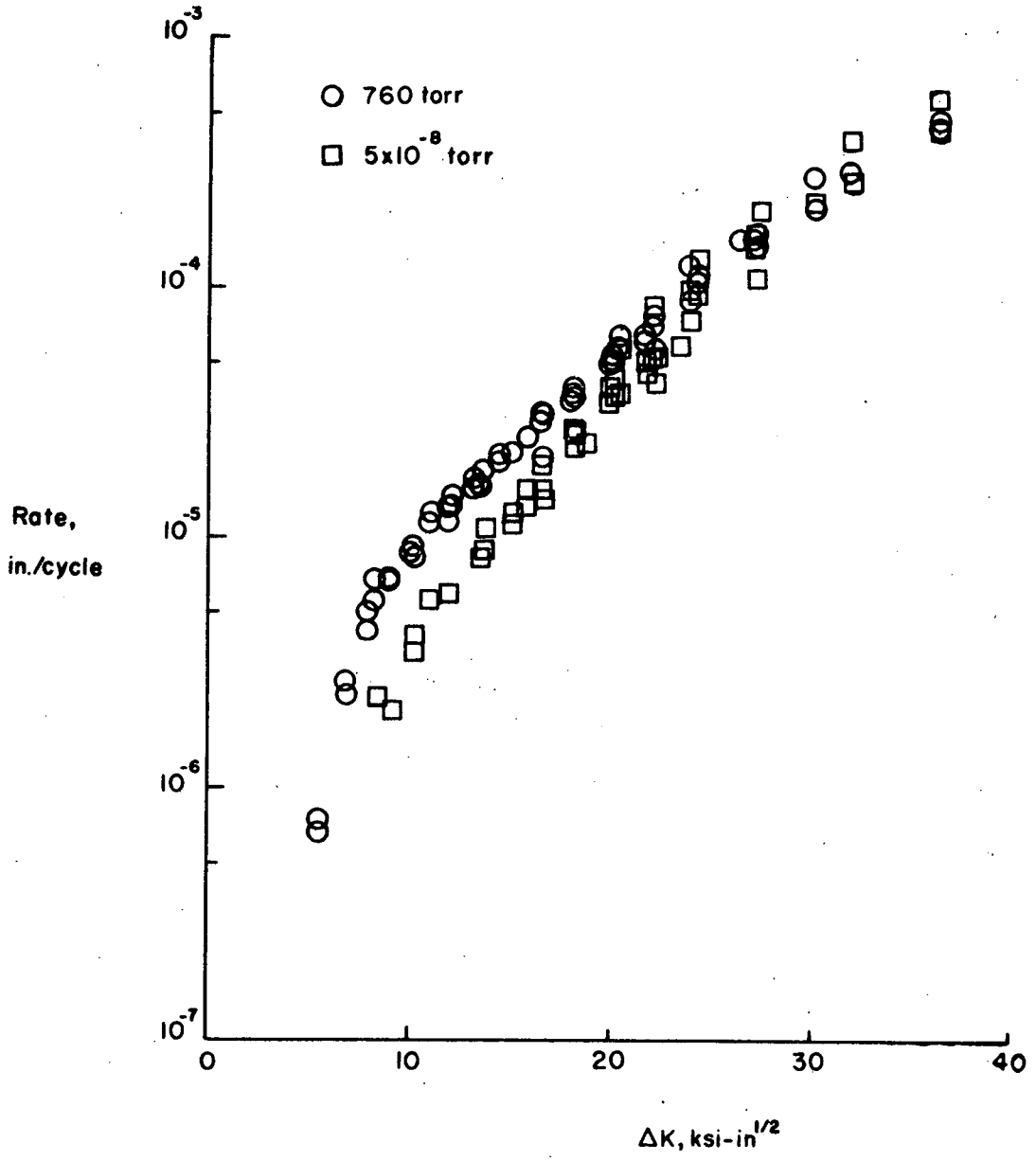

Figure 24.- Variation of fatigue-crack-growth rate with ΔK in 7075-T6 at 760 and 5 X 10^{-8} torr.

24, of the data from figures 22 and 23 shows that at the lower values of ΔK the fatigue-crack-propagation rates were approximately twice as high at a gas pressure of 760 torr than at a 5×10^{-8} torr. At the higher values of ΔK however, the fatigue crack-propagation rates were about the same in vacuum and in air.

An empirical fatigue-crack-propagation equation developed by Forman, Kearney and Engle (1967) was fitted to the rate data. This equation, relating the rate of fatigue-crack-propagation, the stress-intensity range, the stress ratio, and the critical stress-intensity factor at failure, produced an excellent fit to the data from tests at both 760 and 5×10^{-8} torr gas pressure. The equation was, of course, fitted to the two sets of data separately, figures 25 and 26. Least-squares techniques were used to determine the appropriate empirical constants in Forman, Kearney, and Engle's equation. This equation has the form

$$\text{Rate} = \frac{C(\Delta K)^n}{(1-R)K_c - \Delta K} \qquad (1)$$

where C and n are the empirical constants. The values of K_c for 7075-T6 at 760 and 5×10^{-8} torr were determined in the fracture toughness portion of this investigation.

The empirical constants C and n in equation (1) were determined to have values of 5.19×10^{-11} and 2.44 respectively for a gas pressure of 760 torr, and to have values of 1.19×10^{-13} and 3.02 respectively for a gas pressure of 5×10^{-8} torr. Having determined these constants, equation (1) can be used to predict fatigue crack growth behavior in 7075-T6 aluminum alloy at gas pressures of 760 and 5×10^{-8} torr. Numerical

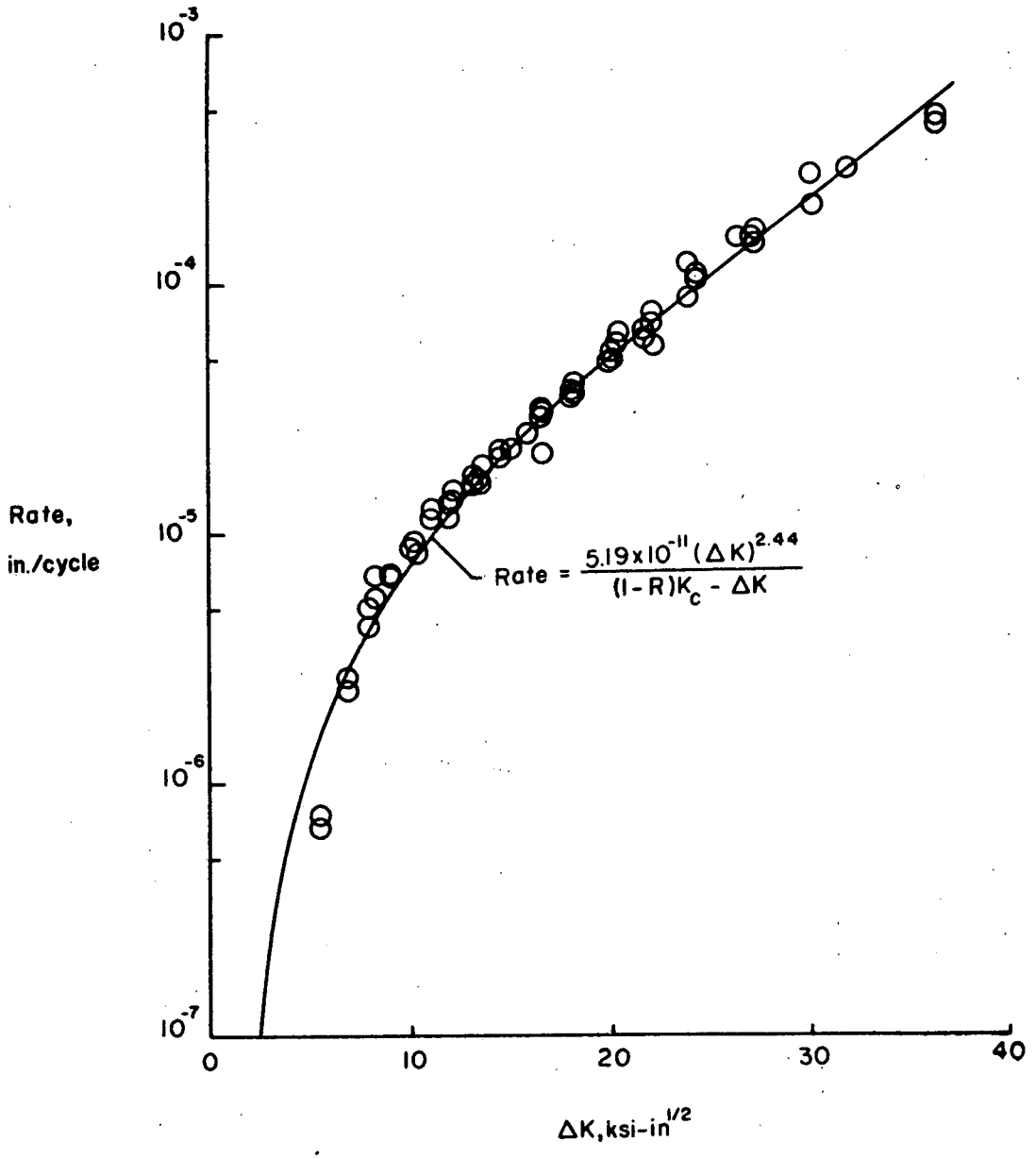

Figure 25.- Correlation of fatigue-crack-growth data from tests at 760 torr with Forman, Kearney, and Engle's equation.

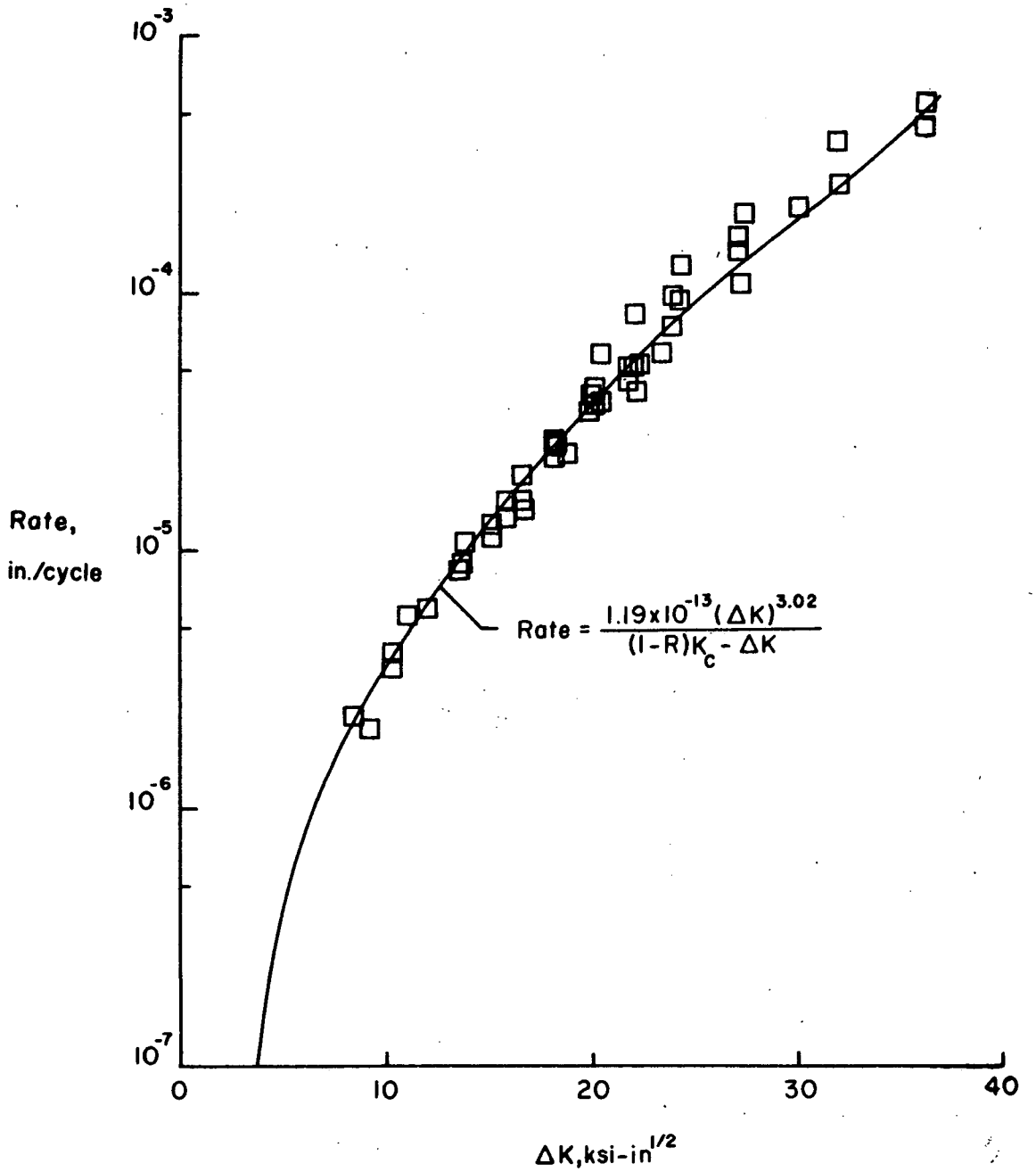

Figure 26.- Correlation of fatigue-crack-growth data from tests at 5×10^{-8} torr with Forman, Kearney, and Engle's equation.

integration of equation (1) is relatively simple on a digital computer, and in-house studies at NASA-Langley have shown that accurate prediction of fatigue-crack-growth curves can be made using such procedures for constant amplitude loading conditions. However, the reader is cautioned against using such procedures to predict fatigue-crack-growth curves for random loading conditions. Significant delays in fatigue-crack growth occur when lower amplitude stress cycles are preceded by stress cycles of significantly higher stress amplitude. The extent of these delays are discussed in reports by Hudson and Hardrath (1961), and Hudson and Raju (1970). Additional research aimed at developing methods of predicting these delays is being actively pursued at NASA-Langley at the present time.

Average fatigue-crack-growth curves were determined for specimens tested at 40, 30, 20, and 15 ksi, figures 27, 28, 29 and 30, respectively. Individual average curves were determined for specimens tested at 760 and 5×10^{-8} torr. These average curves (which are referenced from a half-crack length of 0.10 inch for convenience) show that at 15 ksi approximately twice as many cycles were required to propagate a crack from a half-crack length of 0.10 inch to a given half-crack length when the test was conducted at 5×10^{-8} torr. However, as the stress level was increased, the difference in the number of cycles required to reach a given half-crack length became progressively smaller, and at 40 ksi about the same number of cycles were required to propagate the crack from a half-crack length of 0.10 inch to a given half-crack length in vacuum and in air.

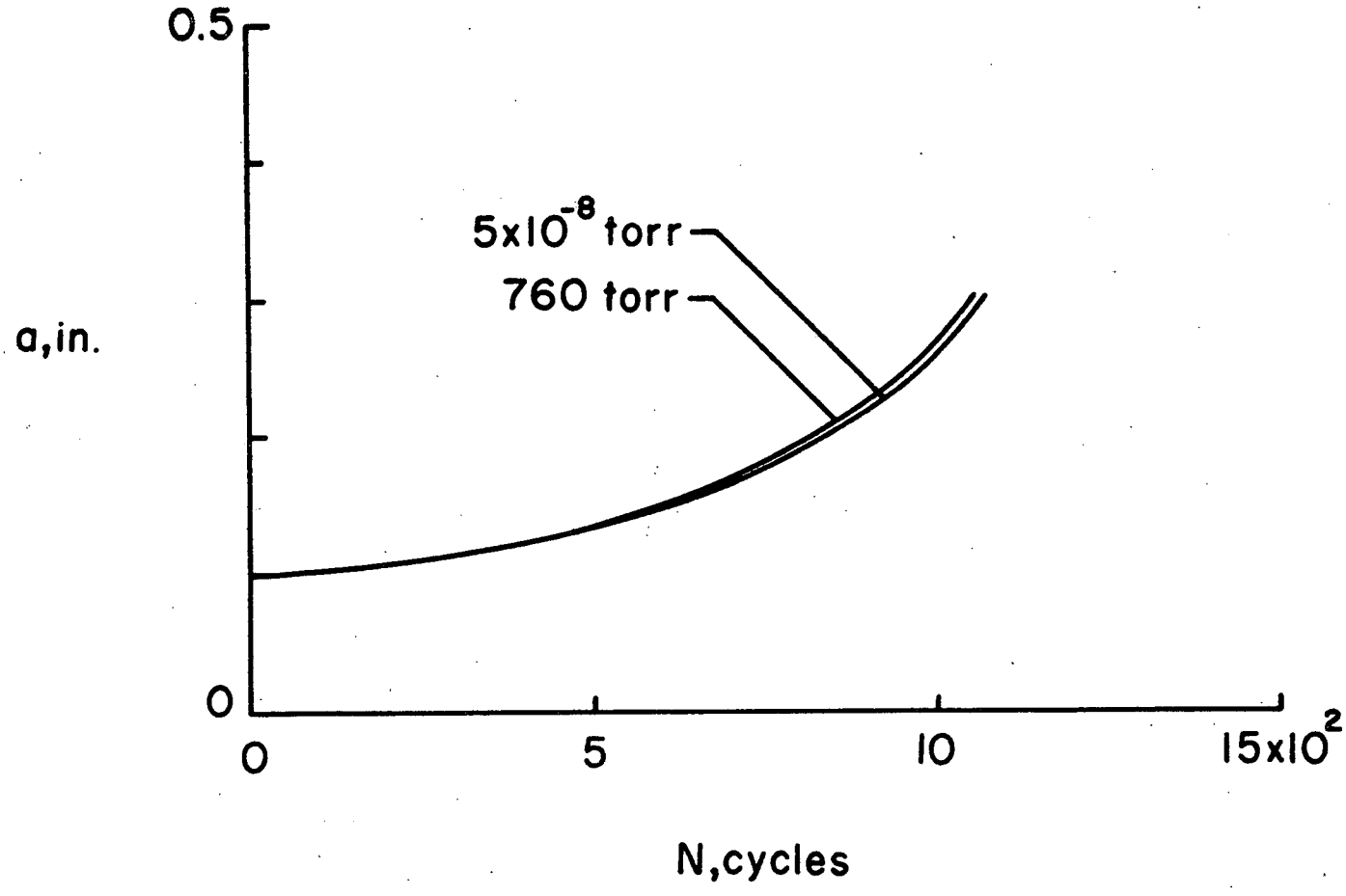

Figure 27.- Average fatigue-crack-growth curves for 7075-T6. S_{max} = 40 ksi.

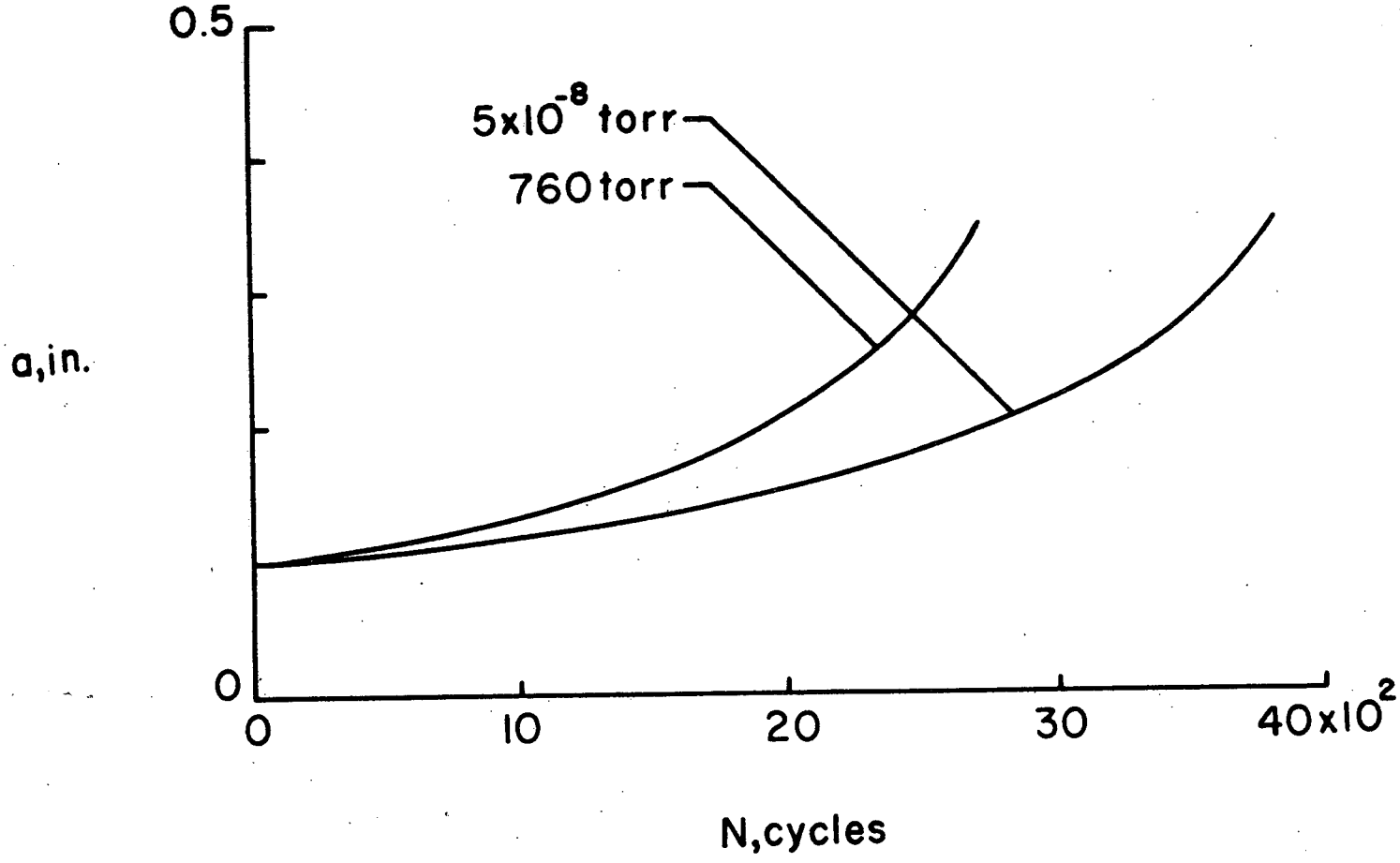

Figure 28.- Average fatigue-crack-growth curves for 7075-T6. S_{max} = 30 ksi.

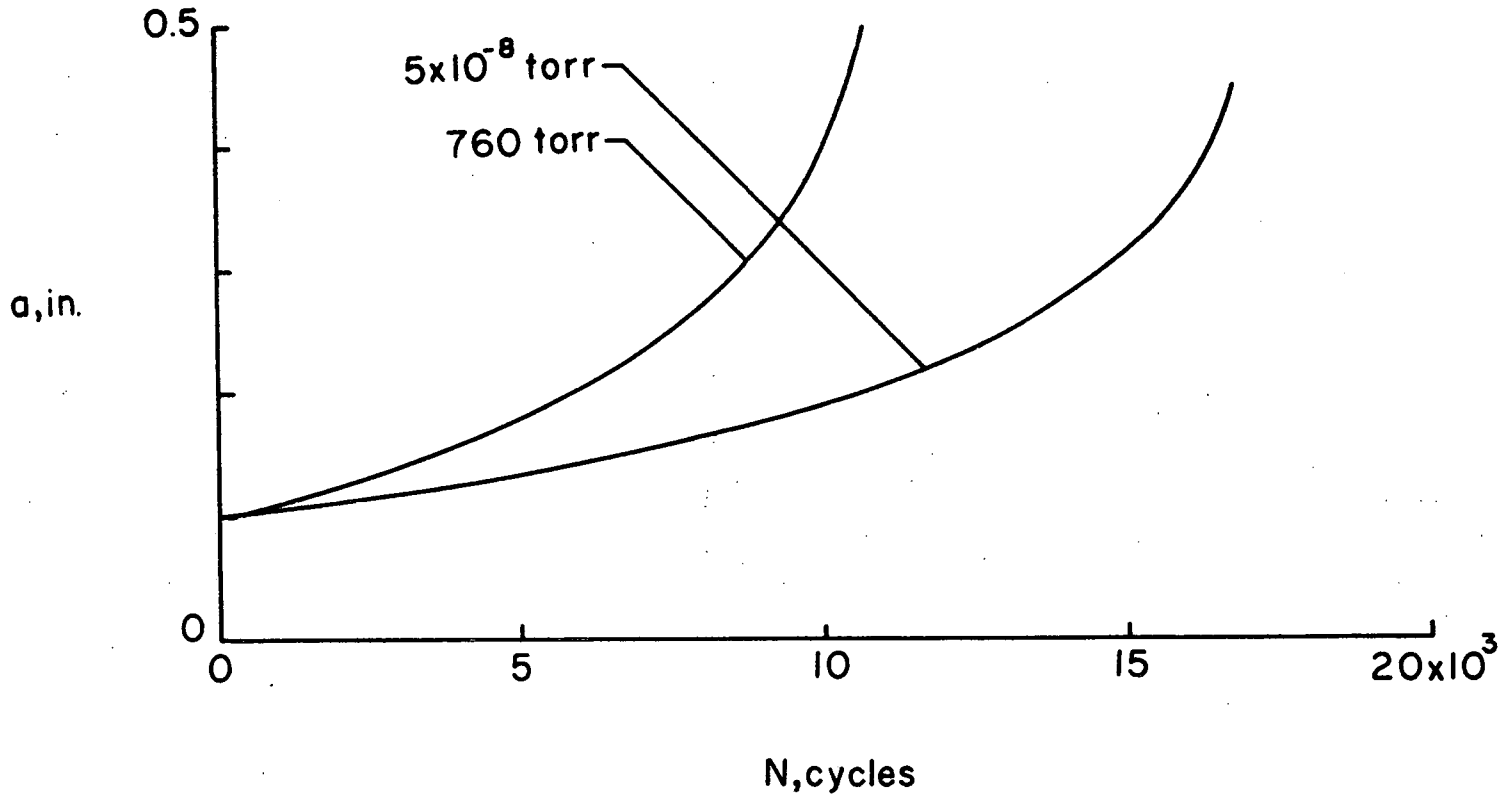

Figure 29.- Average fatigue-crack-growth curves for 7075-T6. S_{max} = 20 ksi.

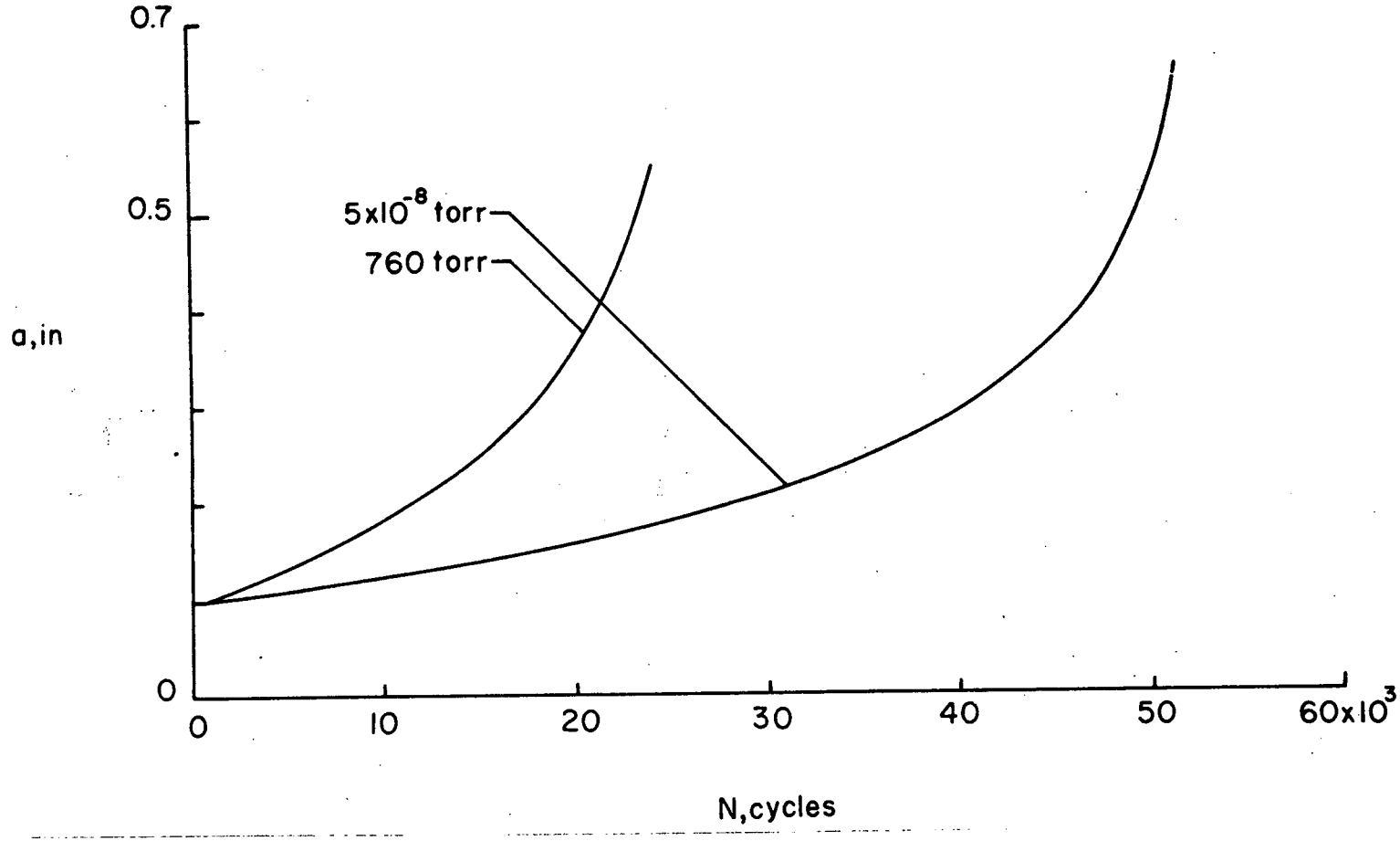

Figure 30.- Average fatigue-crack-growth curves for 7075-T6. S_{max} = 15 ksi.

The average number of cycles required to initiate a fatigue crack and propagate it to a half-crack length of 0.10 inch was also determined for the fatigue-crack-propagation specimens. A plot of maximum stress in the test against the following ratio:

$$\frac{\text{Number of cycles required to obtain a 0.10-inch half-crack length in vacuum}}{\text{Number of cycles required to obtain a 0.10-inch half-crack length in air}}$$

in figure 31. These ratios ranged from 1.8 for tests at 40 ksi to somewhere in excess of 27 for tests at 10 ksi. (Fatigue cracks could not be initiated in vacuum at 10 ksi in 3,909,250 cycles. Consequently testing at that stress level in vacuum was abandoned to expedite testing.) Obviously the vacuum environment had a significantly greater effect on the initiation and propagation of the fatigue cracks to a half-crack length of 0.10 inch than on subsequent fatigue-crack propagation.

Consideration of the facts that (a) the vacuum environment had a significantly greater effect on the initiation and propagation of the fatigue cracks to a half-crack length of 0.10 inch than on subsequent fatigue-crack propagation and (b) that the difference between the number of cycles required to reach a given half-crack length in vacuum and air seldom exceeded a factor of two, while the difference between fatigue lives in vacuum and air ranged from fifteen to thirty (at 5×10^{-8} torr), indicates that for 7075-T6 aluminum alloy the fatigue-crack initiation phase is affected by environment to a much greater extent than the fatigue-crack-propagation phase.

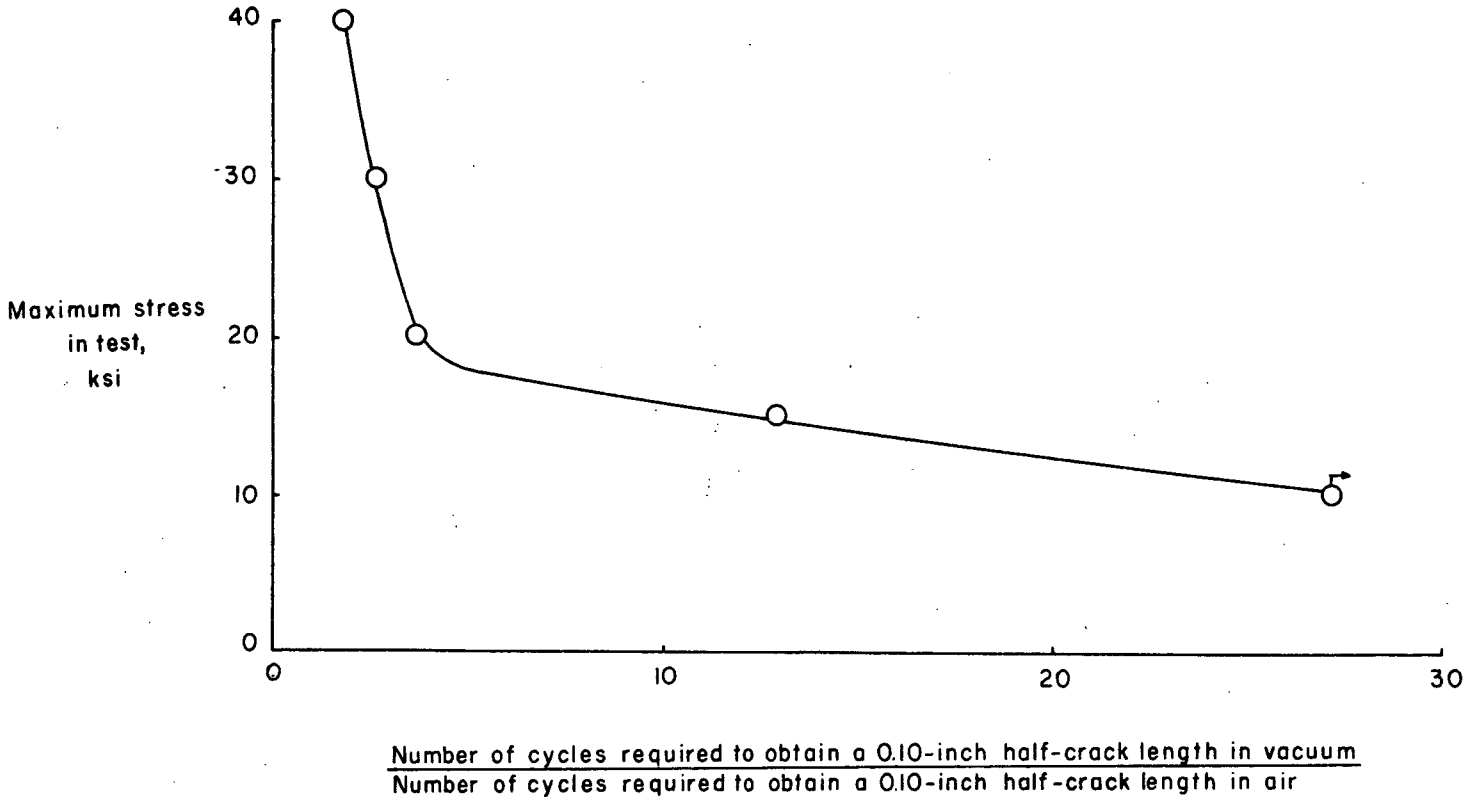

Figure 31.- Variation of the crack-initiation ratio with S_{max}.

Fracture-Toughness Experiments

The stress intensity analysis method used in the analysis of the fracture toughness data is briefly described in Appendix B. The experimental results of the fracture toughness experiments are shown in Tables 14, and 15, and in figures 32 and 33. In these figures the critical stress intensity factor at failure, K_c, is plotted against the half-crack length at failure, a_c. At both 760 and 5×10^{-8} torr the values of K_c are reasonably constant for all values of crack length. These values deviate from the mean value by no more than 8706 psi-$in^{1/2}$. Also, there is virtually no difference between the mean values of K_c in vacuum and in air.

X-Ray Stress Analysis

Results of the residual stress measurements made using X-ray stress analysis techniques are presented in Table 16. This table lists the residual stresses measured in the critical section of selected unnotched fatigue test specimens. These measurements were made on the two flat sides (i.e., the numbered and unnumbered sides) of the test specimens. Also included in this table are the maximum stress applied in fatigue tests on the specimens, the fatigue lives of the test specimens, the gas pressure at which the fatigue tests were conducted, and pertinent remarks relative to the X-ray data. Inspection of Table 16 shows that after polishing approximately 60 percent of the test specimens contained compressive residual stresses on both sides, 36 percent of the specimens contained compressive residual stresses on one side

Table 14. Data from fracture-toughness tests on 7075-T6 specimens tested in air (760 torr).

Specimen Number	a_c, inches	P_c, lbf	A, $(\text{inches})^2$	K_c $\text{psi-in}^{1/2}$
B59N7-10P	0.50	6583	0.1854	51796
B58N7-6P	0.59	5539	0.1888	50034
B58N7-10P	0.42	8374	0.1905	56062
B57N7-4P	0.59	5502	0.1919	48897
B55N7-10P	0.26	9978	0.1871	49677
B52N7-10P	0.40	8094	0.1865	53370
B57N7-8P	0.22	11097	0.1913	49302
B53N7-6P	0.63	4980	0.1871	41553
B52N7-8P	0.39	8094	0.1873	52333
B56N7-2P	0.58	5166	0.1888	45952
B57N7-2P	0.54	6453	0.1917	52644
B51N7-10P	0.42	7460	0.1848	51483

$K_{c_{avg}} = 50259$

Table 15. Data from fracture-toughness tests on 7075-T6 specimens tested in vacuum (5x10-8 torr).

Specimen Number	a_c, inches	P_c, lbf	A, $(\text{inches})^2$	K_c $\text{psi-in}^{1/2}$
B56N7-6P	0.64	5259	0.1875	52374
B55N7-4P	0.67	4252	0.1880	44666
B56N7-10P	0.47	6639	0.1894	48479
B55N7-6P	0.47	6416	0.1856	47810
B60N7-6P	0.40	7488	0.1863	49383
B57N7-10P	0.42	7814	0.1922	51851
B53N7-10P	0.39	8598	0.1859	56062
B57N7-6P	0.40	7612	0.1903	49146
B58N7-4P	0.24	10369	0.1850	50753
B53N7-2P	0.28	10090	0.1867	52884

$K_{c_{avg}} = 50341$

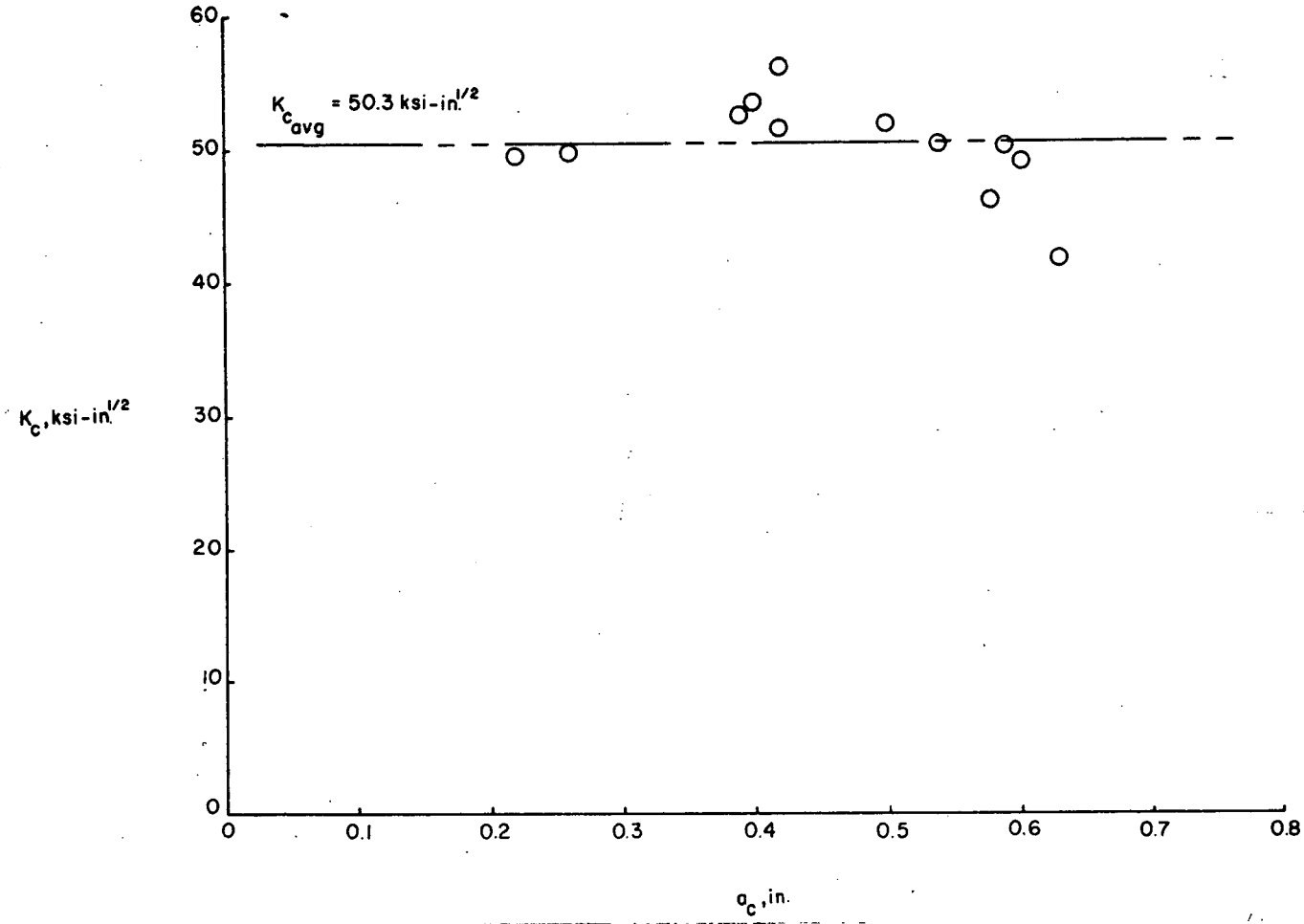

Figure 32.- Variation of K_c with a_c at 760 torr.

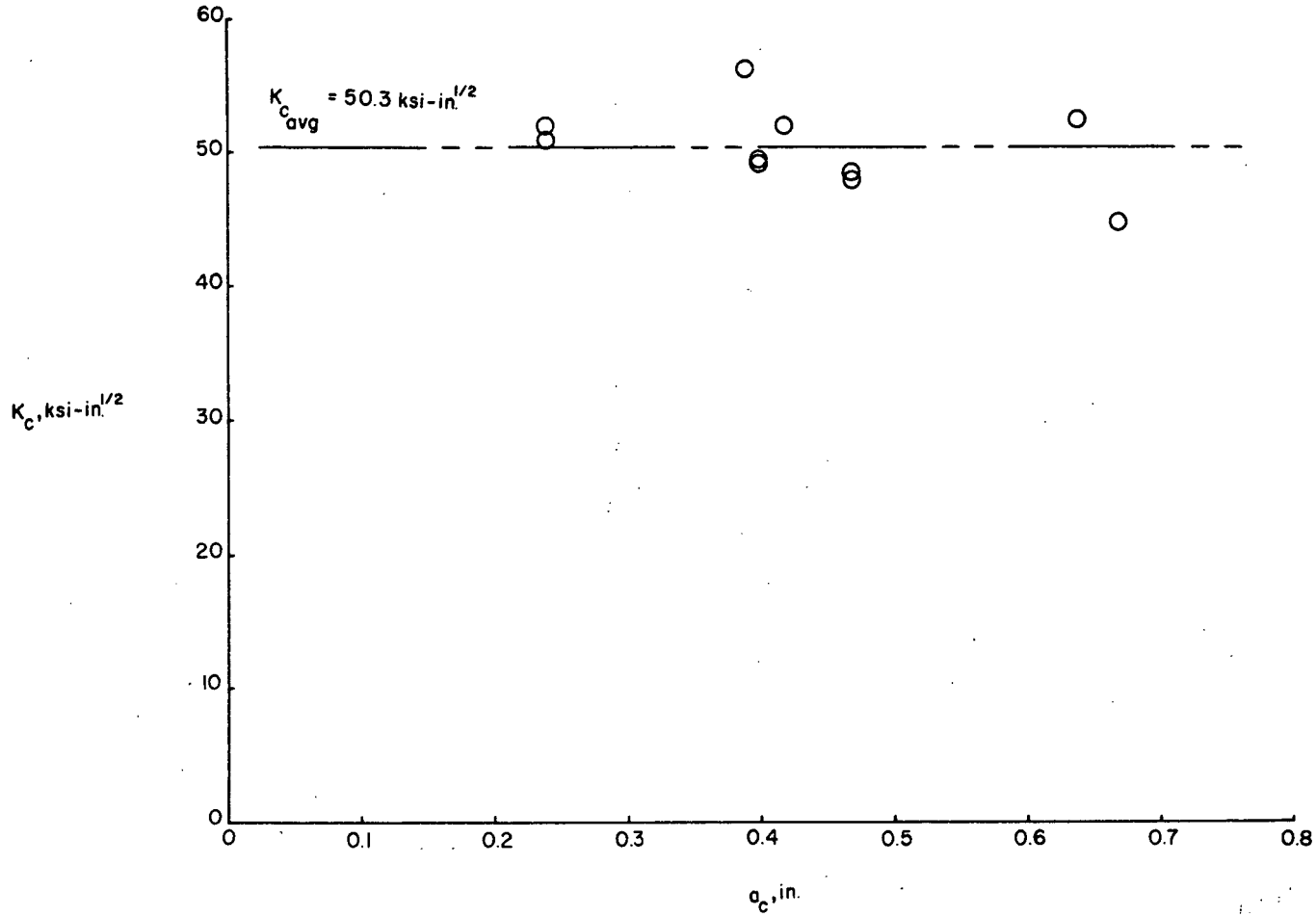

Figure 33.- Variation of K_c with a_c at 5 X 10^{-8} torr.

Table 16. Measurement of residual stresses in unnotched fatigue life specimens.

Specimen Number	Residual Stress on Numbered Side, ksi	Residual Stress on Unnumbered Side, ksi	Maximum Stress Applied in Test, ksi	Fatigue Life, Cycles	Gas Pressure, torr	When X-rayed
B52N7-1	0.5	-0.1	50	251,960	$5X10^{-4}$	After polishing
B52N7-9	3.3	-0.1	45	>5,000,300	$5X10^{-4}$	After polishing
B53N7-9	-5.2	-12.1		Not Tested		After polishing
B56N7-5	-11.2	-9.4	45	844,830	$5X10^{-1}$	After polishing
B58N7-1	-4.4	-3.3	45	5,197,200	$5X10^{-4}$	After polishing
B58N7-3	-2.6	-5.0	45	375,000	$5X10^{-4}$	After polishing
B59N7-7	-0.4	-2.1	60	379,170	$5X10^{-4}$	After polishing
B60N7-7	-7.8	-6.4	45	1,159,740	$5X10^{-1}$	After polishing
B63N7-102	-1.2	-9.2				Before polishing
B63N7-102	-6.0	-5.0		Not Tested		After polishing
B63N7-103	-5.0	-1.3	45	1,168,970	$5X10^{-2}$	After polishing
B63N7-104	-14.6	-5.4	50	1,319,420	$5X10^{-8}$	After polishing
B63N7-105	-6.2	-1.2	40	>8,086,090	$5X10^{-8}$	After polishing
B63N7-106	0.6	-6.5	40	8,243,790	$5X10^{-8}$	After polishing
B63N7-107	-3.7	-0.1	45	1,956,270	$5X10^{-8}$	After polishing
B63N7-108	-2.3	-4.6				Before polishing
B63N7-108	-3.0	-0.8		Not Tested		After polishing
B63N7-109	-4.9	-5.0		Not Tested		After polishing
B63N7-110	-1.9	-8.9				Before polishing
B63N7-110	-4.4	-1.7		Not Tested		After polishing

Table 16 (continued).

Specimen Number	Residual Stress on Numbered Side, ksi	Residual Stress on Unnumbered Side, ksi	Maximum Stress Applied in Test, ksi	Fatigue Life, Cycles	Gas Pressure, torr	When X-rayed
B64N7-114	-6.7	-5.6	40	1,264,000	$5X10^{-1}$	After polishing
B64N7-115	-5.4	-1.7	50	954,680	$5X10^{-8}$	After polishing
B64N7-117	-4.7	0.2	60	137,790	$5X10^{-8}$	After polishing
B64N7-118	9.0	1.3		Not Tested		After polishing
B64N7-119	-0.6	-6.1	50	583,300	$5X10^{-8}$	After polishing
B68N7-156	1.1	-8.4	40	5,008,710	$5X10^{-4}$	After polishing
B68N7-159	-3.8	-0.4		Not Tested		After polishing
B68N7-160	-5.8	1.0	40	2,160,300	$5X10^{-4}$	After polishing
B72N7-191	-9.3	-0.1	50	874,000	$5X10^{-8}$	After polishing
B72N7-192	-1.8	0.3	60	364,880	$5X10^{-8}$	After polishing
B72N7-193	-3.1	0.7		Not Tested		After polishing
B72N7-194	-4.1	0.2	60	570,870	$5X10^{-8}$	After polishing
B74N7-11	-5.0	-4.9	45	805,020	$5X10^{-8}$	After polishing
B74N7-13	-3.4	-1.9		Not Tested		After polishing
B74N7-14	-4.9	-1.3	60	180,310	$5X10^{-4}$	After polishing
B74N7-20	-0.7	-1.2				Before polishing
B74N7-20	-2.0	0.8		Not Tested		After polishing
B83N7-101	-6.5	-5.2		Not Tested		After polishing
B86N7-71	3.0	-1.1	40	2,442,500	$5X10^{-4}$	After polishing
B86N7-72	-5.6	-2.2				Before polishing
B86N7-72	0.9	-4.0		Not Tested		After polishing

Table 16 (continued).

Specimen Number	Residual Stress on Numbered Side, ksi	Residual Stress on Unnumbered Side, ksi	Maximum Stress Applied in Test, ksi	Fatigue Life, Cycles	Gas Pressure, torr	When X-rayed
B86N7-73	9.5	-0.7				Before polishing
B86N7-73	0.2	-2.2		Not Tested		After polishing
B86N7-74	-6.5	0.6	40	7,095,840	$5X10^{-2}$	After polishing
B86N7-75	-1.1	-5.2	50	1,412,010	$5X10^{-8}$	After polishing
B86N7-76	-1.5	-7.6		Not Tested		After polishing
B86N7-77	1.4	2.1	60	296,560	$5X10^{-8}$	After polishing
B86N7-79	0.9	-2.9	45	2,119,710	$5X10^{-8}$	After polishing
B87N7-81	-5.6	1.6	60	188,740	$5X10^{-4}$	After polishing
B87N7-82	-3.8	-7.0	40	>5,799,290	$5X10^{-8}$	After polishing
B87N7-84	-3.6	-1.7	45	340,400	$5X10^{-4}$	After polishing
B87N7-85	-2.8	1.9	40	>7,992,310	$5X10^{-8}$	After polishing
B87N7-86	-2.2	-6.9	40	>8,181,610	$5X10^{-1}$	After polishing
B87N7-87	-4.6	0.3	40	>5,049,570	$5X10^{-4}$	After polishing
B87N7-88	-2.9	1.1	40	>5,000,000	$5X10^{-8}$	After polishing
B87N7-89	-5.4	-2.3	40	Machine Malfunctioned	$5X10^{-2}$	After polishing
B87N7-90	-12.2	-4.3	40	>5,004,290	$5X10^{-1}$	After polishing
B88N7-98	-7.5	-1.8	60	155,460	$5X10^{-8}$	After polishing
B88N7-100	-0.9	-0.5	50	1,194,830	$5X10^{-8}$	After polishing

and tensile residual stresses on the other, and 4 percent of the specimens contained tensile residual stresses on both sides. Seventy eight percent of these surfaces exhibiting compressive residual stresses had residual stresses of 6 ksi or less. The maximum compressive residual stress measured was 14.6 ksi. For specimen surfaces containing tensile residual stresses, the magnitude of these tensile residual stresses was equal to or less than 2 ksi in about 83 percent of the cases. The maximum tensile residual stress measured was 9 ksi. All in all, about 80 percent of the surfaces X-rayed exhibited residual stresses between 6 ksi in compression and 2 ksi in tension.

To study the effects of these residual stresses on the fatigue lives of the test specimens, plots were made of fatigue lives against the algebraically largest residual stress on the specimen surface, figures 34 through 37. For the data in each figure the maximum applied stress and the gas pressure are the same. Thus the only apparent variable is the residual stress in the surface of the specimen. Inspection of figures 34 through 37 indicates there is no consistent variation of fatigue life with residual stress level. There must be other, less obvious factors, which are responsible for the scatter in fatigue lives of these test specimens. Perhaps there were microscopic differences in the surface roughness which were not detected, but which caused the differences in fatigue lives under identical test conditions.

A short study was made to determine the effect of polishing on the residual stress state on the specimen surfaces. Specimen numbers B63N7-104, B63N7-108, B63N7-110, B74N7-20, B86N7-72, and B86N7-73 were

X-rayed both before and after polishing. Examination of table 16 indicates that polishing invariably changed the residual stress state in the specimen surface, however there was no consistent variation in these stresses as a result of polishing. About 50 percent of the time the residual stresses became algebraically larger, and 50 percent of the time they became algebraically smaller.

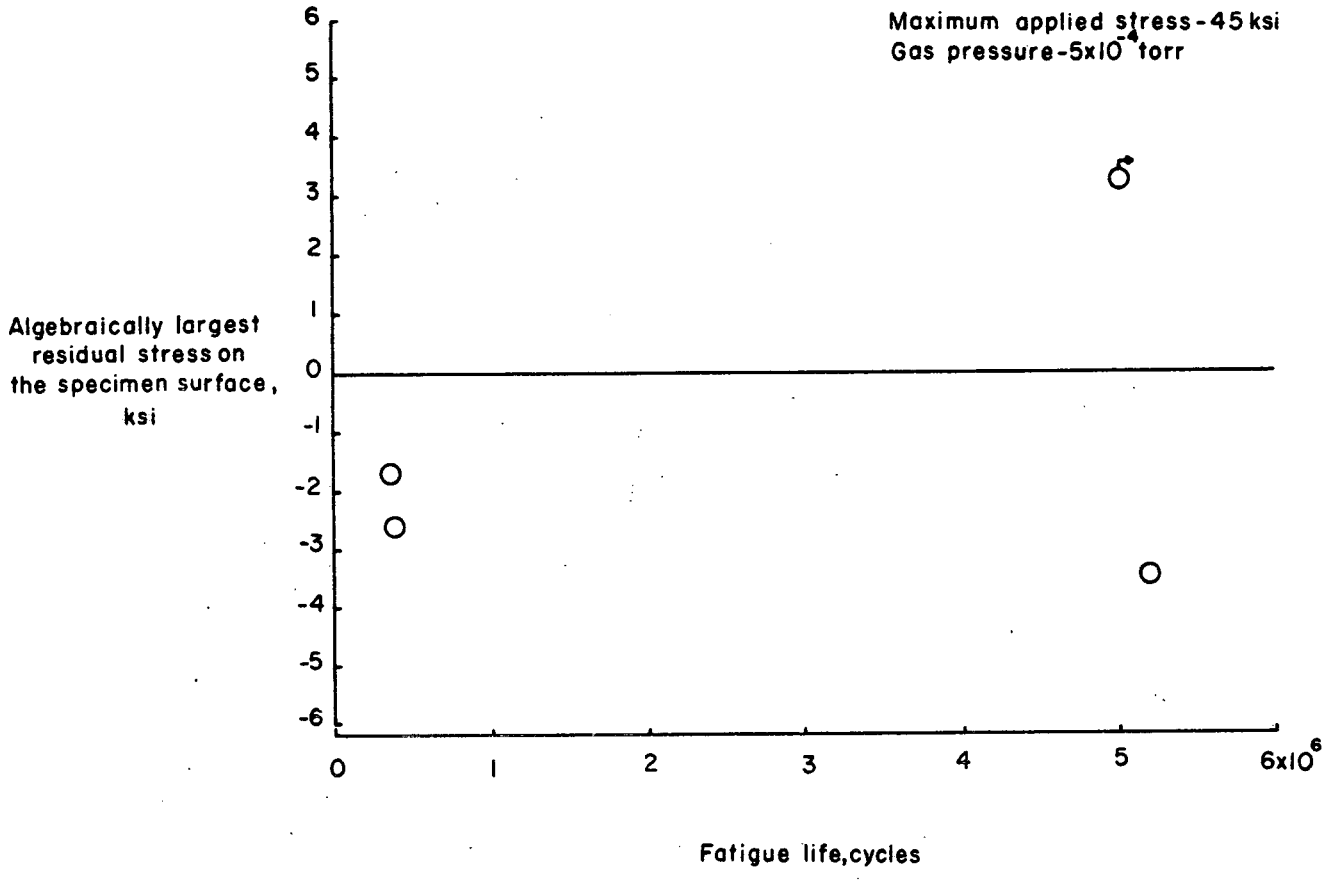

Figure 34.- Variation of fatigue life with residual stress.

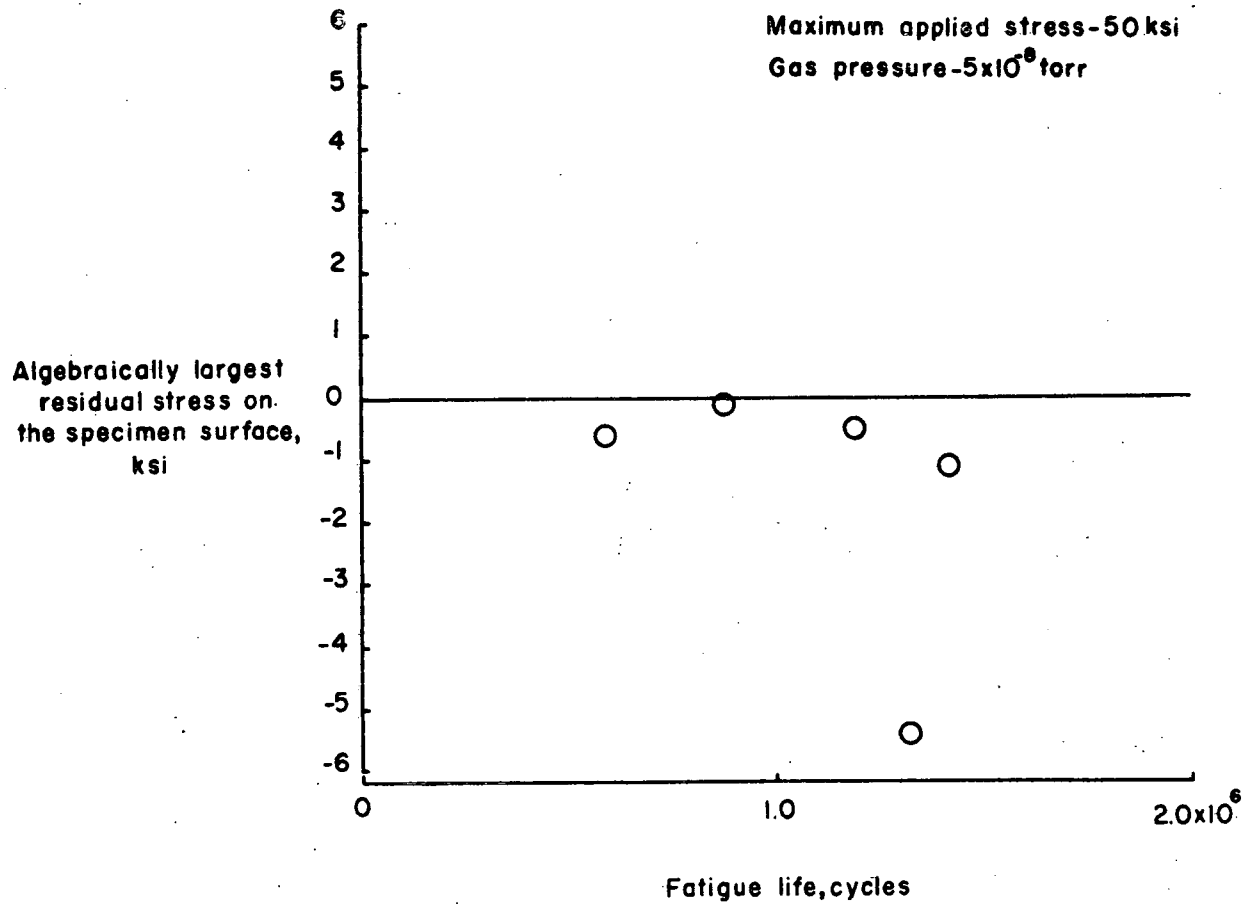

Figure 35.- Variation of fatigue life with residual stress.

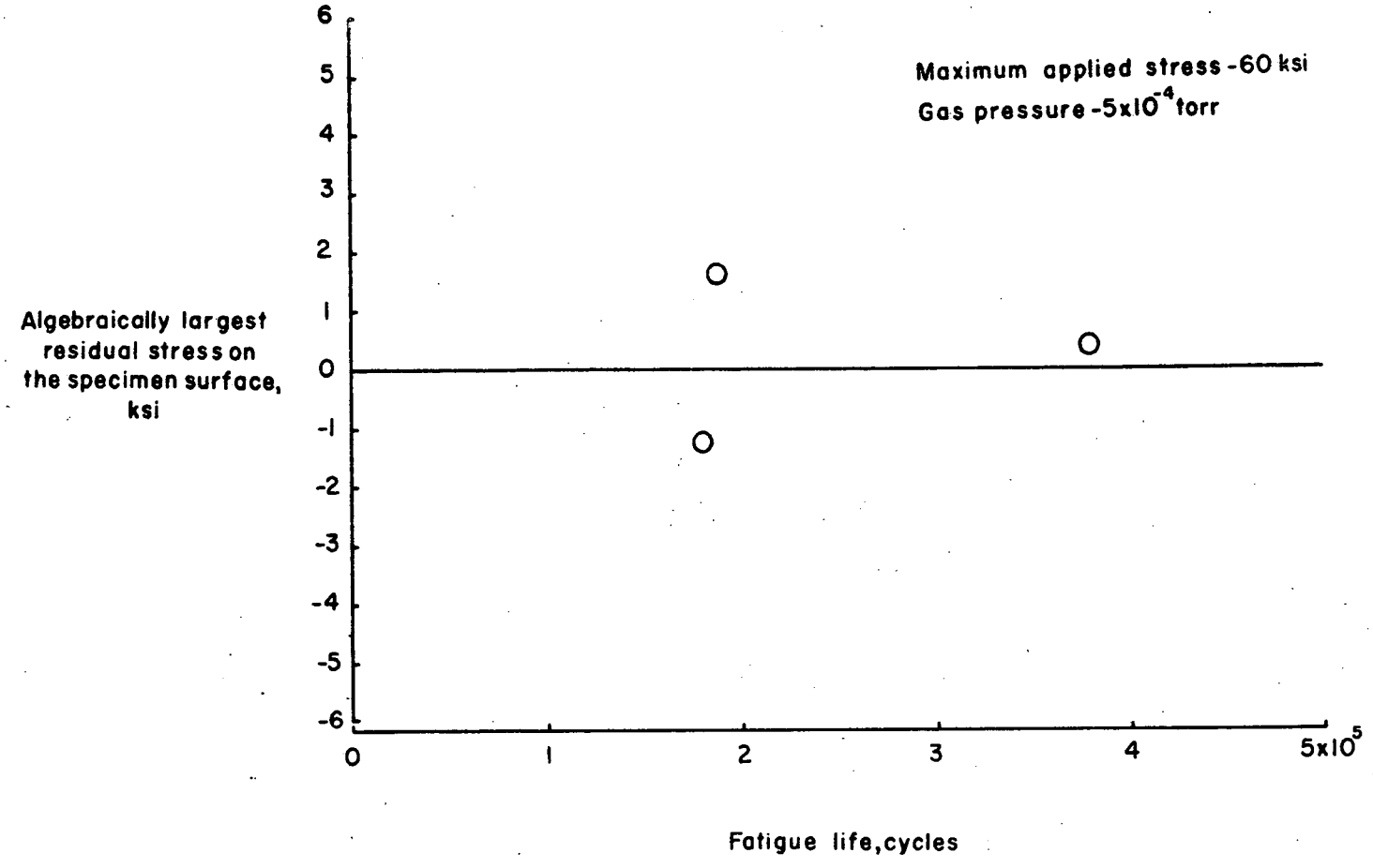

Figure 36.- Variation of fatigue life with residual stress.

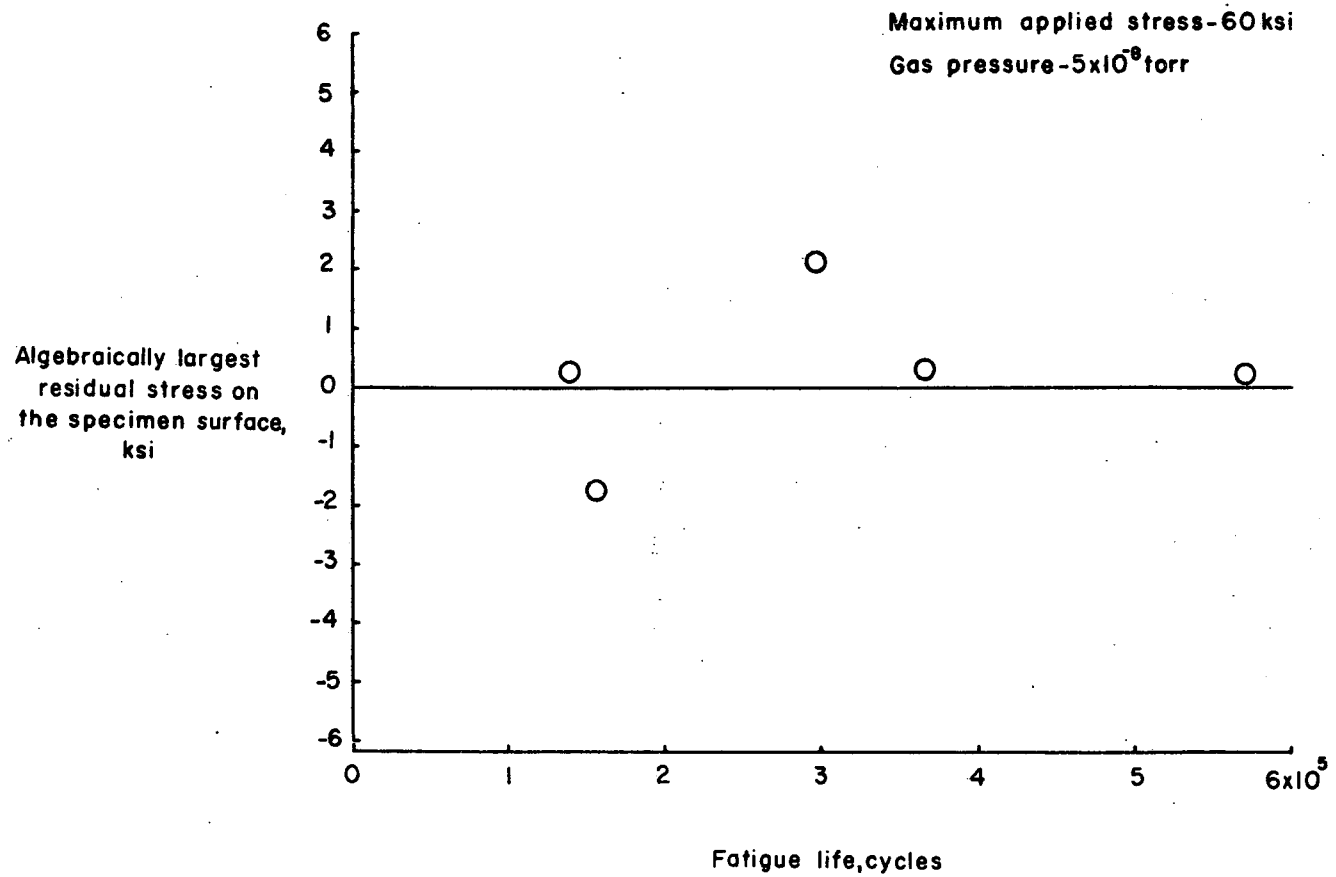

Figure 37.- Variation of fatigue life with residual stress.

Fractographic Examination

Air-Tested Specimens

Typical fractographs from specimens tested in air are shown in figures 38, 39, 40 and 41. Fractographs made using both the transmission- and the scanning-electron microscopes are shown in these figures. Fatigue striations are clearly visible on all of the photographs shown in these figures. The width of each striation represents the advance of the fatigue crack resulting from the application of a single load cycle. At the lower stress levels these striations appeared in fairly large patches on the fracture surfaces. These patches were scattered over the entire fatigue-fractured surface of the specimens. There were large areas of the fatigue-fractured surface which contained no such striations, however. At the higher stress levels the striations appeared in small and widely scattered patches.

Vacuum-Tested Specimens

Typical fractographs from specimens tested in vacuum are shown in figures 42 and 43. Again both transmission- and scanning-electron microscope fractographs are shown. Fatigue striations did form on the surfaces of the vacuum-tested specimens, but were found only in the scanning-electron microscope's fractographs. These striations were very widely scattered over the fatigue-fractured surfaces. This very wide scattering probably accounts for the failure to detect the striations using transmission electron microscope techniques. If the small

(a) Transmission electron microscope

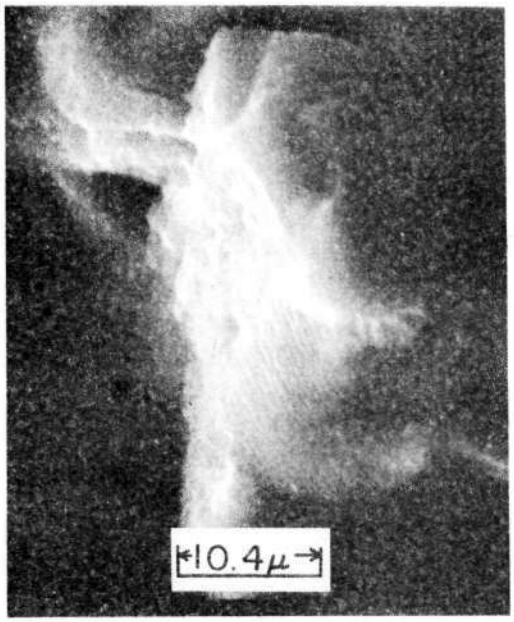

(b) Scanning electron microscope

Figure 38.- Fracture surface of specimen number B83N7-46. S_{max} = 60 ksi. Tested in air.

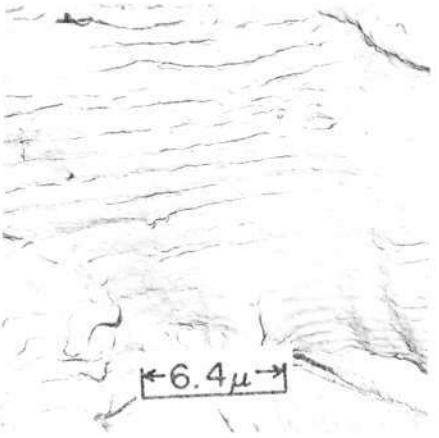

(a) Transmission electron microscope

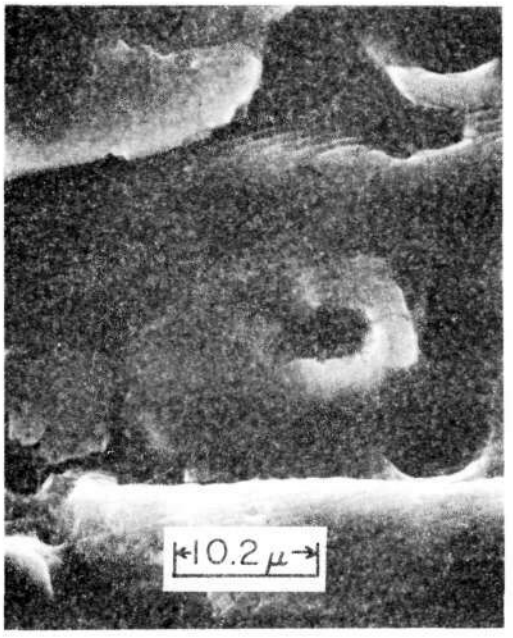

(b) Scanning electron microscope

Figure 39.- Fracture surface of specimen number B84N7-59. S_{max} = 50 ksi. Tested in air.

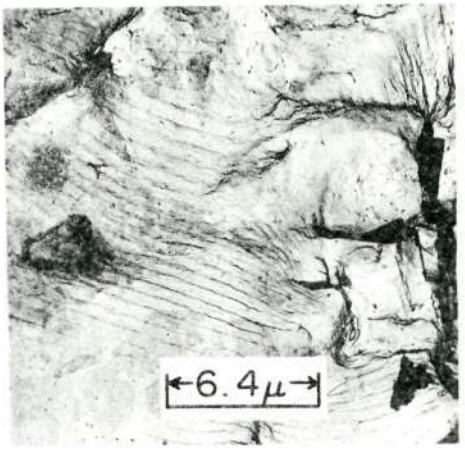

(a) Transmission electron microscope

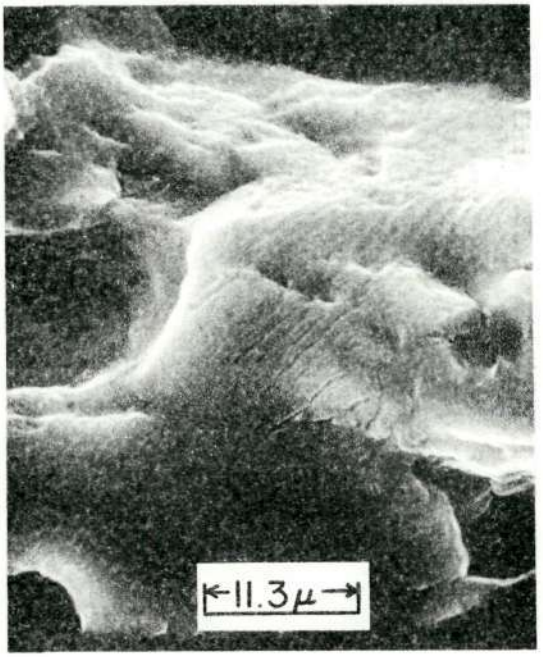

(b) Scanning electron microscope

Figure 40.- Fracture surface of specimen number B71N7-189. S_{max} = 50 ksi. Tested in air.

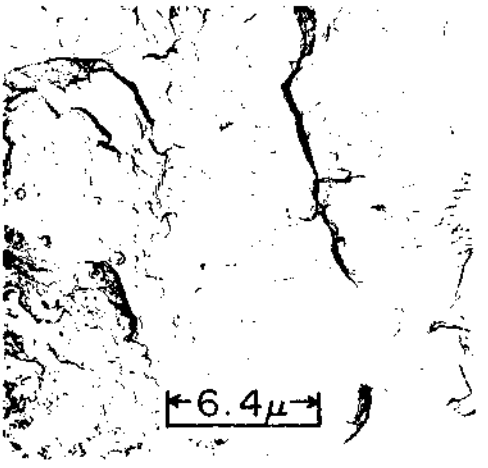

(a) Transmission electron microscope

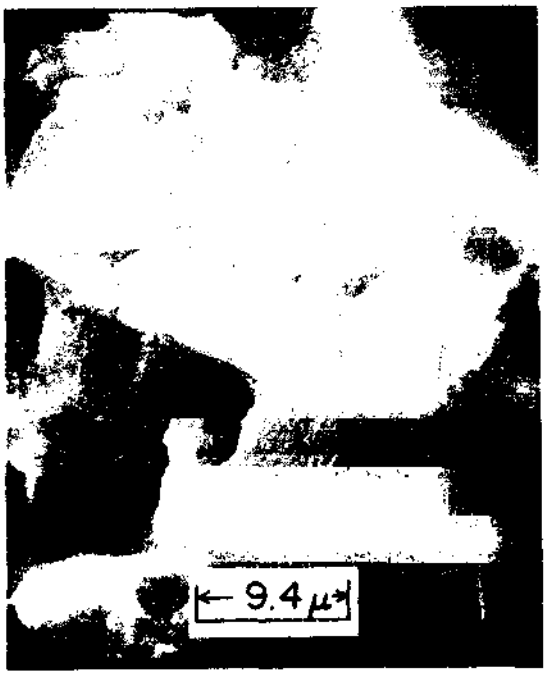

(b) Scanning electron microscope

Figure 41.- Fracture surface of specimen number B65N7-130. S_{max} = 35 ksi. Tested in air.

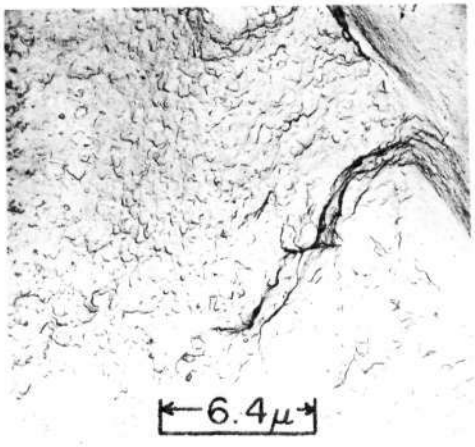

(a) Transmission electron microscope

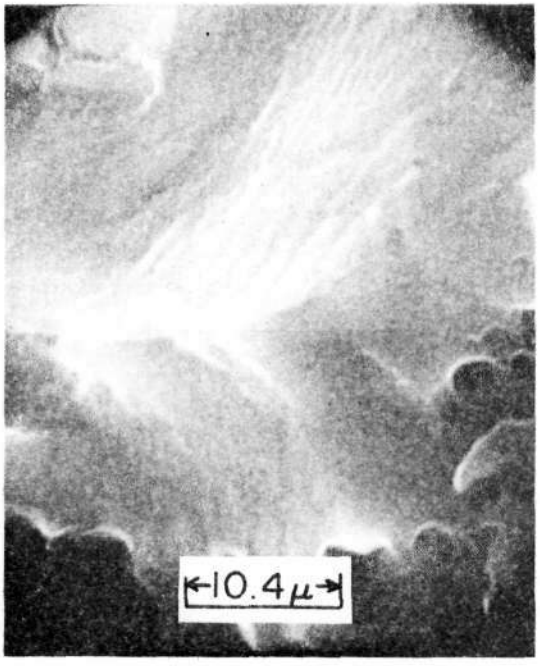

(b) Scanning electron microscope

Figure 42.- Fracture surface of specimen number B64N7-117. S_{max} = 60 ksi. Tested at 5 X 10^{-8} torr.

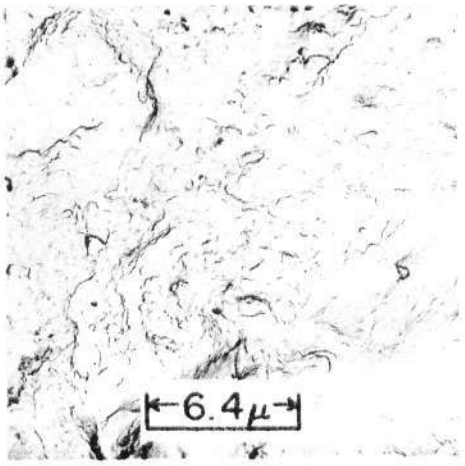

(a) Transmission electron microscope

(b) Scanning electron microscope

Figure 43.- Fracture surface of specimen number B64N7-119. S_{max} = 50 ksi. Tested at 5 X 10^{-8} torr.

areas containing the striations did not replicate well during the preparation of the replicas, or if the areas did replicate well but were covered by the grid, then they could not be detected using transmission electron microscope techniques. This underscores two very basic advantages of the scanning electron microscope, (a) the observer directly observes the specimen surface, not a replica, and (b) the entire surface is available for examination, not just those portions uncovered by the grid. Inspection of figures 38 through 43 also show that much greater depth perception is afforded by the scanning electron microscope.

CONCLUSIONS

A series of axial-load fatigue-life, fatigue-crack growth, and fracture toughness tests were conducted on 0.090-inch thick specimens made of 7075-T6 aluminum alloy. The fatigue life and fatigue crack-propagation experiments were conducted at a stress ratio of 0.02.

The maximum stresses in the fatigue-life experiments ranged from 33 to 60 ksi, and from 10 to 40 ksi in the fatigue-crack-growth experiments. Fatigue life experiments were conducted at gas pressures of 760, $5x10^{-1}$, $5x10^{-2}$, $5x10^{-4}$, and $5x10^{-8}$ torr. Fatigue-crack-growth and fracture toughness experiments were conducted at gas pressures of 760 and $5x10^{-8}$ torr.

Residual stress measurements were made on selected specimens to determine the effect of residual stresses on fatigue behavior. These measurements were made using X-ray diffraction techniques.

Fracture surfaces of typical specimens were examined using scanning and transmission electron microscopes to study fracture modes in vacuum and air.

The following conclusions have been reached on the basis of this investigation.

1. Fatigue lives at a pressure of $5x10^{-8}$ torr were fifteen to thirty times longer than at 760 torr.

2. The fatigue limit was approximately 11 ksi higher at a pressure of $5x10^{-8}$ torr than at 760 torr.

3. Fatigue lives consistently increased with decreasing gas pressure.

4. The fatigue limit consistently increased with decreasing gas pressure.

5. The fatigue resistance of the 7075-T6 used in this investigation decreased by a factor of one and one-half to three (depending upon the stress level) over a twenty-year period.

6. The tensile properties of the 7075-T6 did not change significantly over the twenty-year period.

7. The rate of fatigue-crack-growth for 7075-T6 was a single-valued function of the stress intensity range in both vacuum and air.

8. At lower values of stress-intensity range the rates of fatigue-crack-growth were about twice as high at a gas pressure of 760 torr than at 5×10^{-8} torr.

9. At higher values of stress-intensity range the rates of fatigue-crack-growth were about the same in vacuum and air.

10. An empirical equation developed by Forman et al, produced an excellent fit to the data from both air and vacuum tests.

11. The vacuum environment caused significantly longer delays in the crack initiation phase of fatigue than in the crack propagation phase, although delays occurred in both phases.

12. The vacuum environment had no effect whatever on the fracture toughness of 7075-T6 aluminum alloy.

13. Residual stress measurements indicated the residual stresses in about 80 percent of the specimens ranged between 6 ksi in compression and 2 ksi in tension.

14. The residual stresses did not appear to exert a significant effect on the fatigue lives of the test specimens.

15. Fatigue striations appeared on the fatigue-fractured surfaces of both air and vacuum tested specimens. However, for a given stress level considerably more striations occurred in the air-tested specimens.

REFERENCES

Achter, M. R., Danek, G. J., Jr., and Smith, H. H. 1963. Effect on Fatigue of Gaseous Environments Under Varying Temperature and Pressure. Trans. Met. Soc. AIME. 227(6):1296-1301.

Annual Book of ASTM Standards. 1970. Part 31. Amer. Soc. Testing and Matls.

Azároff, L. V. 1968. Elements of X-ray Crystallography. McGraw-Hill Book Company.

Bennett, J. A., Hoshouser, W. L., and Utech, H. P. 1961. The Importance of Environment in Fatigue Failure of Metals. Rept. to the Aerospace Gearing Committee of the AGMA.

Bennett, J. A. 1964. Effect of Reactions with the Atmosphere During Fatigue of Metals. Fatigue—An Interdisciplinary Approach, J. J. Burke, N. L. Reed, and V. Weiss, eds., Syracuse Univ. Press. 209-227.

Bradshaw, F. J., and Wheeler, C. 1965. The Effect of Environment on Fatigue Crack Propagation. 1. Measurements on Al. Alloy DTD 5070A, S.A.P., Pure Aluminum, and a Pure Al-Cu-Mg Alloy. RAE Tech. Rept. No. 65073.

Broom, T., and Nicholson, A. 1961. Atmospheric Corrosion-Fatigue of Age-Hardened Aluminum Alloys. J. Inst. Metals. 89:183-190.

Christensen, R. H. 1963. Fatigue Cracking of Metals Accelerated by Prolonged Exposure to High Vacuum. Eng. Paper No. 1636, Missile and Space Systems Div., Douglas Aircraft Co.

Christenson, A. L., Koistinen, D. P., Marburger, R. E., Semchyshen, M., and Evans, W. P. 1960. The Measurement of Stress by X-ray. SAE TR-182.

Cullity, B. D. 1956. Elements of X-ray Diffraction. Addison-Wesley Publishing.

Elber, W. 1970. The Significance of Fatigue Crack Closure. Presented at the 1970 Ann. Meeting of ASTM, Toronto, Canada.

Feeney, J. A., McMillan, J. L., and Wei, R. P. 1969. Environmental Fatigue Crack Propagation of Aluminum Alloys at Low Stress Intensity Levels. Boeing Comp. Rept. D6-60114.

Figge, I. E., and Newman, J. C., Jr. 1967. Fatigue Crack Propagation in Structures With Simulated Rivet Forces. Spe. Tech. Publ. No. 415. Amer. Soc. Testing Mater. 71-94.

Forman, R. G., Kearney, V. E., and Engle, R. M. 1967. Numerical Analysis of Crack Propagation in Cyclic-Loaded Structures. Trans. ASME, Ser. D. J. Basic Eng. 89(3):459-464.

Gough, H. J., and Sopwith, D. G. 1946. Inert Atmospheres as Fatigue Environments. J. Inst. Metals. 72:415-421.

Grosskreutz, J. C. 1960. Research in Mechanisms of Fatigue. M.R.I. Proj. No. 2279-P. (Contract No. AF 33(616)-6383), Midwest Res. Corp. Quarterly Prog. Rept. No. 5a.

Grosskreutz, J. C., and Bowles, C. Q. 1965. Effect of Environmental Gases on the Surface Deformation of Aluminum and Gold in Fatigue, Metallurgical Society Conf. 35:67-105.

Grosskreutz, J. C. 1967. The Effect of Oxide Films on Dislocation-Surface Interactions in Aluminum. Surface Science 8:173-190.

Grover, H. J., Bishop, S. M., and Jackson, L. R. 1951. Fatigue Strengths of Aircraft Materials Axial-Load Fatigue Tests on Unnotched Sheet Specimens of 24S-T3 and 75S-T6 Aluminum Alloys and of SAE 4130 steel. NACA TN 2324.

Ham, J. L. 1962. Investigation of Adhesion and Cohesion of Metals in Ultrahigh Vacuum. NRC Proj. No. 42-1-0121 (Contract No. NASr-48), Natl. Res. Corp. (Cambridge, Mass.).

Ham, J. L. and Rechenbach, G. S. 1962. Fatigue Testing of Aluminum in Vacuum and the Effect of Pressure on Life and Surface Appearance. Trans. Fourth Pacific Area Natl. Meeting of the ASTM. Paper No. 56A.

Ham, J. L. 1963. The Influence of Surface Phenomena on the Mechanical Properties of Structural Materials (Fatigue of Aluminum in Vacuum). NRC Proj. No. 42-1-0105 (Contract No. AF 49(638)-1005), Natl. Res. Corp. (Cambridge, Mass.).

Hartman, A., Jacobs, F. A., Nederveen, A., and DeRijk, P. 1967. Some Tests on the Effect of the Environment on the Propagation of Fatigue Cracks in Aluminum Alloys. NLR TN M.2182.

Hoeppner, D. W., and Hyler, W. S. 1966. The Effect of Vacuum Out-Gassing Time on the Fatigue Behavior of Two Structural Aluminum Alloys. Natl. Res. Std. 6(12):599-601.

Hordon, M. J., and Wright, M. A. 1968. Mechanism of the Atmospheric Interaction with the Fatigue of Metals. NASA CR-1165.

Hudson, C. M., and Hardrath, H. F. 1961. Effects of Changing Stress Amplitude on the Rate of Fatigue-Crack Propagation in Two Aluminum Alloys. NASA TN D-960.

Hudson, C. M., and Raju, K. N. 1970. Investigations of Fatigue-Crack Growth Under Simple Variable-Amplitude Loading. NASA TN D-5702.

Irwin, G. R. 1957. Analysis of Stresses and Strains Near the End of a Crack Transversing a Plate. Trans. ASME 79:361-364.

Ishii, H., and Weertman, J. 1969. The Effect of Air Pressure on the Rate of Fatigue Crack Growth. Scripta Metallurgica. 3(4):229-232.

Kodak Industrial Data Book P-7. 1962.

Kramer, I. R., and Podlaseck, S. E. 1961. Effect of Vacuum Environment on the Mechanical Behavior of Materials. RM-102 (Contract AF49(638)-946), Martin-Marietta Corp.

Mabberley, J. C. 1966. The Effect of Environment on Fatigue Crack Propagation in Age Hardened Aluminum Alloy Al-7% Zn-5% Mg-1% Mn. RAE Tech. Memo. CPM. 53.

Martin, D. E. 1965. Plastic Strain Fatigue in Air and Vacuum. Trans. ASME, J. of Basic Eng. 850-856.

Meyn, D. A. 1968. The Nature of Fatigue-Crack Propagation in Air and Vacuum for 2024 Aluminum. Trans. ASM. 61:52-61.

Nelson, H. G. and Williams, D. P. 1967. The Effect of Vacuum on Various Mechanical Properties of Magnesium. Proc. Eleventh National SAMPE Symposium. 11:291-297.

Paris, P. E. 1964. The Fracture Mechanics Approach to Fatigue. Fatigue—An Interdisciplinary Approach, J. J. Burke, N. L. Reed, and V. Weiss, eds., Syracuse Univ. Press. 107-132.

Paris, P. E., and Sih, G. C. 1965. Stress Analysis of Cracks. Fracture Toughness Testing and Its Application. ASTM STP 381. 30-83.

Pelloux, R. M. N. 1969. Mechanisms of Formation of Ductile Fatigue Striations. Trans. of the ASM. 62:281-285.

Shen, H., Podlaseck, S. E., and Kramer, I. R. 1966. Effect of Vacuum on the Fatigue Life of Aluminum. Acta Metallurgica. 14(3):341-346.

Shen, H. 1967. Effect of Vacuum Environment on the Mechanical Behavior of Materials. Martin-Marietta Corp. Rept. No. MCR-67-423.

Shives, T. R., and Bennett, J. A. 1968. The Effect of Environment on the Fatigue Properties of Selected Engineering Alloys. J. Matls. 3(3):695-715.

Snowden, K. U., and Greenwood, J. N. 1958. Surface Deformation Differences Between Lead Fatigued in Air and in Partial Vacuum. Trans. AIME. 212:626-627.

Snowden, K. U. 1961. Effect of Air Pressure on the Fatigue of Lead and Aluminum. Nature 189(475B):54-54.

Spitzig, W. A., and Wei, R. P. 1967. A Fractographic Investigation of the Effect of Environment on Fatigue-Crack Propagation in an Ultrahigh-Strength Steel. Trans. ASM. 60:279-288.

Sumsion, H. T. 1968. Vacuum Effects on Fatigue Properties of Magnesium and Two Magnesium Alloys. J. Spacecraft and Rockets. 5(6): 700-704.

Thompson, N., Wadsworth, N., and Louat, N. 1956. The Origin of Fatigue Fracture in Copper. Phil. Mag. 1(2):113-126.

Wadsworth, N. J., and Hutchings, J. 1958. The Effect of Atmospheric Corrosion on Metal Fatigue. Phil. Mag. 3(34):1154-1166.

Wadsworth, N. J. 1959. The Effect of Environment on Metal Fatigue. Internal Stresses and Fatigue in Metals, G. M. Rassweiler and W. L. Grube, eds., Elsevier Pub. Co. (Amsterdam), 382-396.

Wilkov, M. A., and Applewhite, B. 1967. The Effect of Vacuum on Surface Damage in Fatigue. Eng. Mechs. Res. Lab., Univ. of Texas, EMRL-RM 1039.

Wright, R. N., and Argon, A. S. 1970. Fatigue Crack Growth in Si-Fe. Met. Trans. 1(11):3065-3074.

APPENDICES

Appendix A. X-Ray Diffraction Stress Analysis

X-ray stress analysis has been used in this investigation to measure the residual stresses acting in the longitudinal direction of selected test specimens. These residual stresses may be introduced into the specimens as a result of the rolling of the original aluminum alloy billet to the desired sheet thickness, by tempering of the alloy to the desired strength level, by fabrication and polishing of the specimens prior to testing, or by some combination of the preceding processes. The point is, these residual stresses do exist in the test specimens, and those residual stresses acting in the longitudinal direction of the specimen will directly add to or subtract from (depending upon the sign of the residual stress) the applied fatigue stress. Consequently, the effects of these residual stresses should be considered in evaluating the results of the fatigue-in-vacuum experiments.

The basic relationships used in the development of X-ray diffraction stress analysis are presented in most texts on X-ray diffraction. See Cullity (1956), Azároff, (1968) or Christenson (1960) for example. The pertinent relationships used in this investigation will be presented herein for completeness.

The measurement of residual stresses involves three basic assumptions:

1. That the strains (which can, of course, be converted to stresses) being measured are elastic.

2. That the specimen being examined is an isotropic body.

3. That the specimen being examined is homogeneous.

According to Christenson et. al. polycrystalline metals, such as the 7075-T6 aluminum alloy tested in this investigation, satisfy these requirements to a good degree. In addition, it is assumed that the stress in the volume of material being examined is zero in the direction normal to the free surface.

To determine the residual stress in the longitudinal direction of the test specimen, see figure 44, the relationships for the strain in the Z-direction, ε_Z, and for the strain in the AO-direction, ε_ψ must be determined. The strain in the Z-direction may be written

$$\varepsilon_Z = \frac{d_n - d_o}{d_o} \tag{A1}$$

where d_n is the spacing (while under stress) between a set of crystallographic planes whose normal points in the Z-direction.

Similarly, the strain in the AO-direction is given by

$$\varepsilon_\psi = \frac{d_i - d_o}{d_o} \tag{A2}$$

where d_i is the spacing (while under stress) of the same crystallographic planes when inclined at an angle ψ to the Z-direction, and d_o is the spacing between these inclined planes while unstressed.

From the theory of elasticity the stress in the Y-direction, σ_y, is related to ε_ψ and ε_Z by

$$\varepsilon_\psi - \varepsilon_Z = \frac{\sigma_y}{E} (1 + \nu) \sin^2 \psi \tag{A3}$$

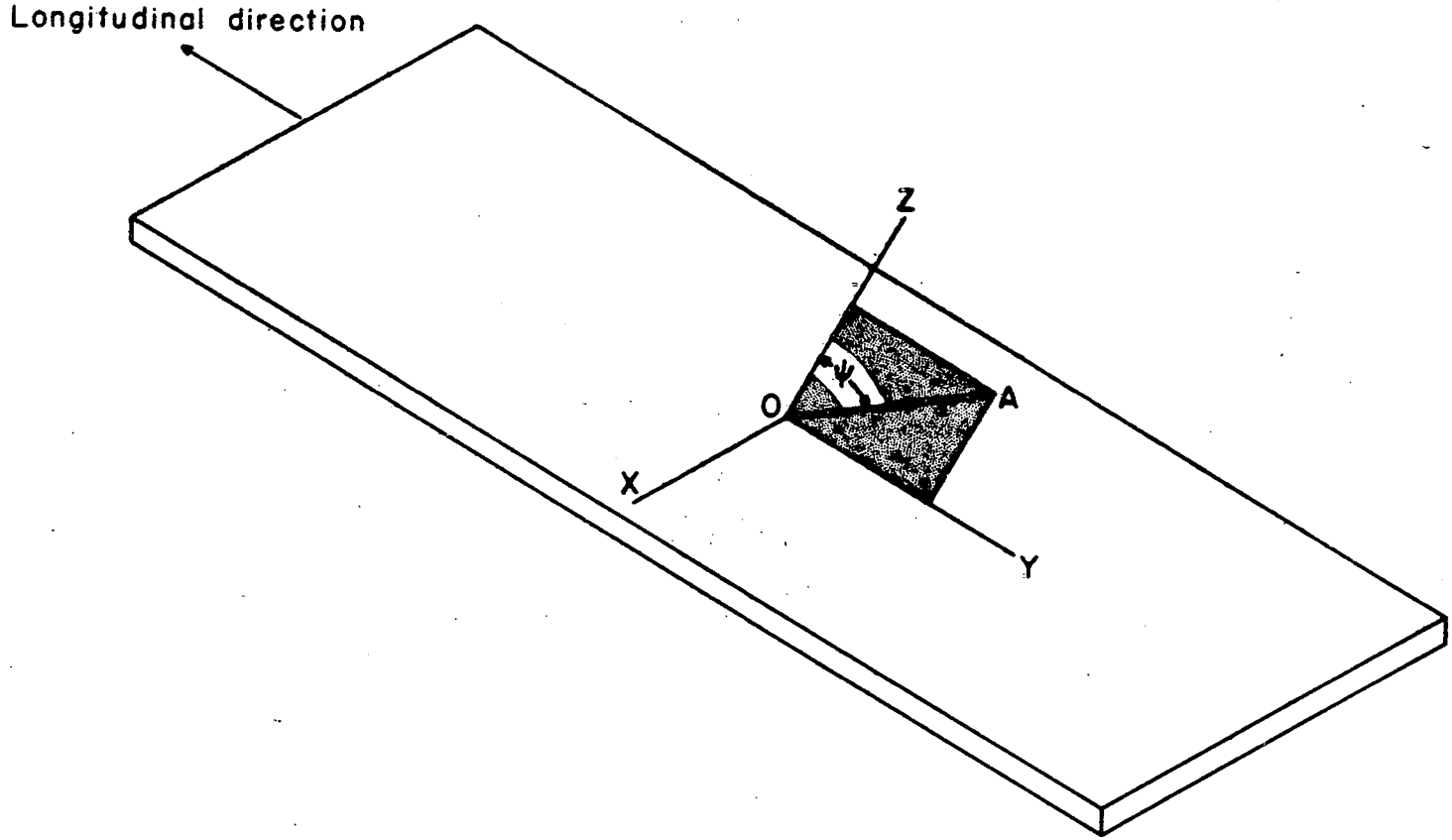

Figure 44.- Test specimen with longitudinal direction indicated.

where E is Young's modulus and ν is Poisson's ratio. The angle ψ is defined in figure 44.

Substituting equations (A1) and (A2) in (A3) there results

$$\frac{d_i - d_o}{d_o} - \frac{d_n - d_o}{d_o} = \frac{\sigma_y}{E} (1 + \nu) \sin^2 \psi \tag{A4}$$

or

$$\frac{d_i - d_n}{d_o} = \frac{\sigma_y}{E} (1 + \nu) \sin^2 \psi \tag{A5}$$

Solving for σ_y and substituting d_o for d_n (which according to Cullity can be done with very little error) Equation (A5) becomes

$$\sigma_y = \frac{E}{(1 + \nu) \sin^2 \psi} \left(\frac{d_i - d_n}{d_n} \right) \tag{A6}$$

For stress analysis using diffractometer X-ray diffraction techniques it is convenient to express Equation (A6) in terms of the Bragg angle θ. Bragg's law is given by

$$\lambda = 2d \sin \theta \tag{A7}$$

where λ is the X-ray wavelength (a constant in this investigation), d is the spacing between crystallographic planes, and θ is the diffraction angle. Differentiating Equation (A7)

$$0 = 2 [d \cos \theta \Delta\theta + \Delta d \sin \theta] \tag{A8}$$

or

$$\frac{\Delta d}{d} = - \cot \theta \Delta\theta = - \cot \theta \frac{\Delta 2\theta}{2} \tag{A9}$$

substituting $\frac{\Delta d}{d}$ for $\frac{d_i - d_n}{d_n}$ in Equation (A6) there results

$$\sigma_y = \frac{E}{(1+\nu)\sin^2\psi}\left(-\cot\theta\,\frac{\Delta 2\theta}{2}\right) \qquad \text{(A10)}$$

or

$$\sigma_y = -\frac{E\cot\theta}{2(1+\nu)\sin^2\psi}(2\theta_c - 2\theta_n) \qquad \text{(A11)}$$

$$= \frac{E\cot\theta}{2(1+\nu)\sin^2\psi}(2\theta_n - 2\theta_i) \qquad \text{(A12)}$$

The term $\frac{E\cot\theta}{2(1+\nu)\sin^2\psi}$ in Equation (A12) is called the stress factor which can be denoted as F. Therefore Equation (A12) is usually written

$$\sigma_y = F\,(2\theta_n - 2\theta_c) \qquad \text{(A13)}$$

The stress factor contains two elastic constants of the material being investigated, i.e., Young's modulus and Poisson's ratio. For most engineering materials the average values of these constants are readily found in materials handbooks. However, for most crystalline materials these constants vary with crystal direction. Consequently, the average properties may not apply in the direction associated with the particular set of crystallographic planes being used for stress measurement. To circumvent the determination of E and ν in the appropriate direction, the stress factor for 7075-T6 was determined empirically in this investigation. This determination was made as follows:

1. An angle ψ of 45 degrees was selected at the inclined angle for the X-ray stress measurements. According to Christenson, et al., this angle should be between 45 and 60 degrees for adequate sensitivity.

2. The 2θ angle, i.e. twice the Bragg angle, was determined. According to Christenson et al., this 2θ angle should exceed 130 degrees for satisfactory sensitivity. A set of diffracting planes having a 2θ value of approximately 136 degrees was selected.

3. Having defined ψ and θ, a strip of 7075-T6 aluminum alloy having two strain gages glued to it was bent around and fastened to a circular wooden disk of known radius, figures 45 and 46. The tensile stress introduced in the outer fiber of this strip, σ_y, was computed using the following equation.

$$\sigma_y = \frac{tE}{D} \qquad \text{(A14)}$$

where t is the material thickness, E is the handbook value of Youngs modulus, and D is the diameter of the circular disk. The strain gages were used to verify the calculated stress.

4. The stressed strip was then mounted in the diffractometer and aligned such that the strip was equally inclined to the incident and diffracted beams. For such an arrangement, the normal to the reflecting planes points exactly in the Z-direction as required in Equation (A1). The strip was subjected to a monochromatic X-ray flux using copper $K\alpha$ radiation. A three-degree beam slit was used at the X-ray source for beam alignment. The diffraction data were obtained using fixed-count scaling, i.e., the time required to accumulate a given number of photon counts on the diffractometer counter was measured. These measurements were made over a range of 2θ values which included the diffraction peak. These data were then corrected using the appropriate Lorentz-

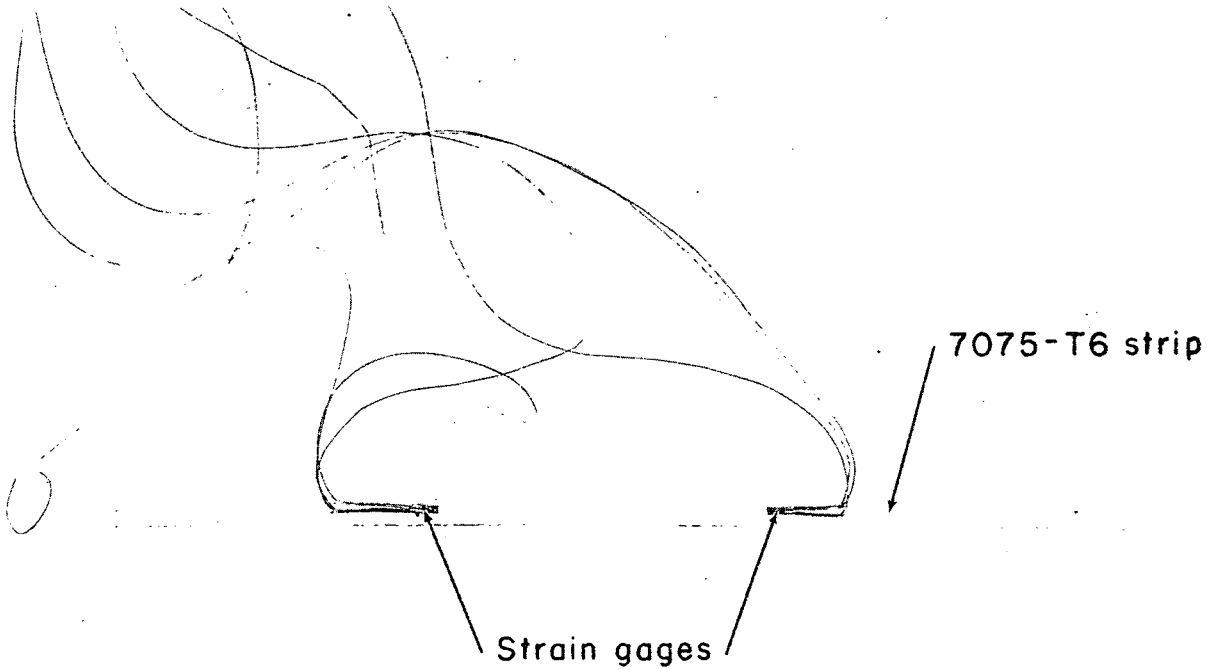

Figure 45.- 7075-T6 strip used in determination of the stress factor.

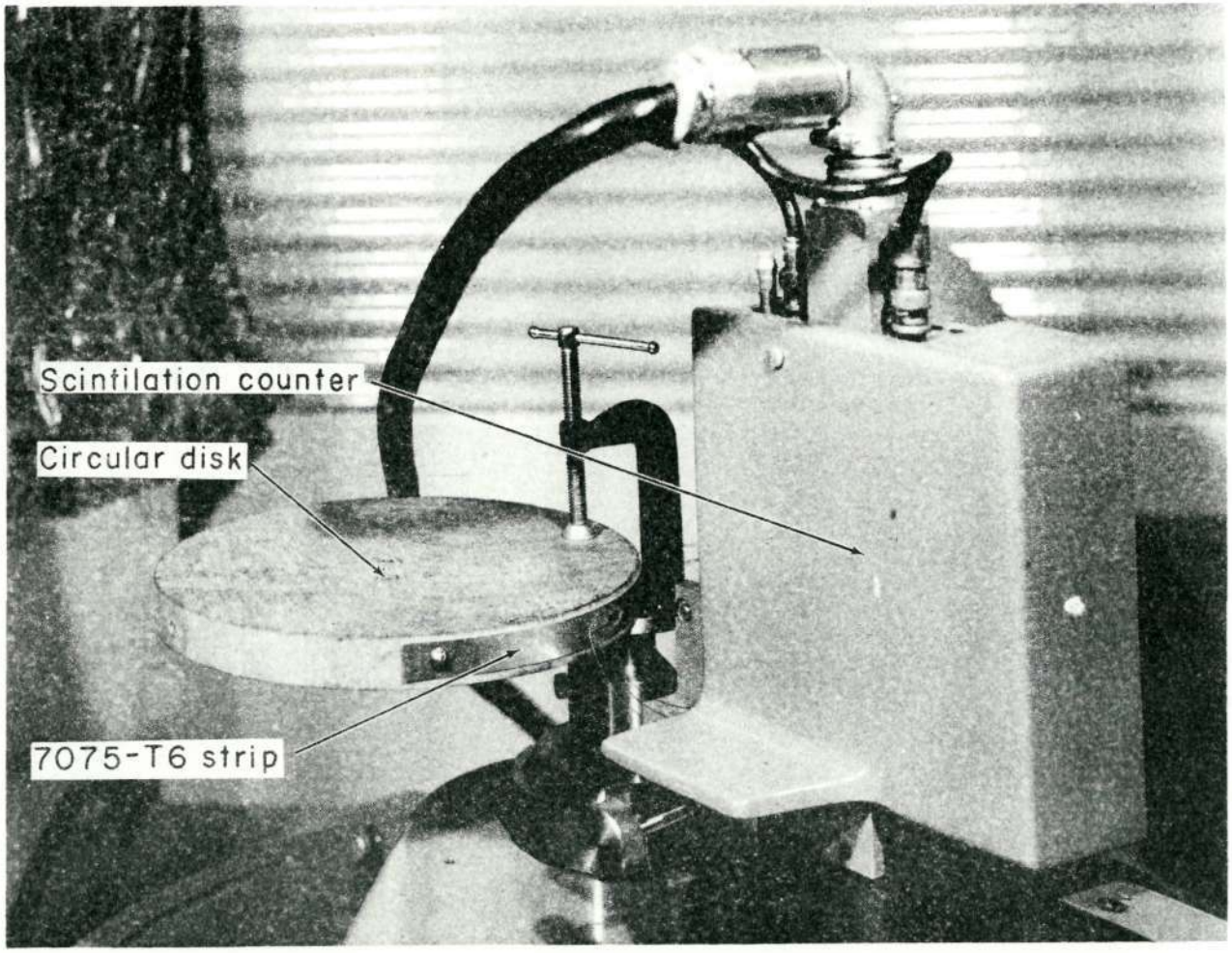

Figure 46.- 7075-T6 strip fastened to a circular wooden disk.

Polarization correction as explained by Christenson et al. A parabola was then fitted to the corrected data and the diffraction peak calculated. This gave $2\theta_n$ for the known stress on the specimen.

5. The stressed strip was then rotated through an angle ψ of 45 degrees for the inclined measurement, and the diffractometer counter refocused. Measurements were again made over a range of 2θ values which included the diffraction peak. The data were corrected using the appropriate Lorentz-Polarization and absorption corrections, and a parabola fitted to the corrected data. The value of $2\theta_i$ was then calculated for the known applied stress.

6. Steps 4 and 5 were repeated with the same aluminum strip bent around blocks having other radii (and consequently other outer fiber stresses). A picture of the strip fastened around one of the wooden blocks and mounted in the diffractometer is shown in figure 47.

7. From the preceding measurements a plot of $(2\theta_n - 2\theta_i)$ was made against the known stresses introduced in the strip. The result was a linear plot, figure 48, the slope of which is the stress factor F in equation (A13). For the test conditions used, the stress factor for 7075-T6 was 76 ksi per degree.

8. Having determined the stress factor for 7075-T6, the fatigue test specimens were mounted in the diffractometer and the techniques described in the preceding steps 4 and 5 were used to calculate $2\theta_n$ and $2\theta_i$. Knowing F, $2\theta_n$ and $2\theta_i$ the residual stresses in the longitudinal direction of the specimen were computed using Equation (A13).

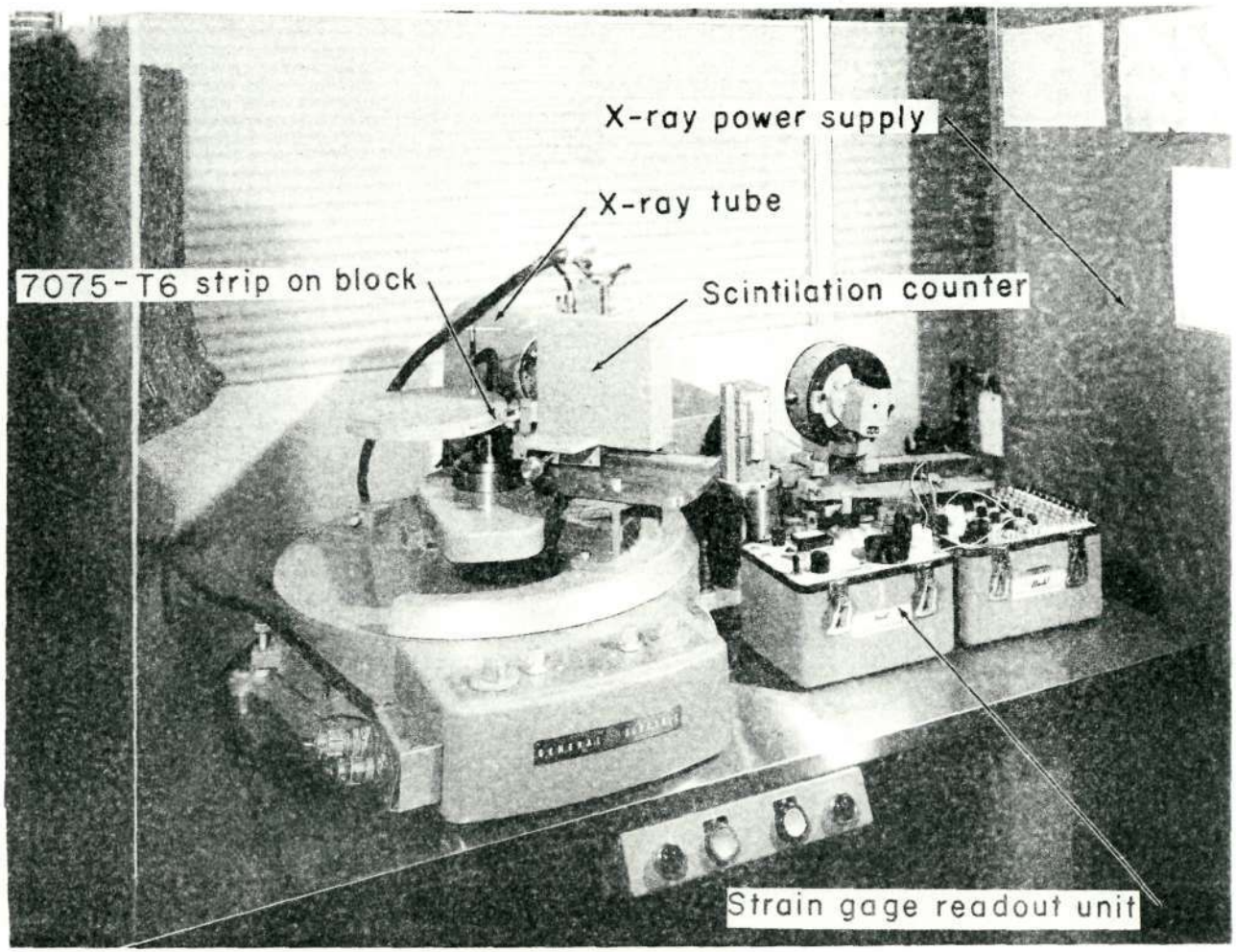

Figure 47.- 7075-T6 strip fastened to a circular wooden disk and mounted in the diffractometer.

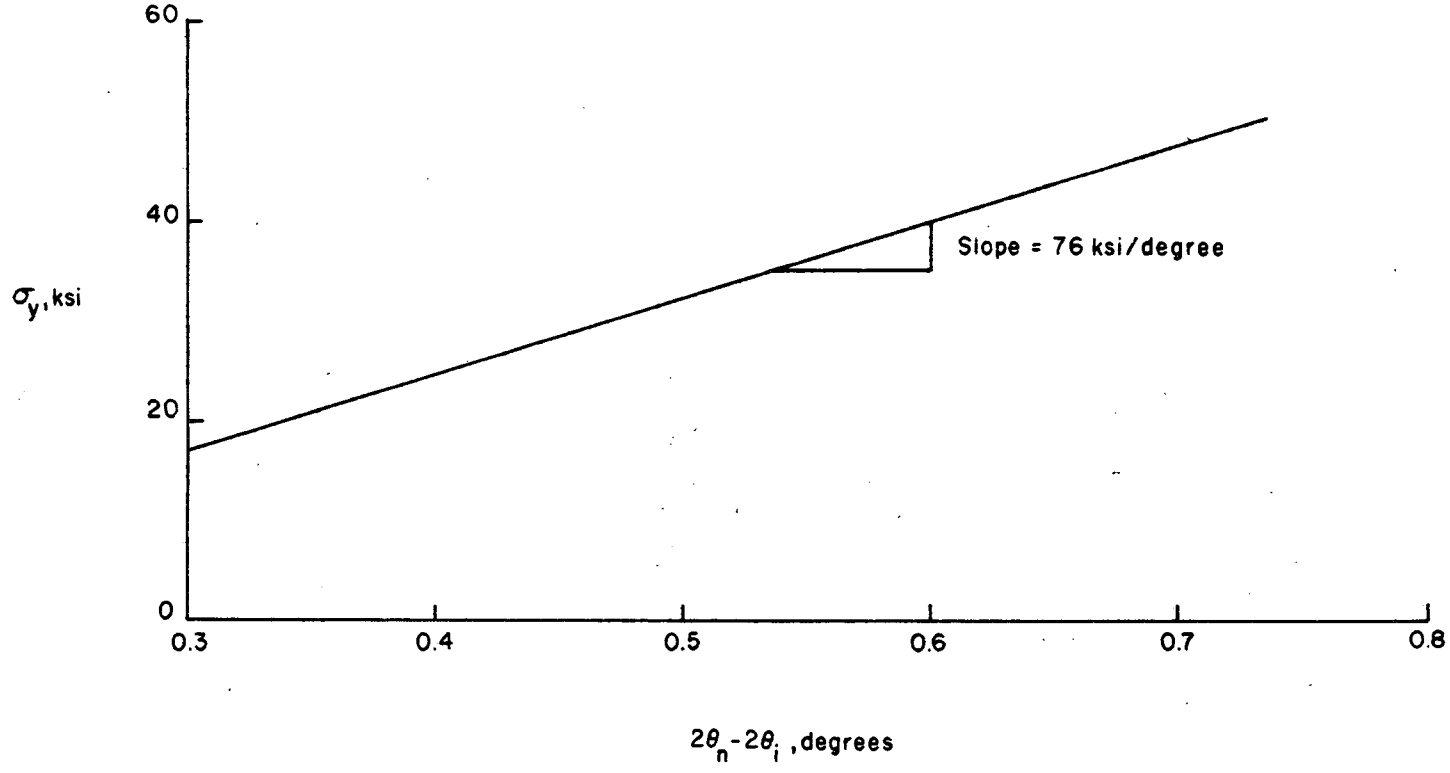

Figure 48.- Plot of $(2\theta_n - 2\theta_i)$ versus stress.

Appendix B. Stress Intensity Analysis

The stress solution for a transverse crack in an infinitely wide plate loaded in tension was developed by Irwin (1957) among others. This solution showed that the stresses near the tip of a crack were given by:

$$\sigma_y = \frac{K_I}{\sqrt{2\pi r}} \cos\frac{\delta}{2}\left[1 + \sin\frac{\delta}{2}\sin\frac{3\delta}{2}\right] \qquad \text{(B1)}$$

$$\sigma_x = \frac{K_I}{\sqrt{2\pi r}} \cos\frac{\delta}{2}\left[1 - \sin\frac{\delta}{2}\sin\frac{3\delta}{2}\right] \qquad \text{(B2)}$$

$$\tau_{xy} = \frac{K_I}{\sqrt{2\pi r}} \sin\frac{\delta}{2}\cos\frac{\delta}{2}\cos\frac{3\delta}{2} \qquad \text{(B3)}$$

where σ_y is the stress in the longitudinal direction (see figure 49), σ_x is the stress in the long transverse direction, τ_{xy} is the shear stress, r is the distance from the tip of the crack to the point at which the stress is being calculated, δ is the angle between the X-axis and r, and K_I is the stress-intensity factor. This stress-intensity factor is a local stress parameter which reflects the intensity of the stress at all points surrounding the tip of the crack. This factor has been used successfully by a number of investigators to correlate fracture toughness, and fatigue-crack growth data generated under different test conditions, e.g. different loading conditions and different specimen configurations.

For the crack configuration used in the fatigue-crack-growth and fracture-toughness tests conducted in this investigation, the stress-intensity factor, K_I, is given by

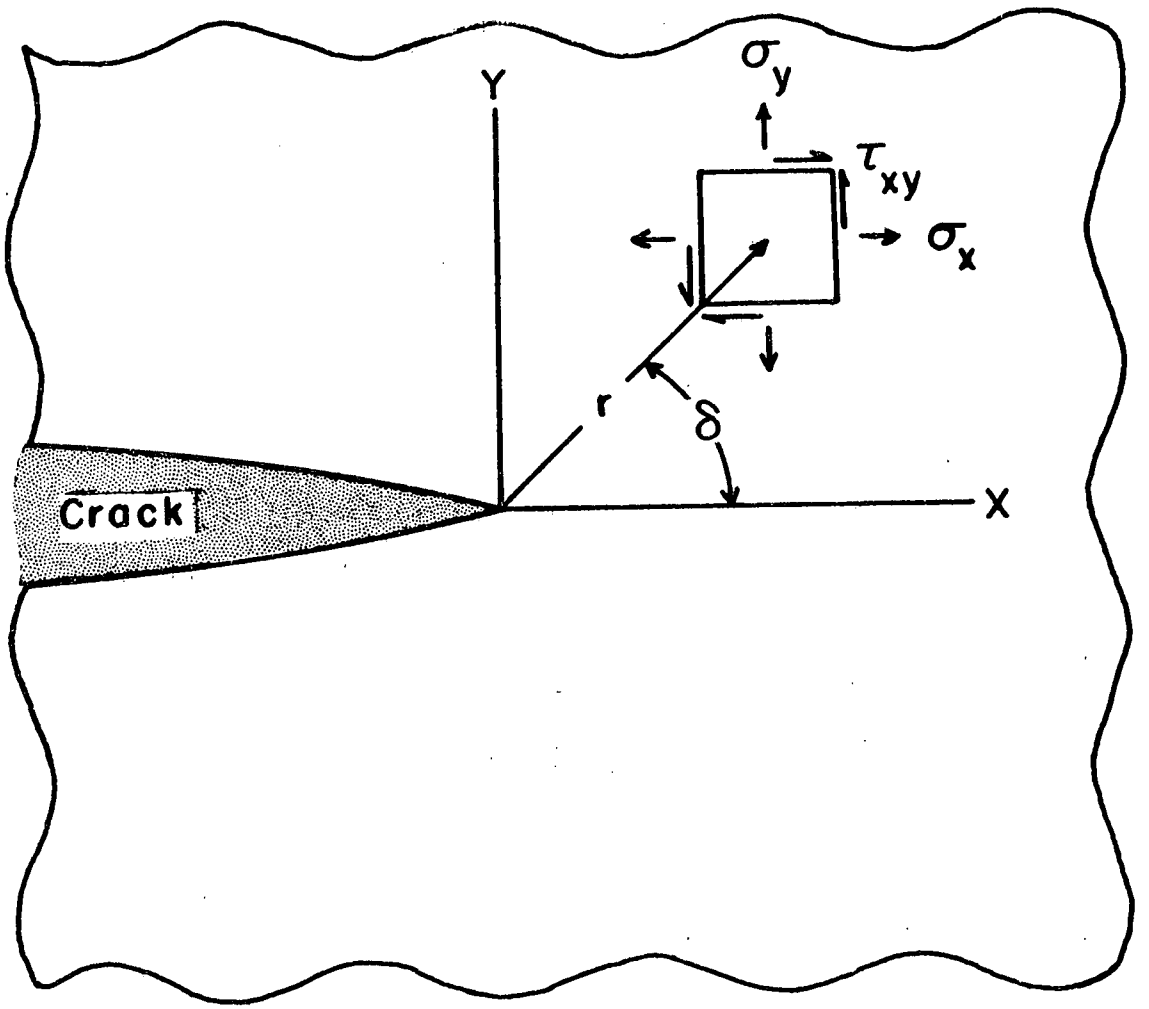

Figure 49.- Definition of stresses near the tip of a crack.

$$K_I = S\sqrt{\pi a} \qquad (B5)$$

where S is the uniformly-distributed axial stress, and a is one-half the length of the crack. For finite width specimens, such as the ones used in this investigation, K_I is multiplied by a finite width correction ω where

$$\omega = \sqrt{\sec \frac{\pi a}{w}}$$

and w is the width of the test specimen. Equation (B4) thus becomes

$$K_I = S\sqrt{a\pi \sec \frac{\pi a}{w}} \qquad (B6)$$

The value of K_I at which unstable crack growth begins in the test specimen is called the critical stress intensity factor, K_c. This K_c is an important material parameter which can be used to compare the relative fracture toughnesses of different materials to determine the effect of environment on fracture toughness, or to predict the stress level at which failure will occur in a cracked structure. Such predictions can be made for relatively complex structures provided K_c is known for the material and there is a stress-intensity solution for the structure under investigation. Stress intensity solutions for a wide range of configurations are presented in a report by Paris and Sih(1965). Numerous other solutions are presented in journals such as the Journal of Fracture Mechanics published by P. Noordhoff, Ltd., and Engineering Fracture Mechanics published by Pergamon Press.

The values of S and a associated with K_c are the applied stress and half-crack length at the onset of unstable crack growth. In this investigation, S_c was obtained using a calibrated recording oscillograph, and a_c was obtained through visual observation of the specimen during fracture-toughness testing.

Paris (1964) showed that the rate of fatigue-crack propagation, $\frac{d(2a)}{dN}$, was a function of the stress-intensity factor range, ΔK, i.e.

$$\frac{d(2a)}{dN} = C_1(\Delta K)^m \tag{B7}$$

where

$$\Delta K = K_{max} - K_{min} \tag{B8}$$

and C_1 is an empirical constant.

Paris found that a value of $m = 4$ fits the broad trend of the data. For the specimen configuration used in this investigation,

$$K_{max} = S_{max}\sqrt{\pi a}\,\omega \tag{B9}$$

and

$$K_{min} = S_{min}\sqrt{\pi a}\,\omega \tag{B10}$$

where S_{max} is the maximum gross stress, and S_{min} is the minimum gross stress.

In view of the success enjoyed by numerous investigators in correlating fatigue-crack-growth data using the ΔK parameter, this parameter has been used to correlate the fatigue-crack-growth data generated in this investigation.

Appendix C. Symbols

A	cross-sectional area of a test specimen
a	one-half the total length of a central crack
a_c	one-half of the total length of a central crack at the onset of unstable crack growth
C, C_1	empirical constants in fatigue-crack-propagation equations
D	diameter of a circular disk
d	spacing between crystallographic planes
da/dN	rate of fatigue-crack propagation
d_i	spacing (while under stress) between a set of crystallographic planes whose normal is inclined at an angle ψ to the Z-direction
d_n	spacing (while under stress) between a set of crystallographic planes whose normal points in the Z-direction
d_o	spacing (while not under stress) between a set of crystallographic planes whose normal points in the Z-direction
E	Young's modulus
e	percent elongation in a 2-inch gage length
F	stress factor
K_c	stress intensity factor at the onset of unstable crack growth
K_I	stress intensity factor
K_{max}	stress-intensity factor associated with the maximum cyclic stress
K_{min}	stress-intensity factor associated with the minimum cyclic stress
LN_2	liquid nitrogen
m,n	exponents in fatigue-crack-propagation equation
N	number of applied fatigue cycles

N_{ip}	number of cycles required to initiate fatigue cracks at each end of a central notch and to propagate them to specified half-lengths
P_c	load at the onset of unstable crack growth
R	stress ratio (ratio of the minimum gross stress to the maximum gross stress)
r	distance from the tip of a crack to the point at which the stress is being calculated
S	uniformly-distributed axial stress
S-N curve	plot of maximum gross stress against fatigue life
S_c	uniformly-distributed axial stress at the onset of unstable crack growth
S_{max}	maximum gross stress
S_{mean}	mean gross stress
S_{min}	minimum gross stress
t	material thickness
w	width of the test specimen
Δd	change in the spacing between crystallographic planes
ΔK	stress intensity range
$\Delta\theta$	change in the Bragg angle
δ	angle between the X-axis and r
ε	maximum gross strain
ε_Z	strain in the Z-direction
ε_ψ	strain in AO-direction
θ	Bragg angle
θ_i	Bragg angle for incident diffraction
θ_n	Bragg angle for normal diffraction

λ	X-ray wave length
ν	Poisson's ratio
σ_x	stress in the long transverse direction
σ_y	stress in the longitudinal direction
σ_{ys}	yield strength (0.2-percent offset)
σ_{us}	ultimate tensile strength
τ_{xy}	shear stress
ψ	the inclination angle to the Z-axis at which X-ray diffrac - tion measurements were made
ω	finite width correction for the stress intensity factor